Copy

NASA TM X-742

GRO ... at 3 year ... assified
Do ...
in ...

(NASA-TM-X-742) LONGITUDINAL AERODYNAMIC CHARACTERISTICS OF SEVERAL THICK-SLAB DELTA WINGS AT MACH NUMBERS OF 3.00, 4.50, AND 6.00 AND ANGLES OF ATTACK TO 95 DEG W.B. Olstad (NASA) Feb. 1963 70 p
N72-73531
Unclas
00/99 32632

TECHNICAL MEMORANDUM

X-742

LONGITUDINAL AERODYNAMIC CHARACTERISTICS OF SEVERAL THICK-SLAB DELTA WINGS AT MACH NUMBERS OF 3.00, 4.50, AND 6.00 AND ANGLES OF ATTACK TO 95°

By Walter B. Olstad

Langley Research Center
Langley Station, Hampton, Va.

CLASSIFICATION CHANGED
TO ...
By authority of ... Date ...
CLASSIFIED DO...

NATIONAL AERONAUTICS AND SPACE ADMINISTRATION
WASHINGTON
February 1963

Reproduced by
NATIONAL TECHNICAL
INFORMATION SERVICE
U S Department of Commerce
Springfield VA 22151

NATIONAL AERONAUTICS AND SPACE ADMINISTRATION

TECHNICAL MEMORANDUM X-742

LONGITUDINAL AERODYNAMIC CHARACTERISTICS OF SEVERAL THICK-SLAB DELTA WINGS AT MACH NUMBERS OF 3.00, 4.50, AND 6.00 AND ANGLES OF ATTACK TO 95°*

By Walter B. Olstad

SUMMARY

Results are presented of an investigation of the effects of slab thickness, or volume-area parameter, and dihedral angle on the longitudinal aerodynamic characteristics of several slab delta wings. The effects of nose deflection and elevon planform shape and deflection were studied to obtain data on the trim, stability, and control characteristics of these configurations in the angle-of-attack range which encompasses maximum lift-drag ratio and maximum lift coefficient. Modified Newtonian impact theory was used to estimate the force and moment coefficients and comparisons between the estimated results and experimental results are presented.

Reasonably good agreement between the theory and experiment was obtained at a Mach number of 6.00. A positive shift in pitching moment occurred in the angle-of-attack range from 50° to 65° for all models tested. This shift apparently was caused by the flow on the lower surface changing from supersonic to subsonic in this angle-of-attack range. Values of the maximum lift-drag ratio and maximum lift coefficient decreased with increasing volume-area parameter $V^{2/3}/S$. Increasing the wing dihedral angle, at least up to 30°, increased slightly the maximum lift-drag ratio for a slab delta wing of constant volume-area parameter and decreased the maximum lift coefficient. A positive nose deflection provided a positive increment in pitching moment and increased the stability level of the model at angles of attack greater than 30° at the expense of decreased lift and increased drag.

INTRODUCTION

The corridor for entry into the earth's atmosphere at supercircular velocities can be greatly widened over that available to a ballistic vehicle through the use of aerodynamic lift. (See ref. 1.) Aerodynamic lift can also provide the vehicle with some maneuverability and range control. High values of aerodynamic drag are desired in order to reduce the heat load associated with

*Title, Unclassified.

atmospheric entry. During entry, then, it is desirable to have both high lift and high drag which leads to rather low values of lift-drag ratio of 1.0 or less.

Vehicles with highly swept thick delta wings can provide the required aerodynamic performance. In addition, the blunt nose and highly swept blunt leading edges of such configurations would tend to reduce the heat load to these critical areas.

The purpose of the investigation reported herein was to determine the effects of slab thickness, or volume-area parameter, and dihedral angle on the longitudinal aerodynamic characteristics of several slab delta wings. Also, the effects of nose deflection and elevon planform shape and deflection were studied to obtain data on the trim, stability, and control characteristics of these configurations in the angle-of-attack range from maximum lift-drag ratio to maximum lift coefficient. The results of an investigation of somewhat similarly shaped sharp- and blunt-nose elliptic cone models are presented in reference 2.

Modified Newtonian impact theory was used to estimate the force and moment coefficients at hypersonic speeds and comparisons between these estimated results and experimental results are presented.

SYMBOLS

The force and moment coefficients were referred to the wind and body axes systems with the origin located at the centroid of the planform area of the undeflected delta wing, as shown in figure 1.

t slab thickness

A_b base area

b width of model at base

C_A axial-force coefficient, $\frac{\text{Axial force}}{q_\infty S}$

C_D drag coefficient, $\frac{\text{Drag}}{q_\infty S}$

C_L lift coefficient, $\frac{\text{Lift}}{q_\infty S}$

C_m pitching-moment coefficient, $\frac{\text{Pitching moment}}{q_\infty S l_1}$

C_N normal-force coefficient, $\frac{\text{Normal force}}{q_\infty S}$

C_P pressure coefficient, $\frac{p - p_\infty}{q_\infty}$

l_1 body length

l_2 body length before blunting (see fig. 1)

$\frac{L}{D}$ lift-drag ratio, $\frac{C_L}{C_D}$

M free-stream Mach number

p pressure

p_∞ free-stream static pressure

q_∞ free-stream dynamic pressure

r radius

S planform area

V total volume of configuration

α angle of attack, deg

δ_e elevon deflection angle (positive when trailing edge is down), deg (see fig. 3)

δ_n nose deflection angle (positive when nose is up), deg (see fig. 3)

Γ angle of dihedral, deg (see fig. 1)

σ angle of shock from stream direction, deg

Subscript:

max maximum

MODELS AND APPARATUS

Dimensional details of the five basic models used during this investigation are shown in figure 1, and photographs of these models are shown as figure 2. The models represent blunted slab delta wings with leading edges swept back 75° and with variations in thickness and dihedral angle. The noses of the models were spherical sections and the leading edges were hemicylinders.

Models 1, 2, and 3 form a series of models of varying thickness with thickness-length ratios t/l_1 of 0.117, 0.219, and 0.637, respectively, and of varying volume-area parameter $V^{2/3}/S$ with values of 0.319, 0.441, and 0.663, respectively.

Models 1, 4, and 5 form a series of varying dihedral angle. The dihedral angles for the three models are 0°, 15°, and 30°, respectively. The dihedral angles were obtained by rotating the wing panels about a line on the lower surface of the wing. Rotation of the wing panels in this manner brought about a reduction in planform area and volume. The volume-area parameters $V^{2/3}/S$ for models 4 and 5 are 0.341 and 0.387, respectively.

Model 1 was tested with nose deflection angles δ_n of 0°, 10°, and 20°, whereas model 4 was tested with nose deflection angles of 0° and 10°. (See figs. 3(a) and 3(b).) Model 1 (with $\delta_n = 10°$) was also tested with triangular-planform elevons at elevon deflection angles δ_e of 15°, 0°, -15°, and -30°. (See fig. 3(c).) Rectangular-planform elevons at $\delta_e = -15°$ were also used in conjunction with model 1 (with $\delta_n = 10°$). (See fig. 3(d).) Model 4 (with $\delta_n = 10°$) was tested with both the triangular-planform and rectangular-planform elevons at $\delta_e = -15°$. Photographs of two of the models with deflected nose and tail surfaces are presented as figure 4.

At angles of attack from -6° to 15° the model was supported by a straight sting which extended from the model base and was attached to the central support system of the wind tunnel. In order to obtain angles of attack up to 95°, an adapter was inserted between the model and the sting. (See fig. 2.) This adapter was fixed at angles of 20°, 40°, 60°, and 80°, and the angle of attack of the model was varied about these settings by varying the angle of the central support system. These support systems kept the model near the center line of the tunnel at all angles of attack. It was necessary to remove a small portion of the upper surface of all of the models with the exception of model 3 in order to accommodate the adapter.

TESTS, CORRECTIONS, AND ACCURACY

Tests were conducted in the 2-foot hypersonic facility at the Langley Research Center at free-stream Mach numbers of 3.00, 4.50, and 6.00 and angles of attack from -6° to 95°. A description of the tunnel and its operating characteristics are presented in reference 3. Tunnel test conditions and corresponding Reynolds numbers per foot are presented in the following table:

Mach number, M	Total pressure, psia	Total temperature, °F	Reynolds number per ft
3.00	3.9	130	0.56×10^6
4.50	14.7	300	.67
6.00	46.5	330	1.08

Model forces and moments were measured with a three-component internal strain-gage balance. The measured coefficients are estimated to be accurate within the following limits:

C_N (at α near 0°)	± 0.005
C_N (at α near 90°)	± 0.025
C_A	± 0.002
C_m	± 0.001

The angle-of-attack measurements were corrected for balance and sting deflections under load. The angle of attack is estimated to be accurate within $\pm 0.2^\circ$. Pressures were measured by means of static-pressure orifices on the base and upper surface of model 2. (See fig. 1.) The pressure coefficients are estimated to be accurate within ± 0.01.

Calibrations of the tunnel test section indicate that local deviations from the average free-stream Mach number in the region of the model were no greater than ± 0.03. The average free-stream Mach number was held to within ± 0.02 of the nominal values shown in this paper.

The effects of the presence of the support systems were not determined during these tests and no corrections have been applied to the data to account for support interference. The axial-force and drag coefficients have not been adjusted to free-stream conditions at the model base.

RESULTS AND DISCUSSION

Aerodynamic Characteristics of Basic Models

The experimental results obtained at Mach numbers of 3.00, 4.50, and 6.00 for the five basic models are presented in figures 5 to 9. In these figures the experimental results for a Mach number of 6.00 are compared with estimated values obtained from modified Newtonian impact theory (see ref. 4) together with an estimated local average skin-friction drag coefficient of 0.0015 and an estimated base drag coefficient equivalent to a base pressure coefficient of $-1/M^2$. The modification to the simple impact theory consisted of replacing the Newtonian value of 2.0 for the stagnation pressure coefficient by the values listed in the following table:

α, deg	Value of stagnation pressure coefficient			
	Flat surfaces			Blunt nose and leading edges
	Models 1, 2, 3	Model 4	Model 5	
0	2.40	2.40	2.40	1.80
15	2.40	2.40	2.40	1.80
30	2.40	2.40	2.40	1.80
45	2.30	2.32	2.35	1.80
60	2.11	2.18	2.27	1.80
75	1.92	2.05	2.19	1.80
90	1.80	1.92	2.11	1.80

These particular values were chosen on the basis of the discussion presented in reference 4.

In general, the agreement between the experimental and predicted values for the force coefficient was good. The predicted values of pitching-moment coefficient were generally more negative than the experimental values indicating that the center of pressure was actually 1 or 2 percent of the root chord forward of the predicted position. The agreement between the predicted and experimental values of pitching-moment coefficient for model 3 (fig. 7(c)) was poor, probably because of the pressures induced on the lower surface by the presence of the large blunt nose and leading edges.

All the basic configurations exhibit a positive shift in pitching-moment coefficient (similar to subsonic pitchup). This shift was initiated in the angle-of-attack range from 50° to 65°. A similar shift was noted in reference 5. It is believed that this shift is caused by the flow on the lower surface changing from supersonic to subsonic in this angle-of-attack range. Figure 10, which presents the lower-surface shock angle as a function of angle of attack for model 2, indicates that the shock angle for sonic flow occurs at the angle of attack for which the shift in pitching moment begins.

Measured upper-surface and base pressure coefficients for model 2 are presented in figure 11 together with curves of the empirical base pressure coefficient $-1/M^2$. (See ref. 6 for derivation of this expression.) The empirical values are in good agreement with experimental values at a Mach number of 3.00, whereas at Mach numbers of 4.50 and 6.00 the agreement between the predicted and experimental values is poor.

The effects of wing thickness or volume-area parameter $V^{2/3}/S$ on the performance characteristics are summarized in figure 12. The maximum lift-drag ratio and maximum lift coefficient decreased, as expected, as the volume-area parameter increased. The effects of dihedral angle on the performance characteristics are shown in figure 13. The effects shown in this figure are not entirely due to dihedral inasmuch as models 1, 4, and 5 each had a different value of the volume-area parameter $V^{2/3}/S$. The short-dash curves in figure 13 represent the theoretical estimate of the effects of the variation of the volume-area parameter for the three models (obtained from the theoretical curve of fig. 12), so that the difference between the long-dash curves and the short-dash curves is the estimated increment in maximum lift-drag ratio and maximum lift coefficient due to dihedral angle. It is seen, then, that increasing the dihedral angle, at least up to 30°, theoretically increases the maximum lift-drag ratio by a small amount for a slab delta wing of fixed volume-area parameter. The maximum lift coefficient would be decreased somewhat by an increase in dihedral angle.

Effect of Nose Deflection

The effect of nose deflection on the longitudinal aerodynamic characteristics of models 1 and 4 is presented in figures 14 and 15, respectively. These figures indicate that positive nose deflection produced a positive increment in pitching moment at the expense of decreased lift and increased drag. The

pitching-moment increment generally increased with increasing angle of attack up to an angle of attack of about 30°. (See fig. 16.) Further increases in angle of attack tended to reduce the pitching-moment increment (thereby increasing the stability level). Thus, positive nose deflection not only provides positive increments of pitching moment to aid in trimming a configuration at large angles of attack but also adds to the stability level of the configuration for angles of attack greater than about 30°. Similar results were obtained in the investigation of reference 5.

Theoretical calculations of incremental pitching moment due to nose deflection properly predicted the stability trends (fig. 16) but failed to predict the magnitude of the test results. The difference in the incremental pitching moments between a nose deflection of 20° and a nose deflection of 10° was quite accurately predicted by the theory.

Effects of Elevon Planform and Deflection

The effects of elevon planform and deflection angle on the longitudinal aerodynamic characteristics of models 1 and 4 with positive nose deflection of 10° are presented in figures 17 and 18, respectively. Changing the elevon planform shape from triangular to rectangular did not produce any significant change in the force and moment coefficients for either model.

An increase in negative elevon deflection for the triangular elevons on model 1 with a nose deflection of 10° decreased both lift and drag throughout the angle-of-attack range of the investigation, with the largest change occurring between the elevon deflection angles of 15° and 0°. Deflecting the elevon in the negative (or trailing edge up) direction from an angle of 15° to -30° produced large positive increments in pitching moment allowing the configuration to be trimmed over an angle-of-attack range from less than 6° (the lowest angle of attack at which data were obtained) to approximately 42°.

Theoretical calculations of incremental pitching moment due to elevon deflection properly predicted both the stability trends and magnitudes of the test results for elevon deflection angles of -15° and -30°. (See fig. 19.) For an elevon deflection of 15° the stability trend was predicted but the magnitudes of the test results were underestimated by about 50 percent.

CONCLUSIONS

An investigation of the longitudinal aerodynamic characteristics of several slab delta wings of varying thickness and dihedral angle at Mach numbers of 3.00, 4.50, and 6.00 and angles of attack to 90° has led to the following conclusions:

1. Reasonably good agreement between experimental values and values estimated from modified Newtonian impact theory was obtained at a Mach number of 6.00 for the basic models.

2. A positive shift in pitching-moment coefficient occurred in the angle-of-attack range from 50° to 65° for all models tested. This shift apparently was caused by the flow on the lower surface changing from supersonic to subsonic in this angle-of-attack range.

3. Values of maximum lift-drag ratio and maximum lift coefficient decreased with increasing volume-area parameter $V^{2/3}/S$.

4. According to theory, increasing the wing dihedral angle, at least up to 30°, increased slightly the maximum lift-drag ratio for a slab delta wing of constant volume-area parameter and decreased the maximum lift coefficient.

5. A positive nose deflection provided a positive increment in pitching moment and increased the stability level of the model at angles of attack greater than 30° at the expense of decreased lift and increased drag.

Langley Research Center,
National Aeronautics and Space Administration,
Langley Station, Hampton, Va., September 19, 1962.

REFERENCES

1. Chapman, Dean R.: An Analysis of the Corridor and Guidance Requirements for Supercircular Entry Into Planetary Atmospheres. NASA TR R-55, 1960.

2. McDevitt, John B., and Rakich, John V.: The Aerodynamic Characteristics of Several Thick Delta Wings at Mach Numbers to 6 and Angles of Attack to 50°. NASA TM X-162, 1960.

3. Stokes, George M.: Description of a 2-Foot Hypersonic Facility at the Langley Research Center. NASA TN D-939, 1961.

4. Olstad, Walter B.: Theoretical Evaluation of Hypersonic Forces, Moments, and Stability Derivatives for Combinations of Flat Plates, Including Effects of Blunt Leading Edges, by Newtonian Impact Theory. NASA TN D-1015, 1962.

5. Close, William H.: Hypersonic Longitudinal Trim, Stability, and Control Characteristics of a Delta-Wing Configuration at High Angles of Attack. NASA TM X-240, 1960.

6. Mayer, John P.: A Limit Pressure Coefficient and an Estimation of Limit Forces on Airfoils at Supersonic Speeds. NACA RM L8F23, 1948.

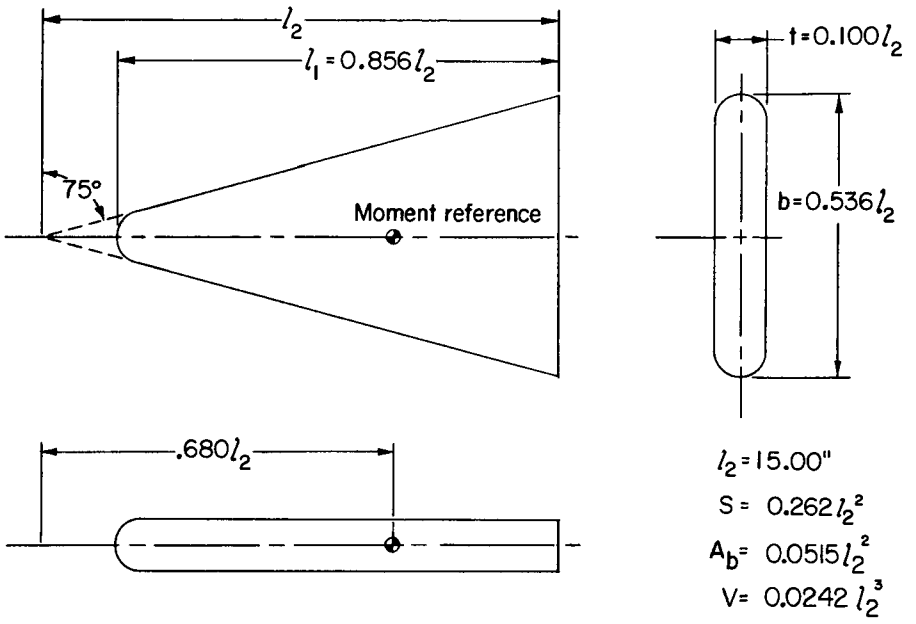

(a) Model 1.

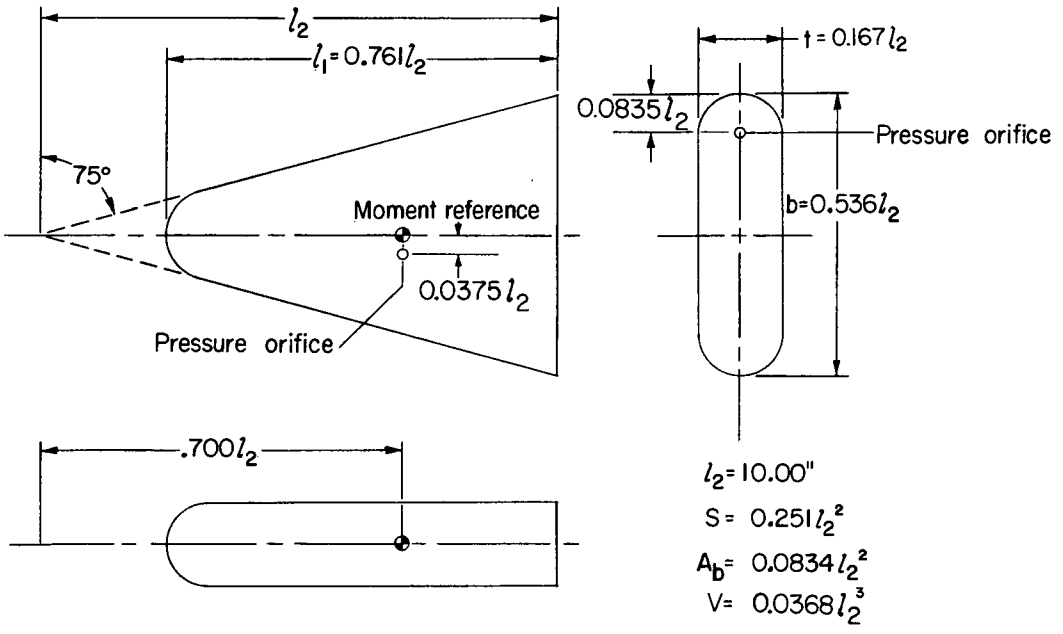

(b) Model 2.

Figure 1.- Geometry of the basic models.

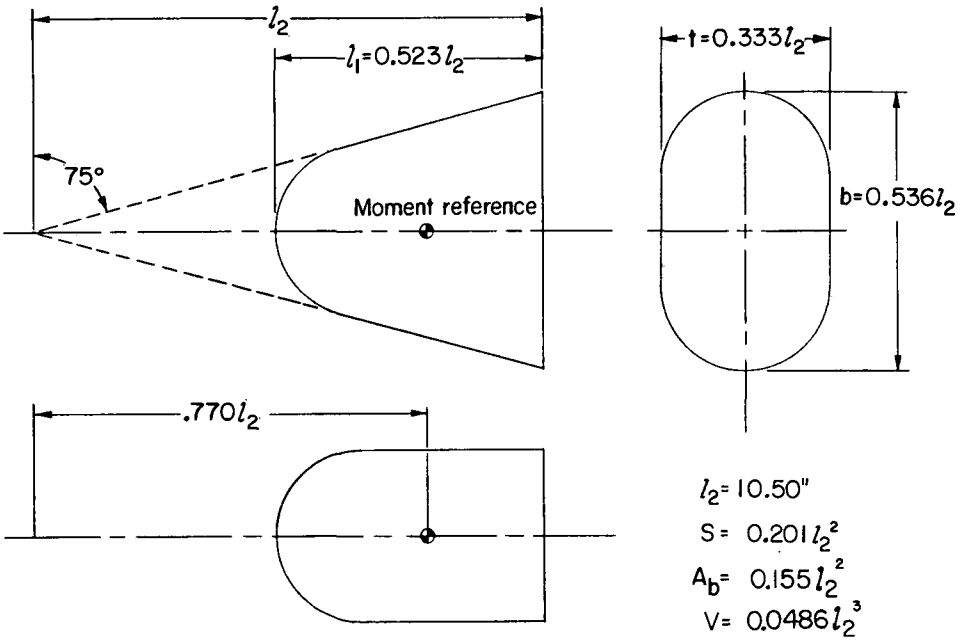

(c) Model 3.

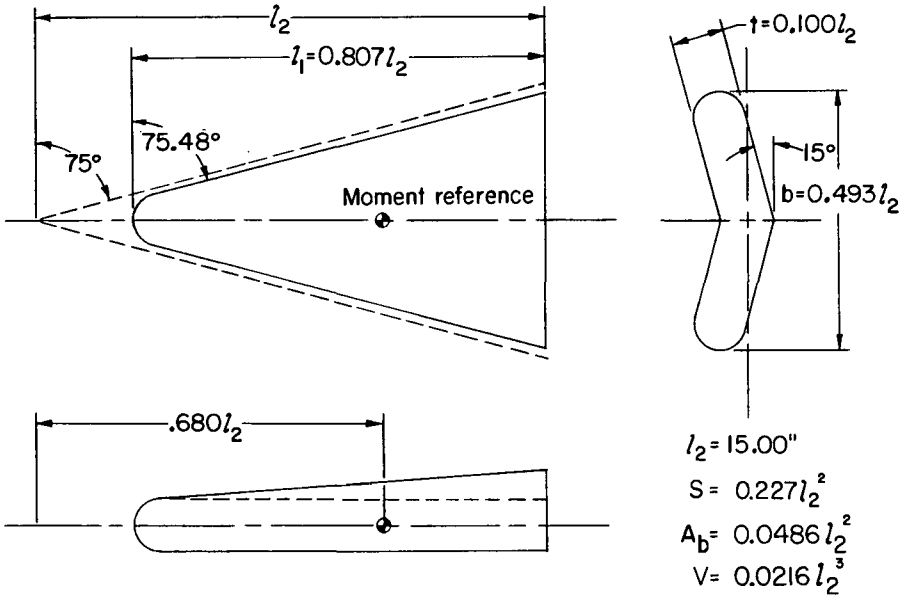

(d) Model 4.

Figure 1.- Continued.

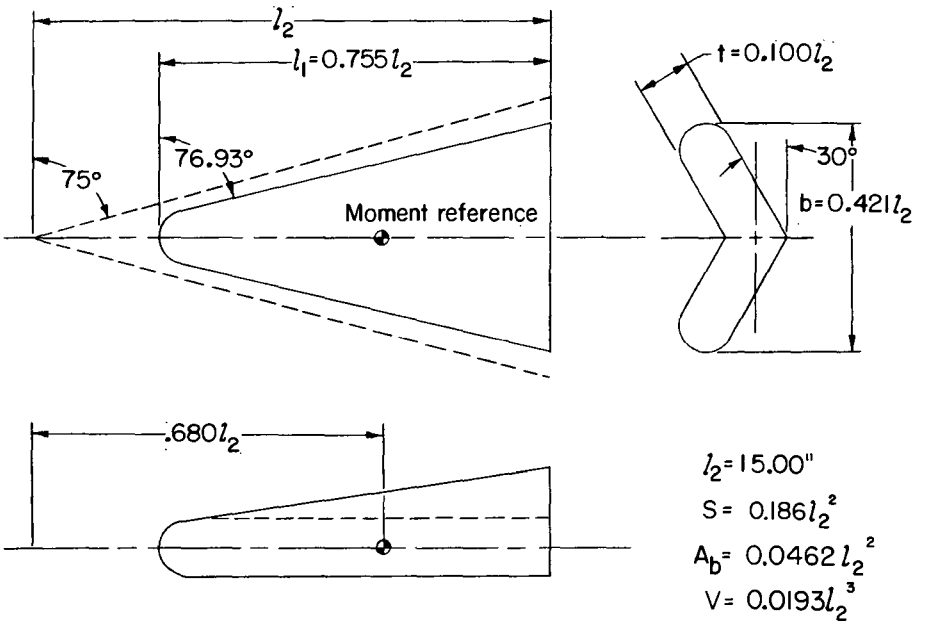

(e) Model 5.

Figure 1.- Concluded.

CONFIDENTIAL

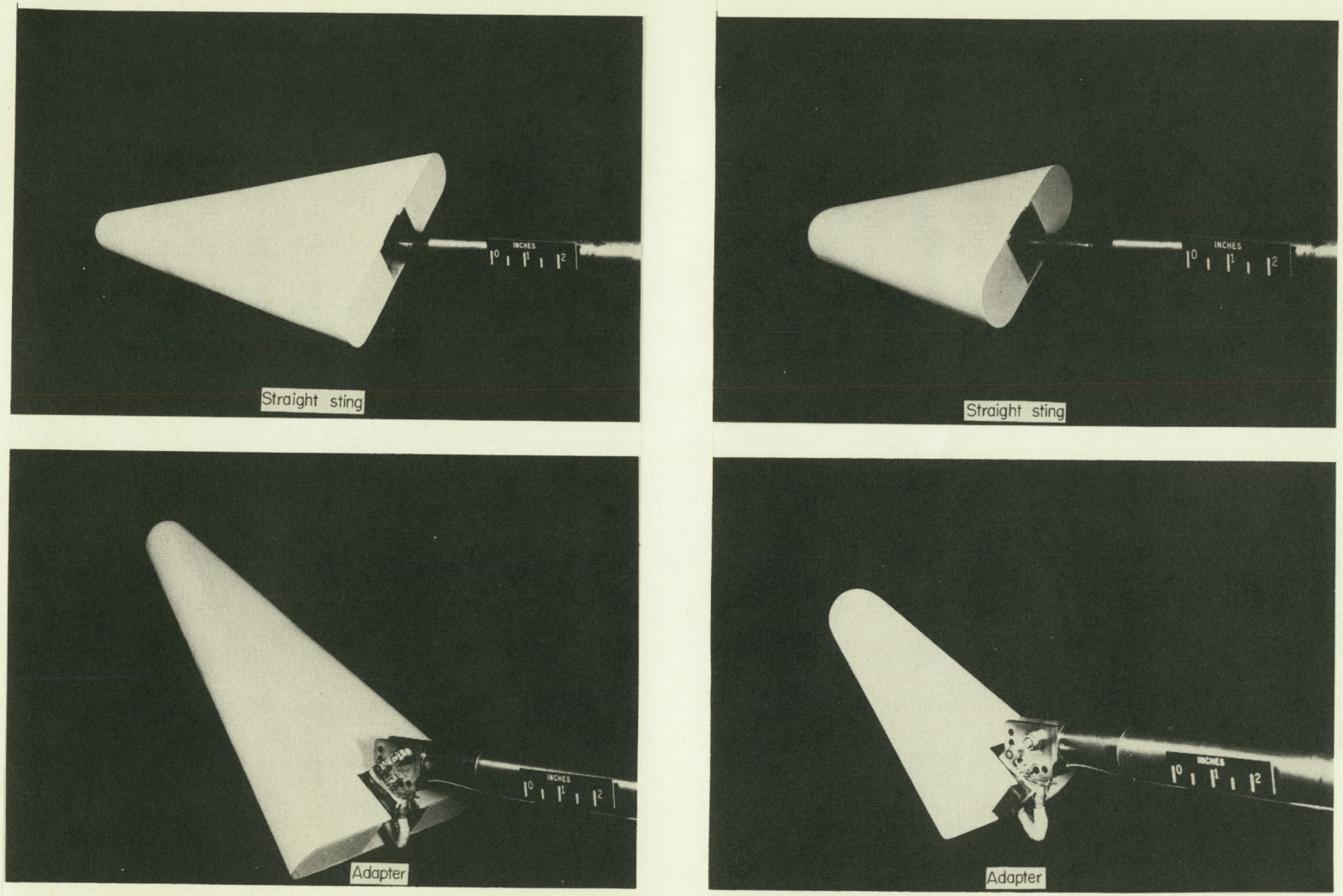

(a) Model 1.

(b) Model 2.

L-63-10

Figure 2.- Models used in the investigation.

CONFIDENTIAL

CONFIDENTIAL

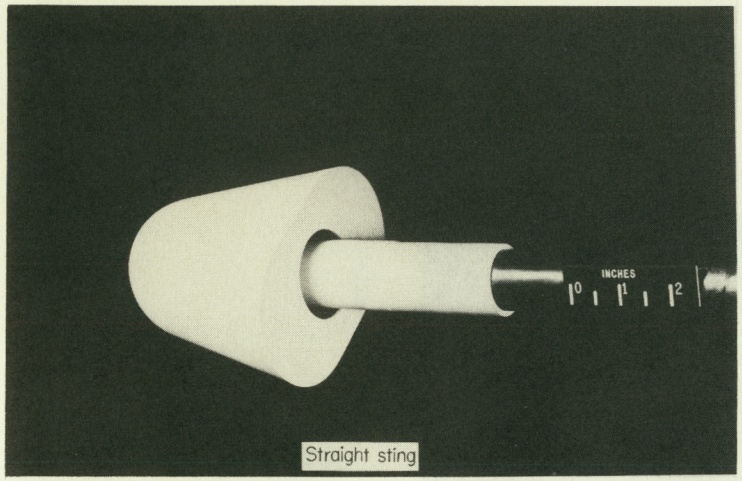

(c) Model 3.

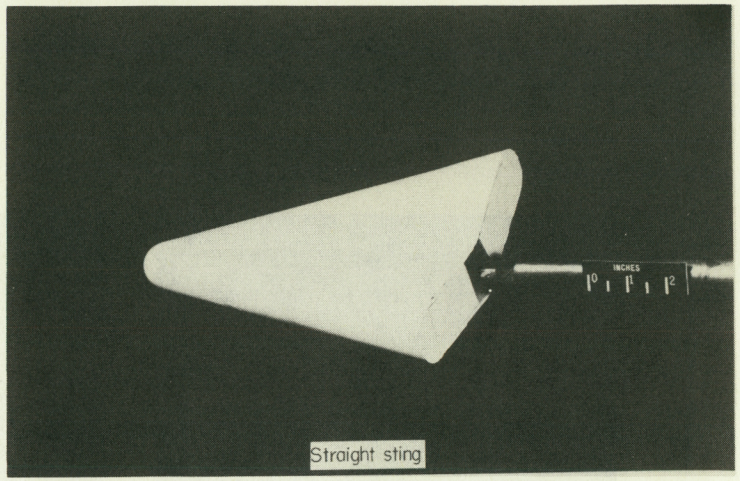

(d) Model 4.

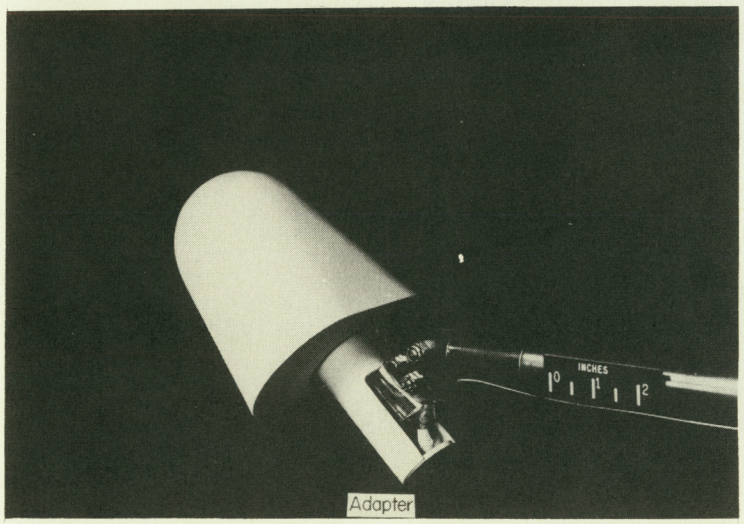

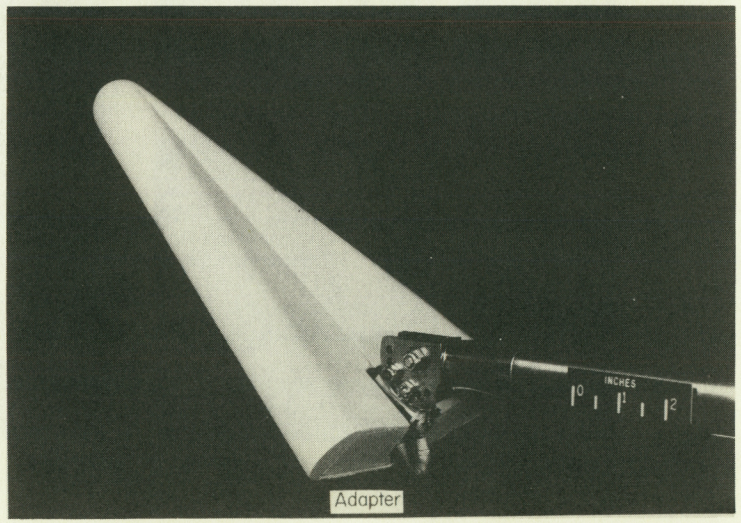

L-63-11

Figure 2.- Continued.

CONFIDENTIAL

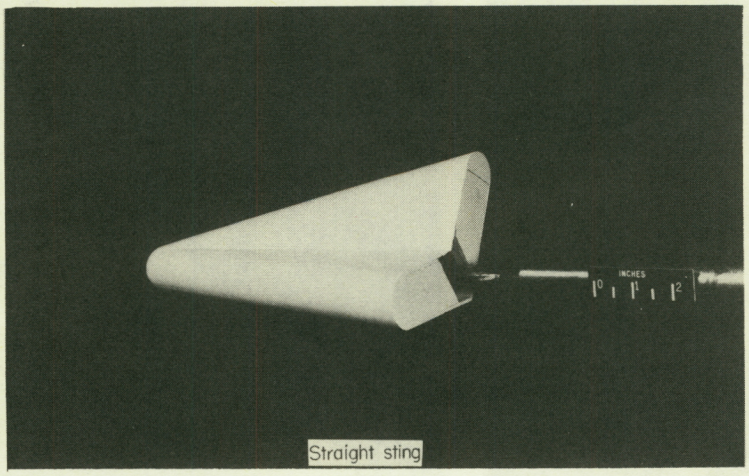

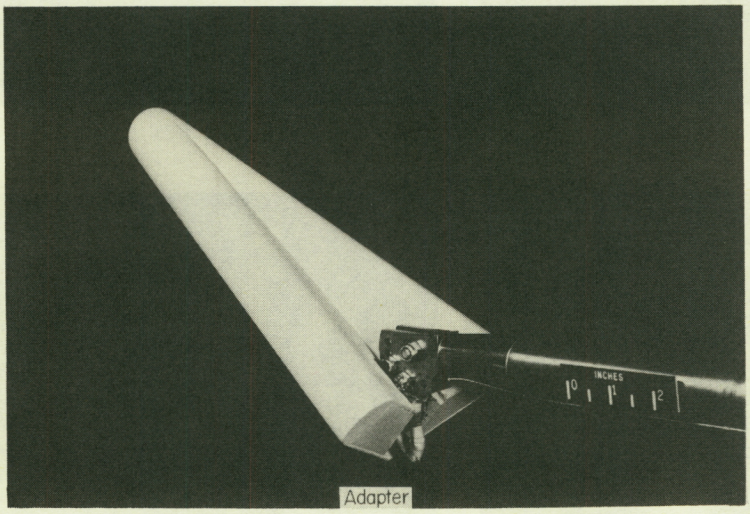

(e) Model 5. L-63-12

Figure 2.- Concluded.

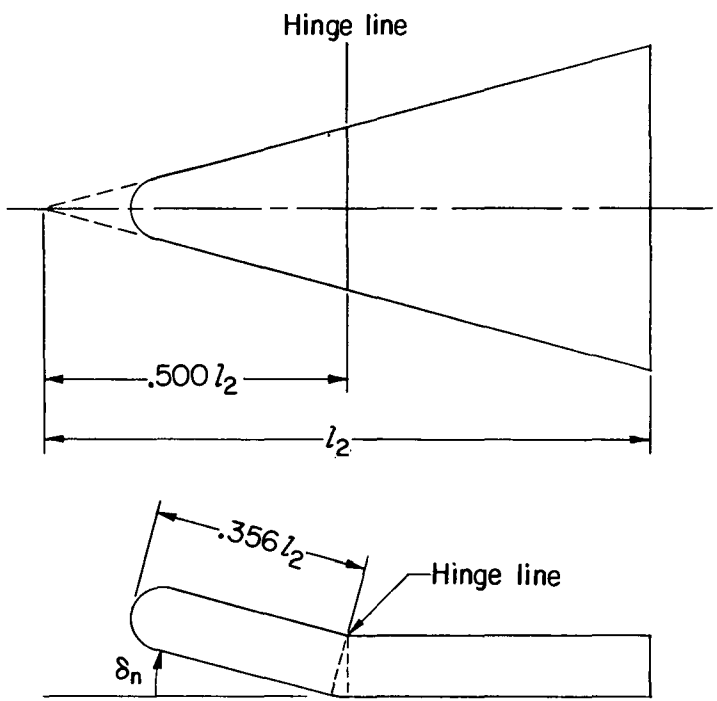

(a) Nose deflection (model 1).

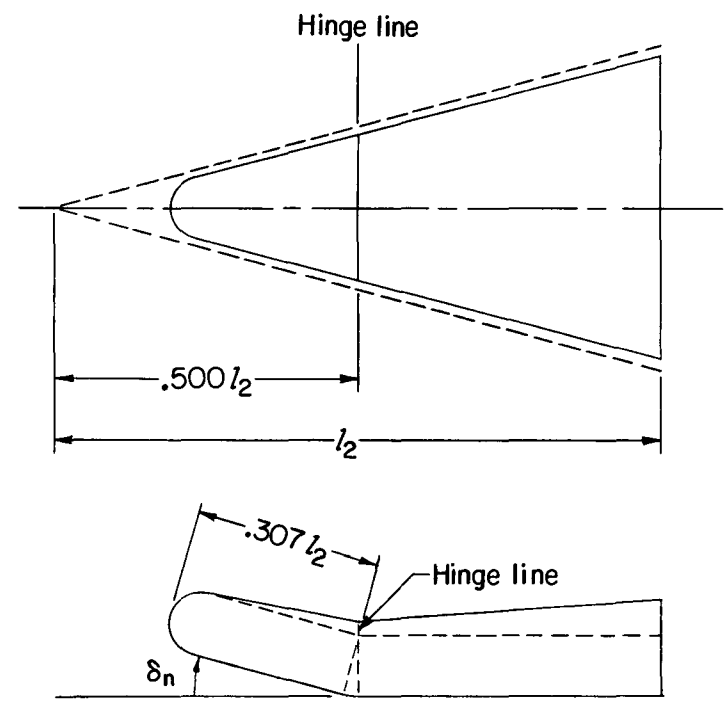

(b) Nose deflection (model 4).

Figure 3.- Geometry of deflected surfaces.

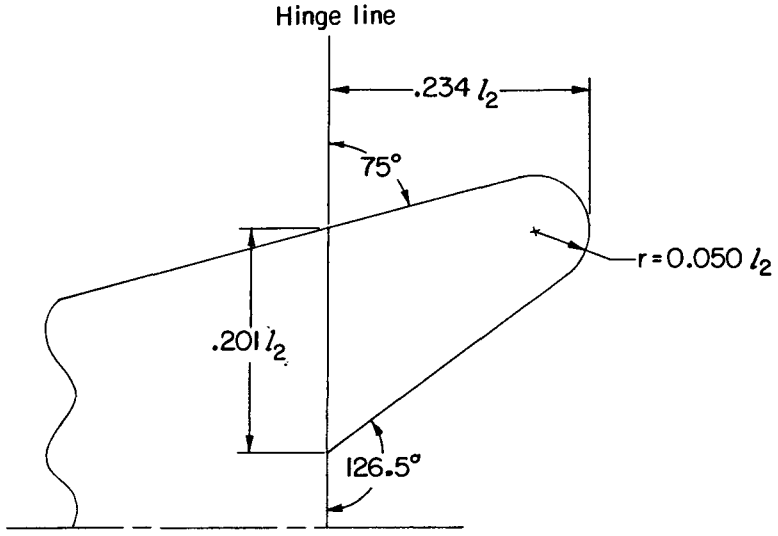

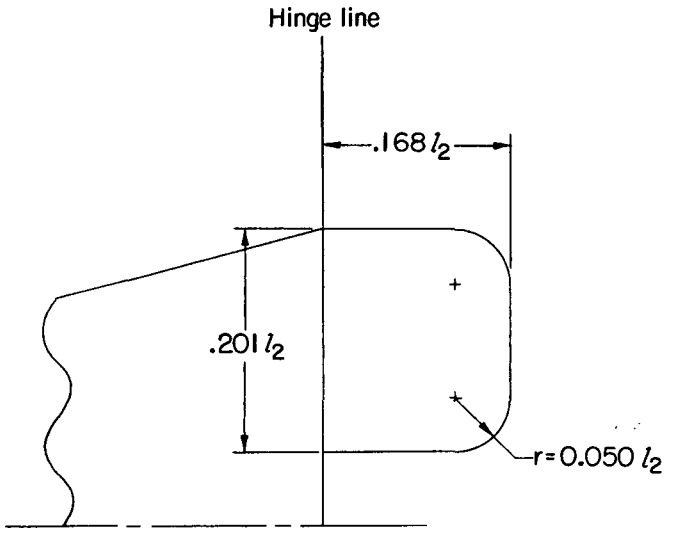

All exposed elevon edges are rounded to r = 0.050 l_2

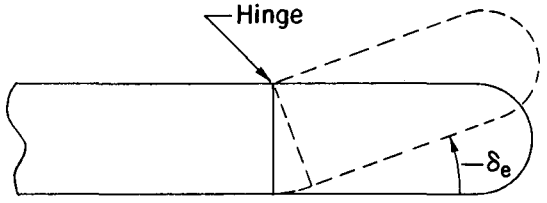

(c) Triangular-planform elevon.

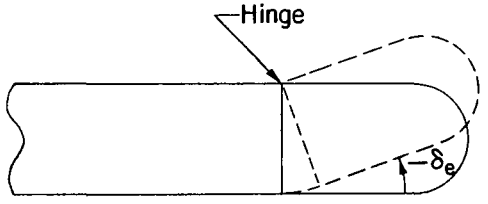

(d) Rectangular-planform elevon.

Figure 3.- Concluded.

CONFIDENTIAL

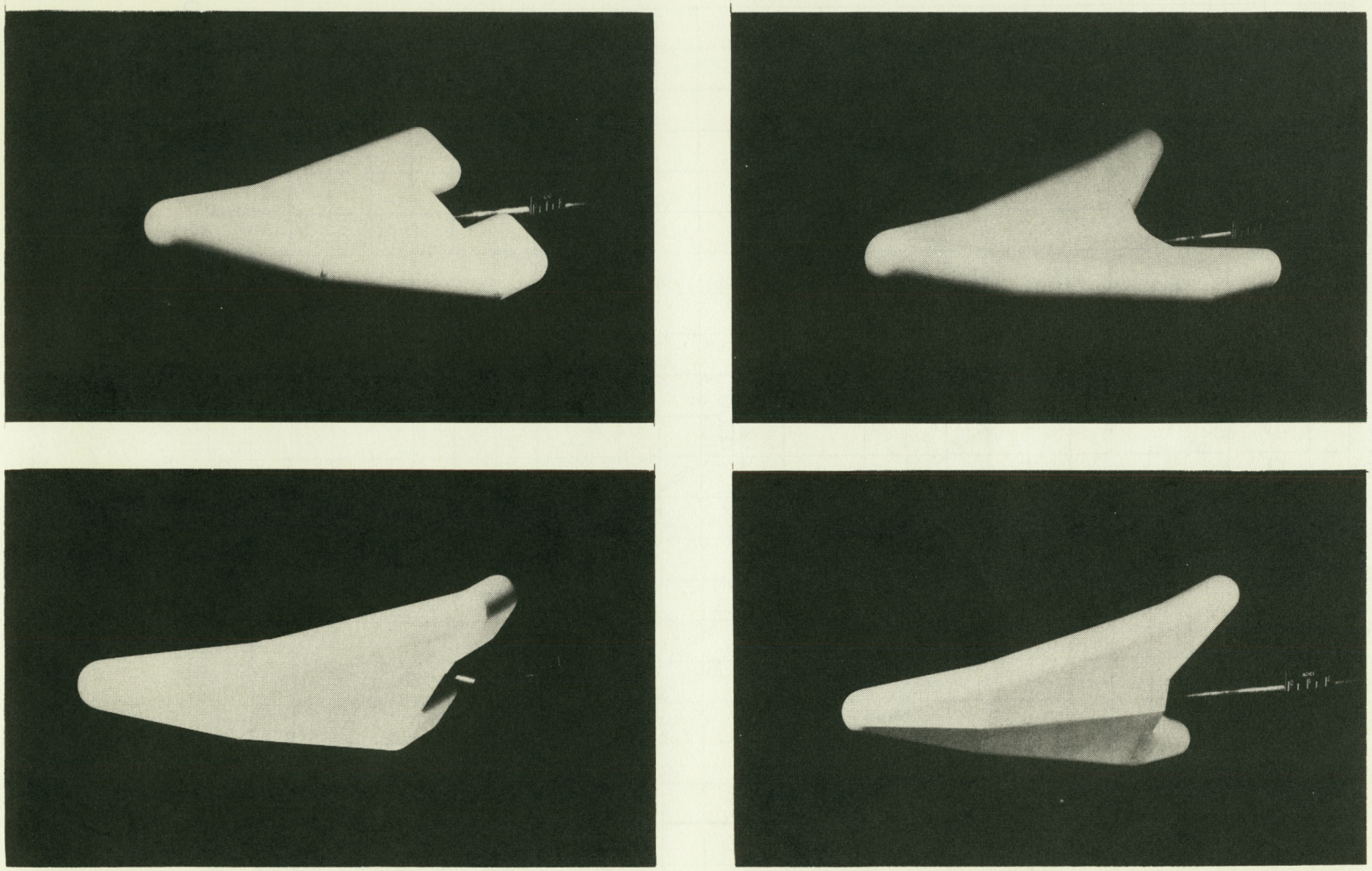

(a) Model 1 with rectangular-planform elevons. $\delta_n = 10^\circ$; $\delta_e = -15^\circ$.

(b) Model 4 with triangular-planform elevons. $\delta_n = 10^\circ$; $\delta_e = -15^\circ$.

L-63-13

Figure 4.- Models with deflected surfaces.

CONFIDENTIAL

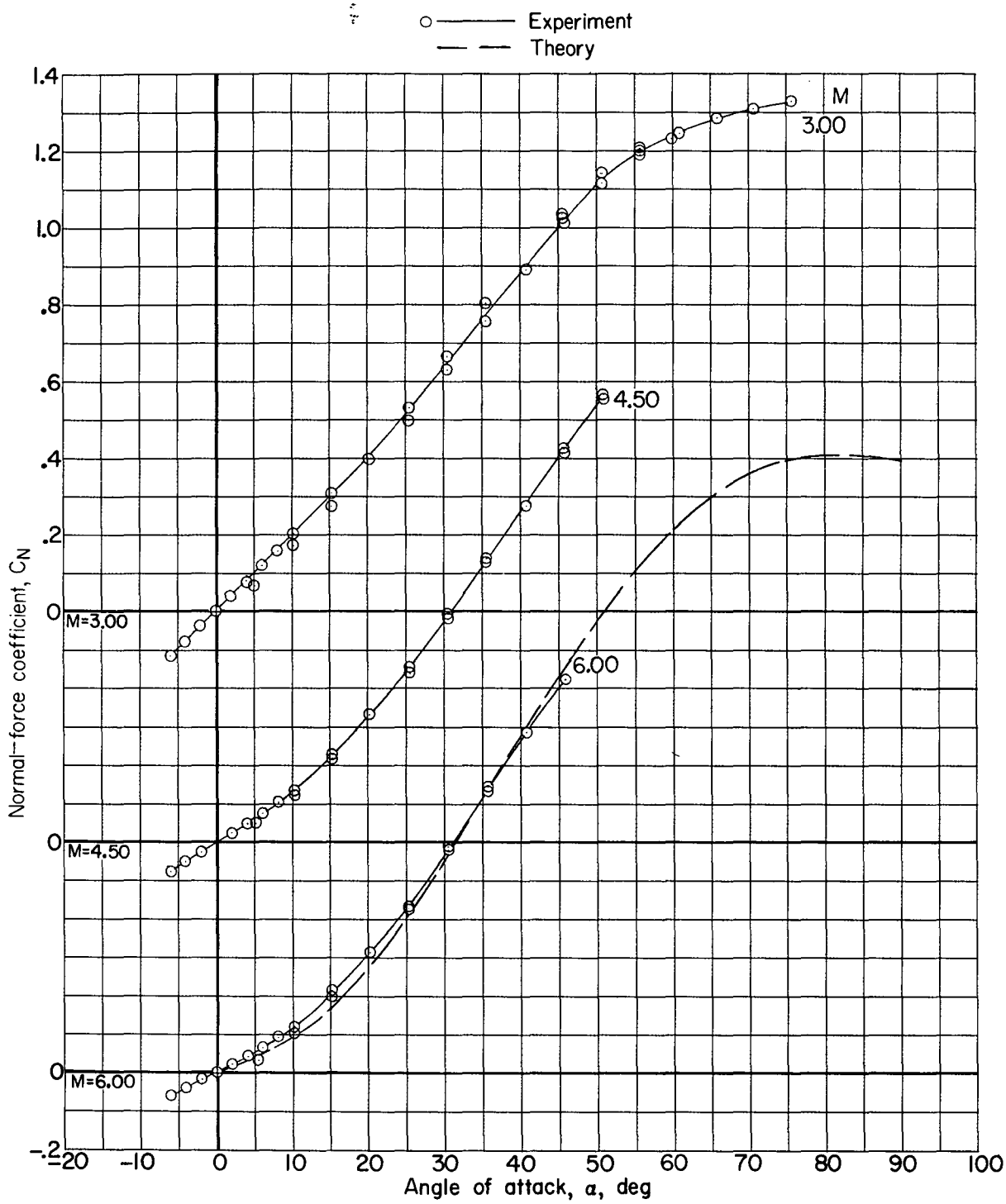

(a) Normal force.

Figure 5.- Longitudinal aerodynamic characteristics of model 1.

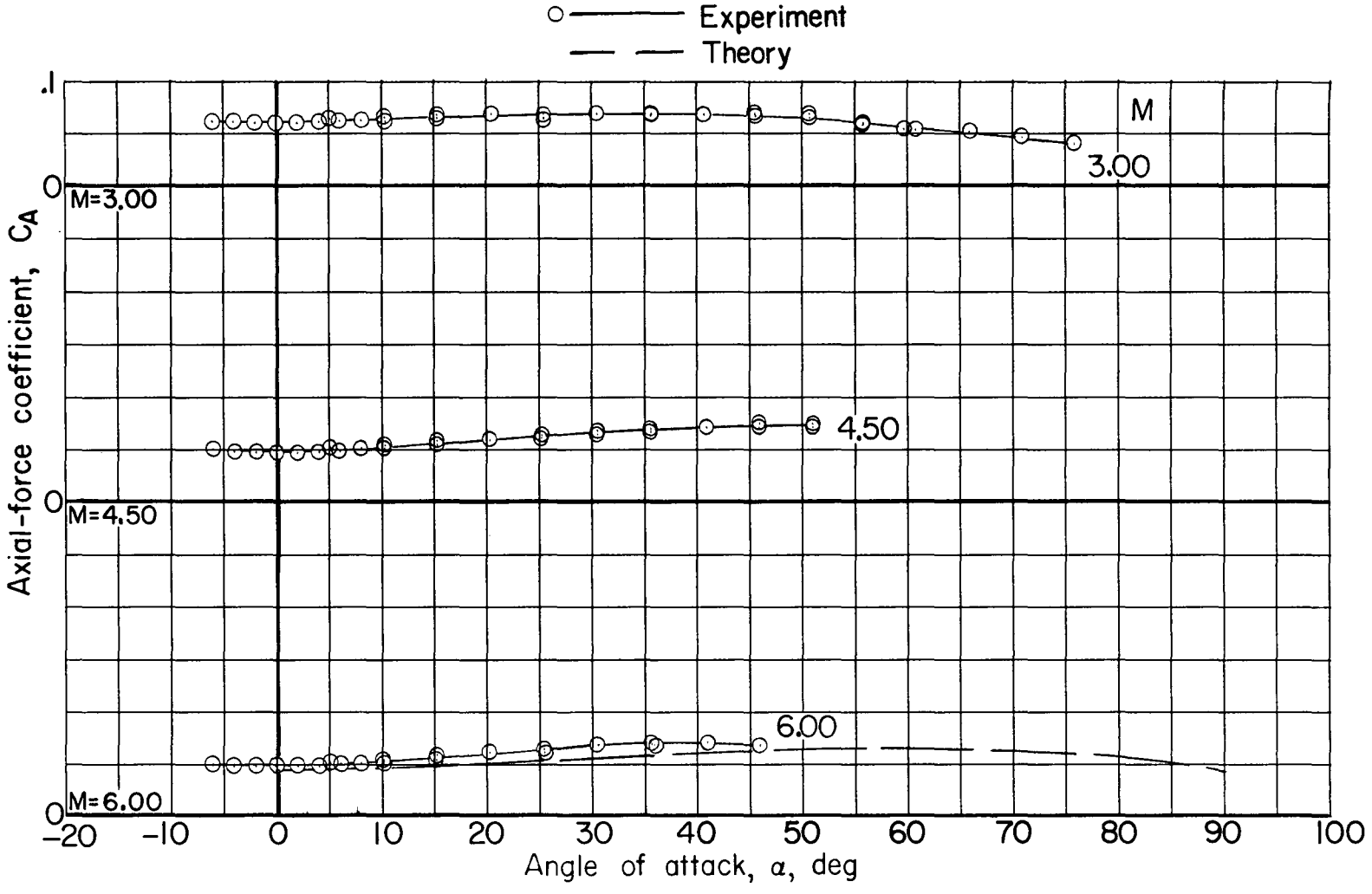

(b) Axial force.

Figure 5.- Continued.

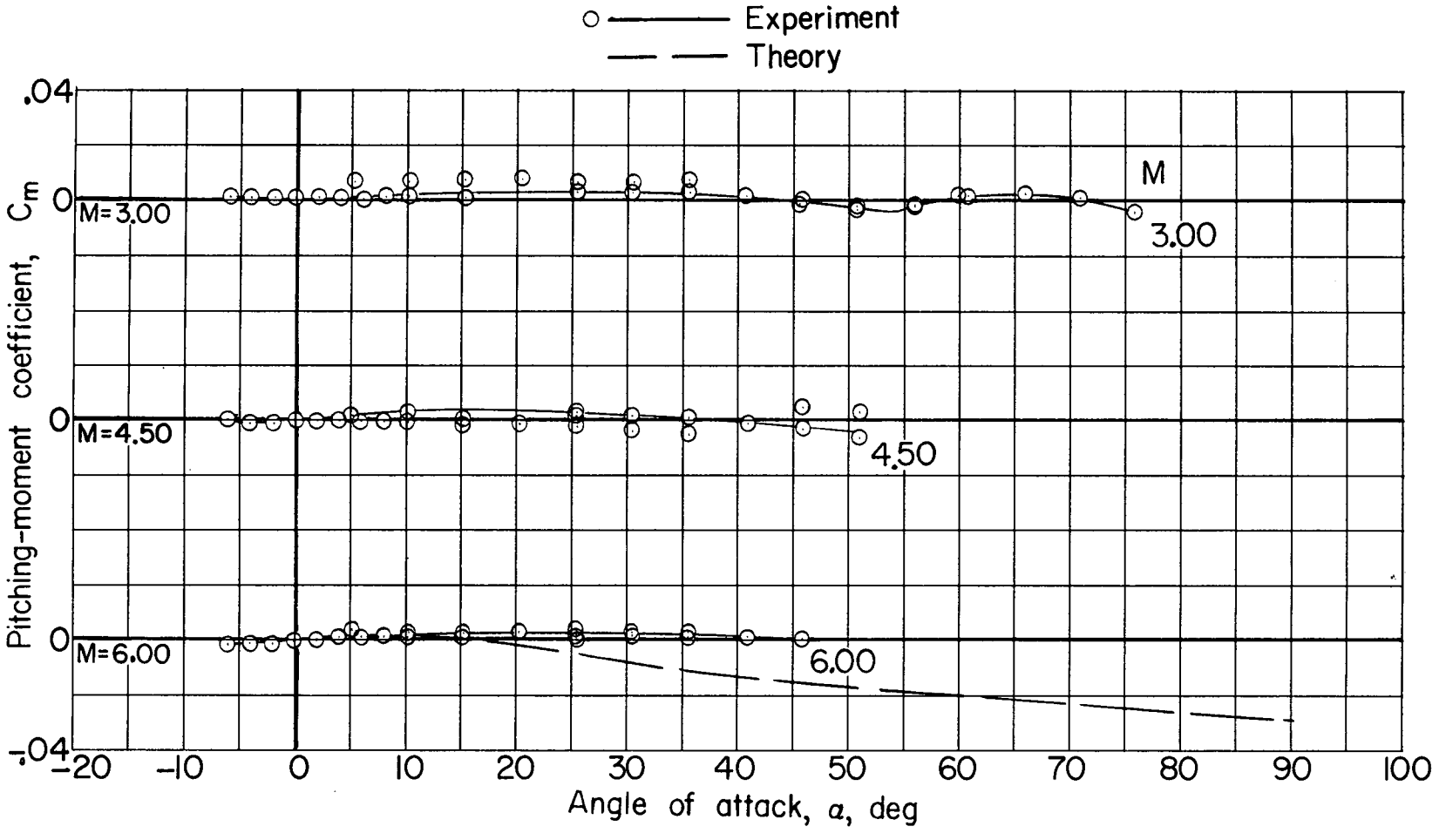

(c) Pitching moment.

Figure 5.- Continued.

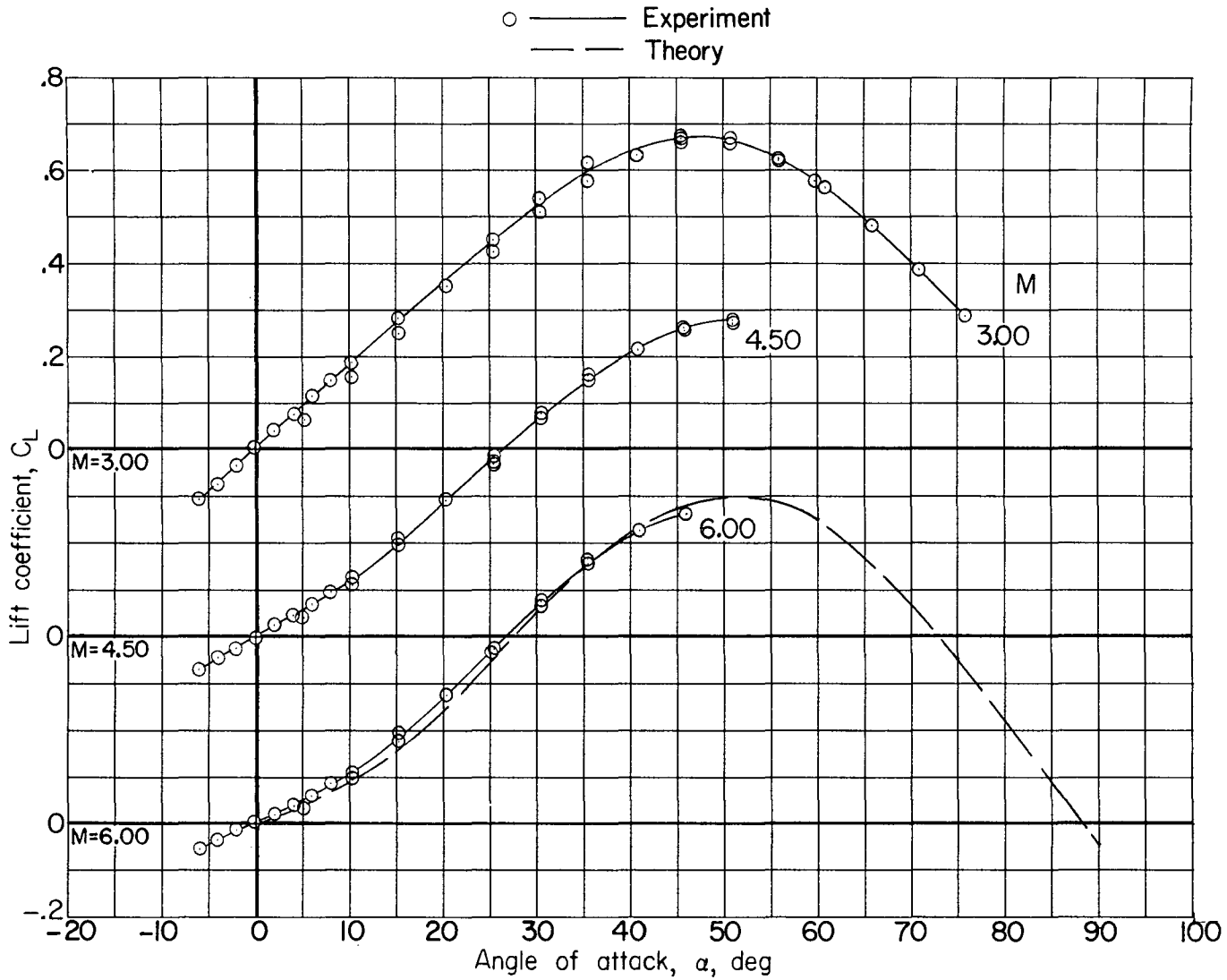

(d) Lift.

Figure 5.- Continued.

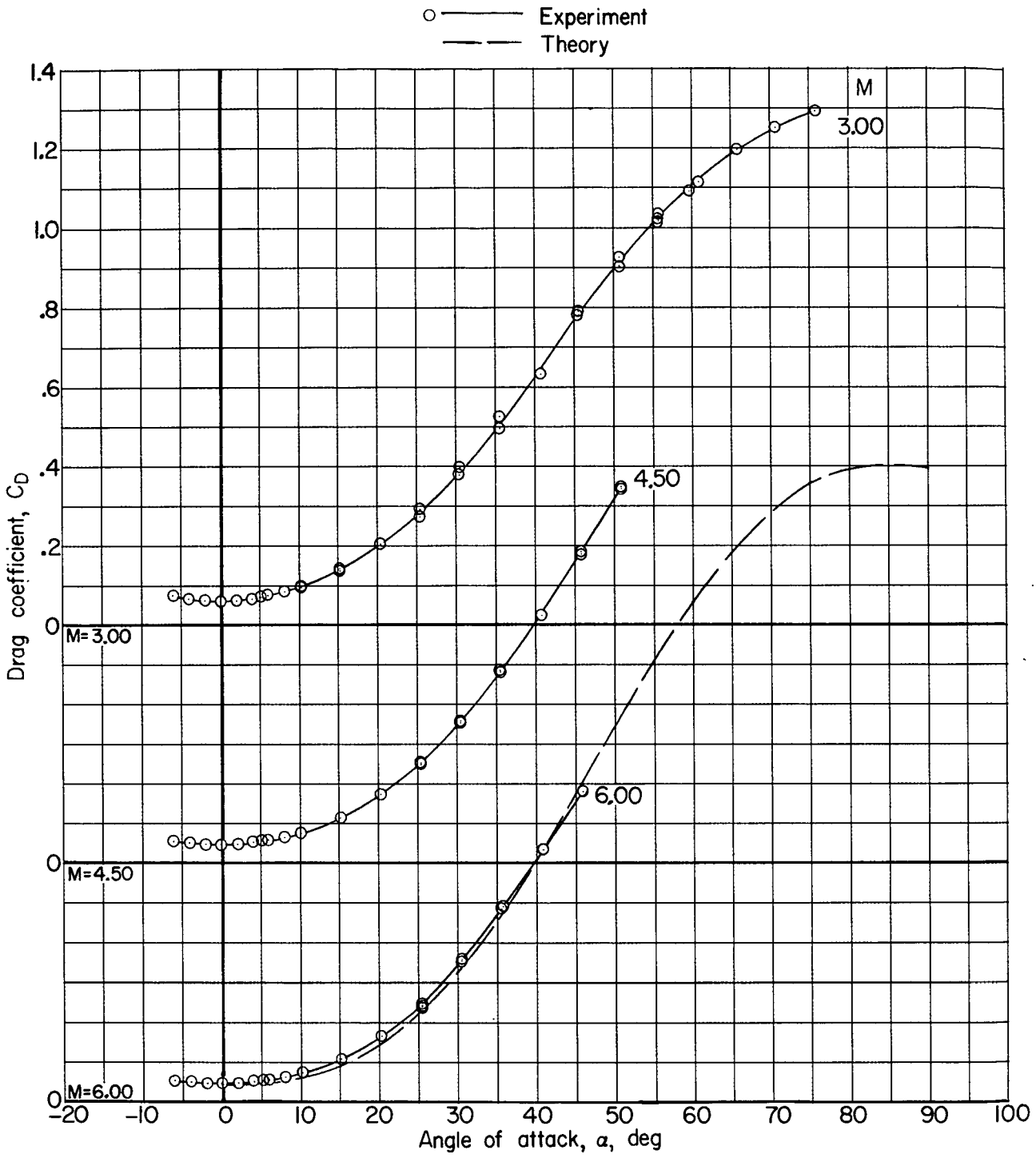

(e) Drag.

Figure 5.- Continued.

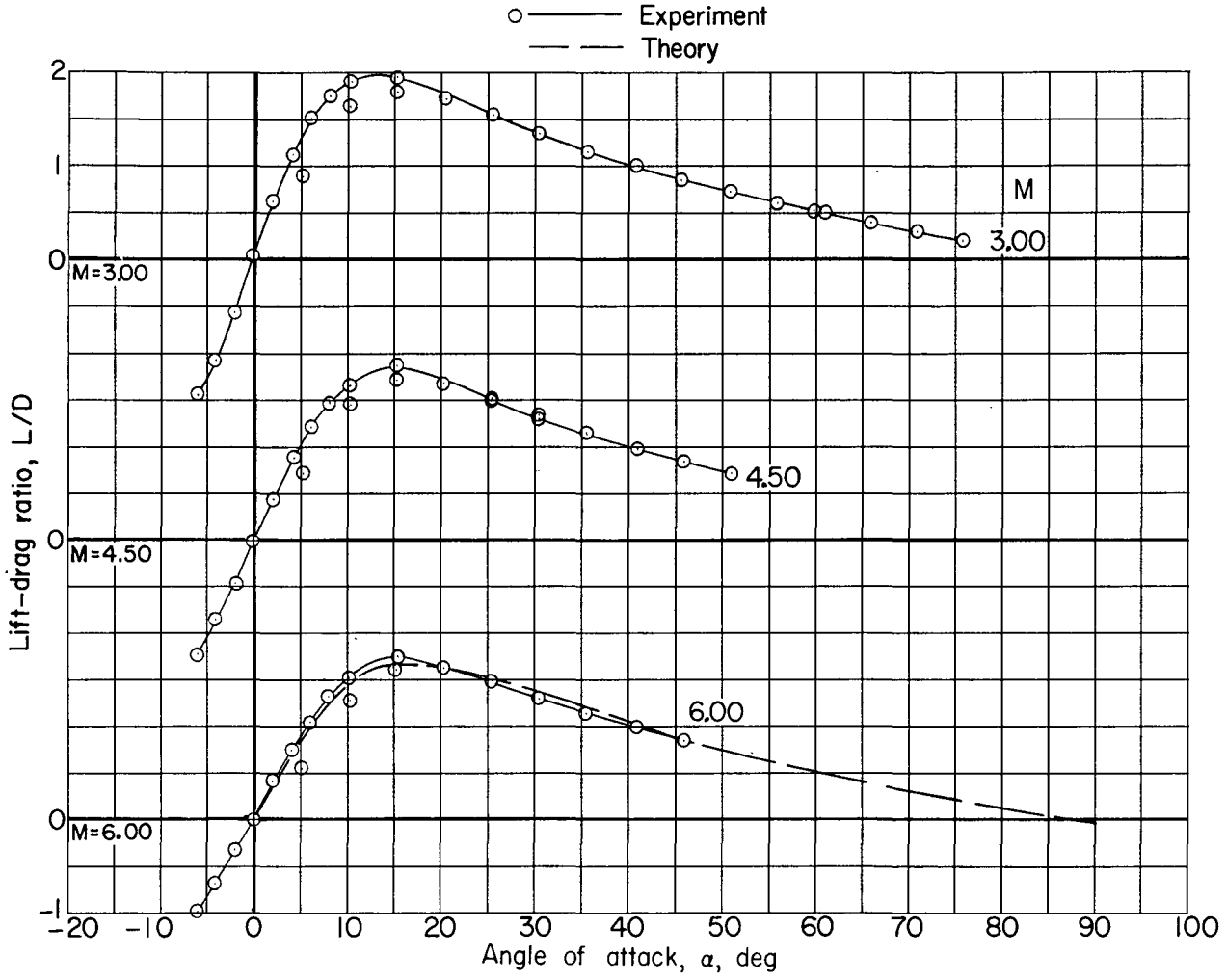

(f) Lift-drag ratio.

Figure 5.- Concluded.

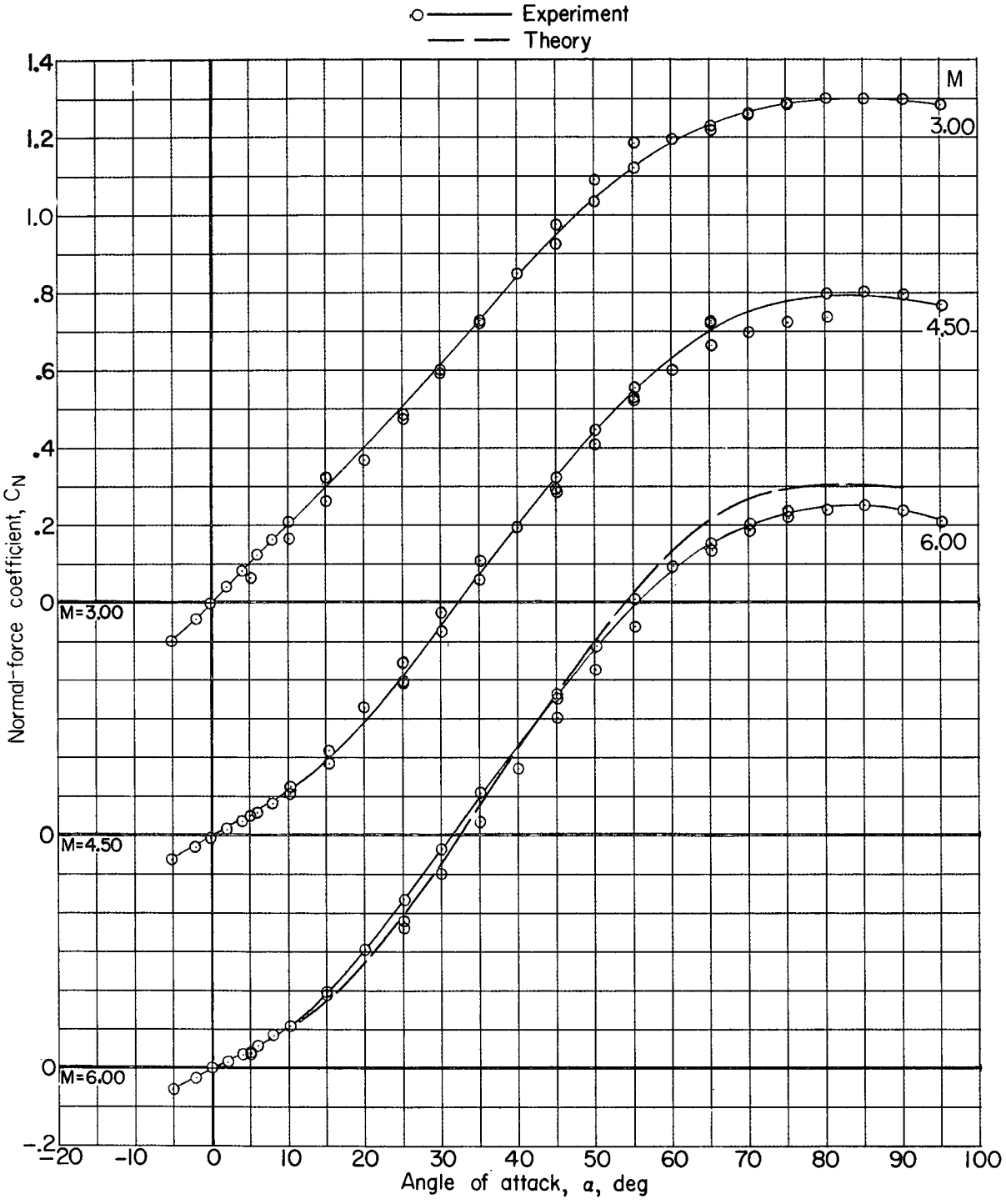

(a) Normal force.

Figure 6.- Longitudinal aerodynamic characteristics of model 2.

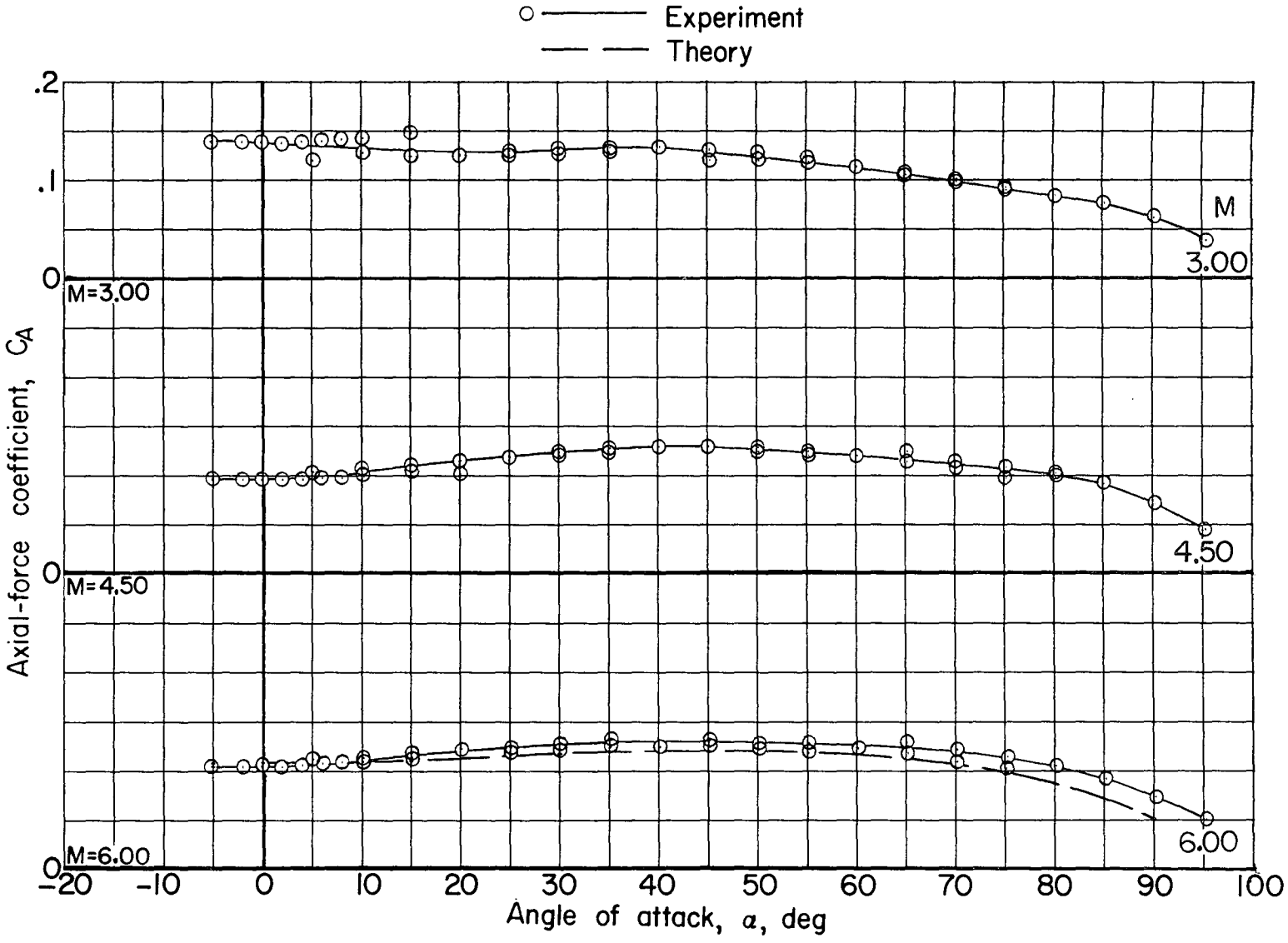

(b) Axial force.

Figure 6.- Continued.

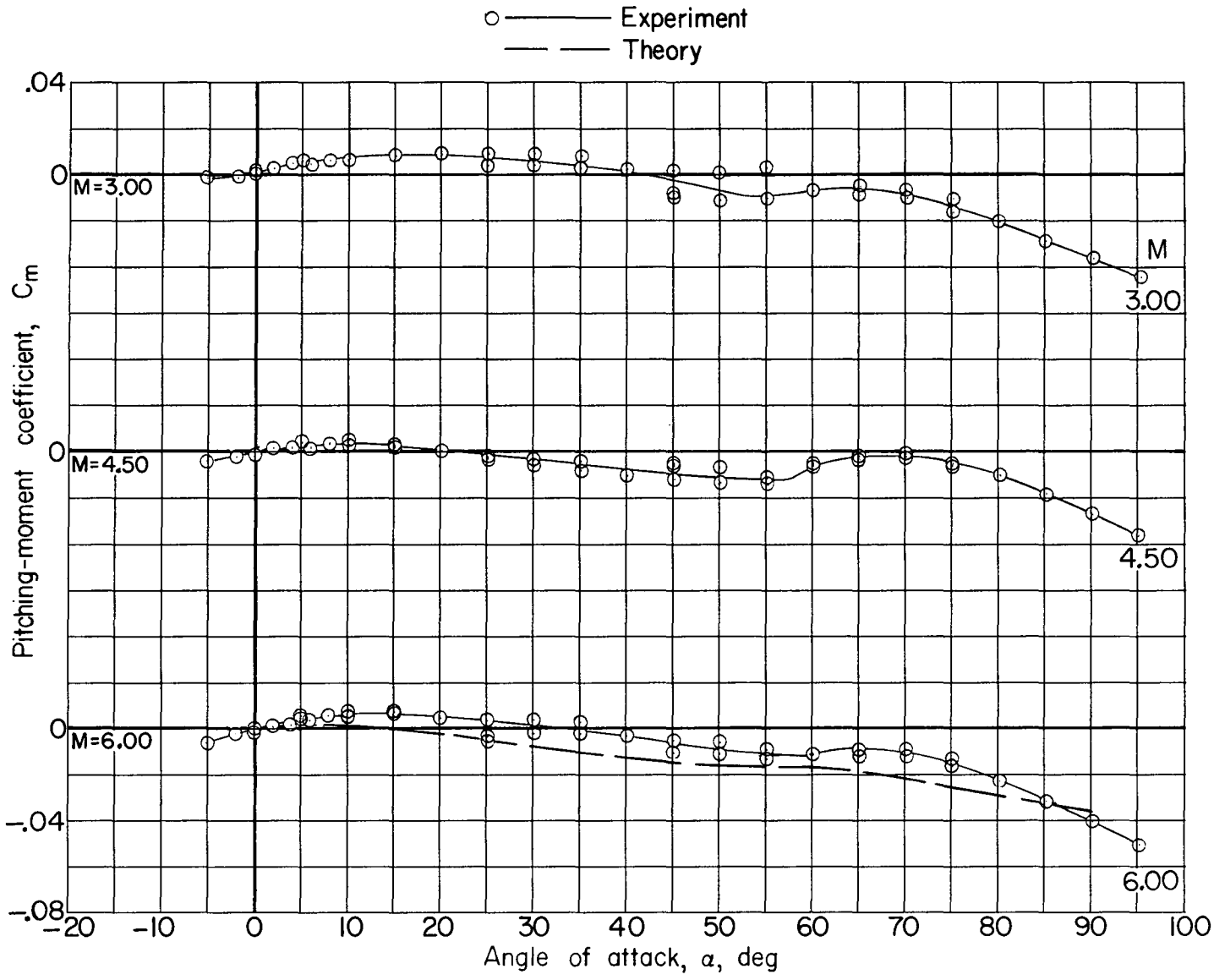

(c) Pitching moment.

Figure 6.- Continued.

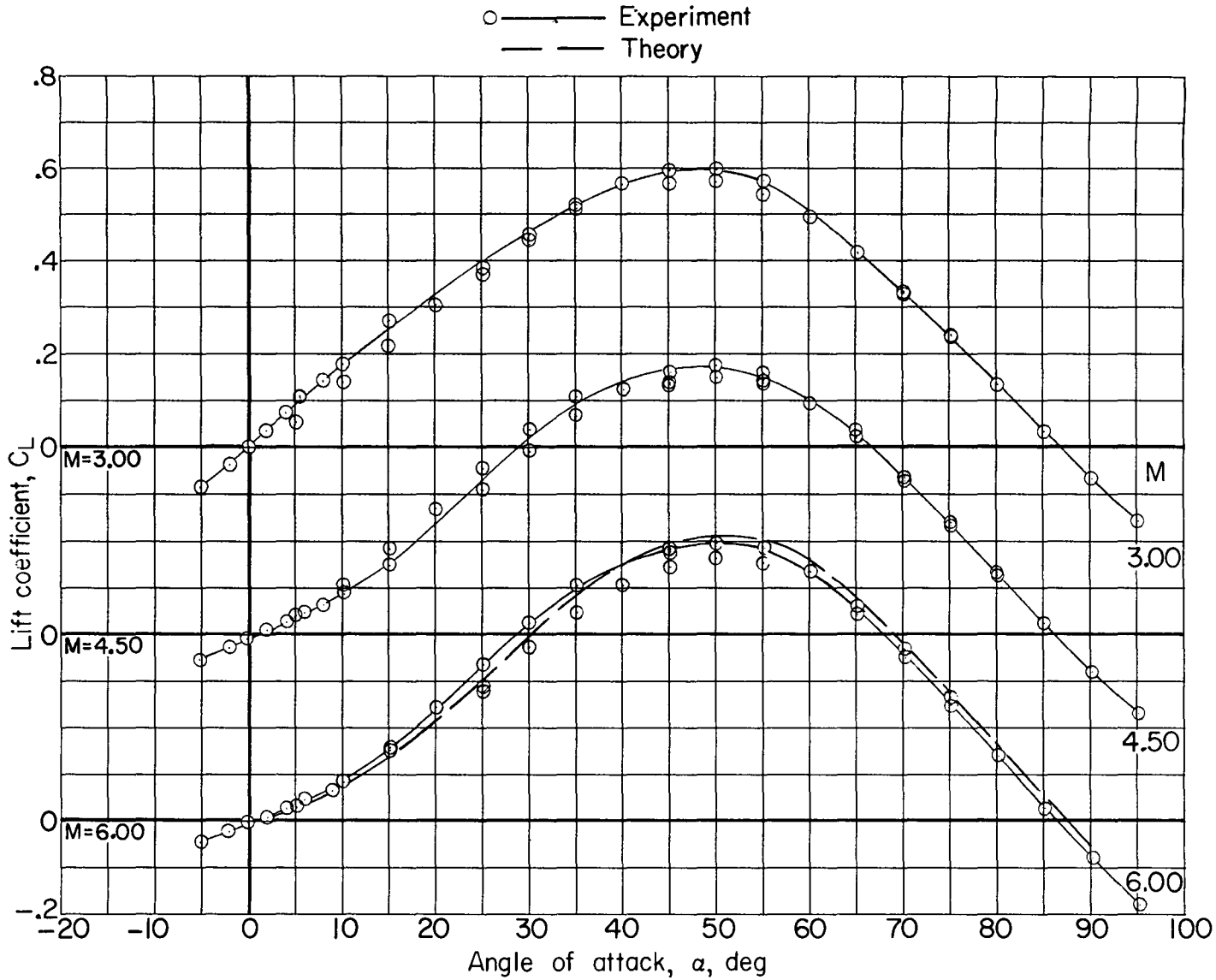

(d) Lift.

Figure 6.- Continued.

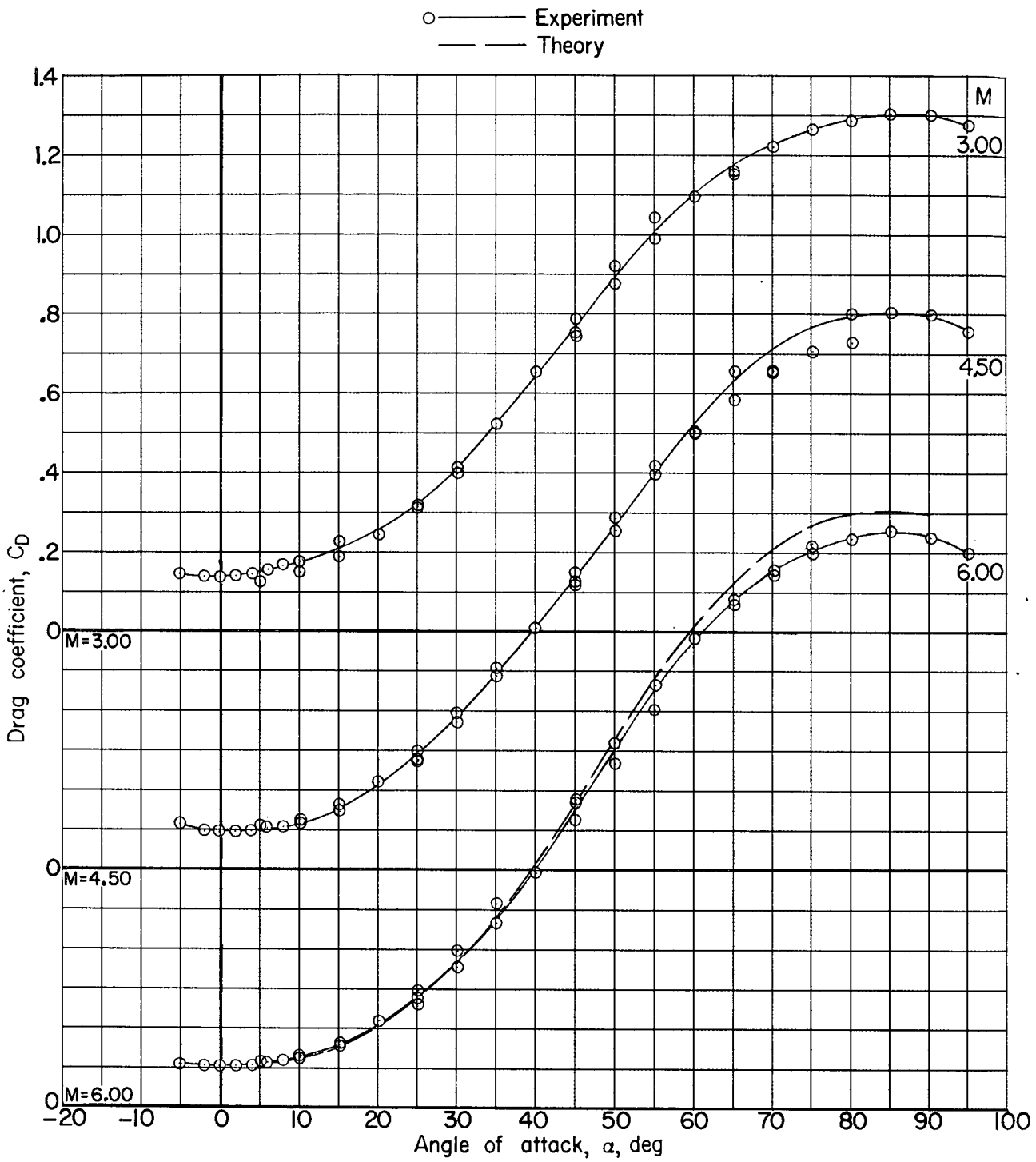

(e) Drag.

Figure 6.- Continued.

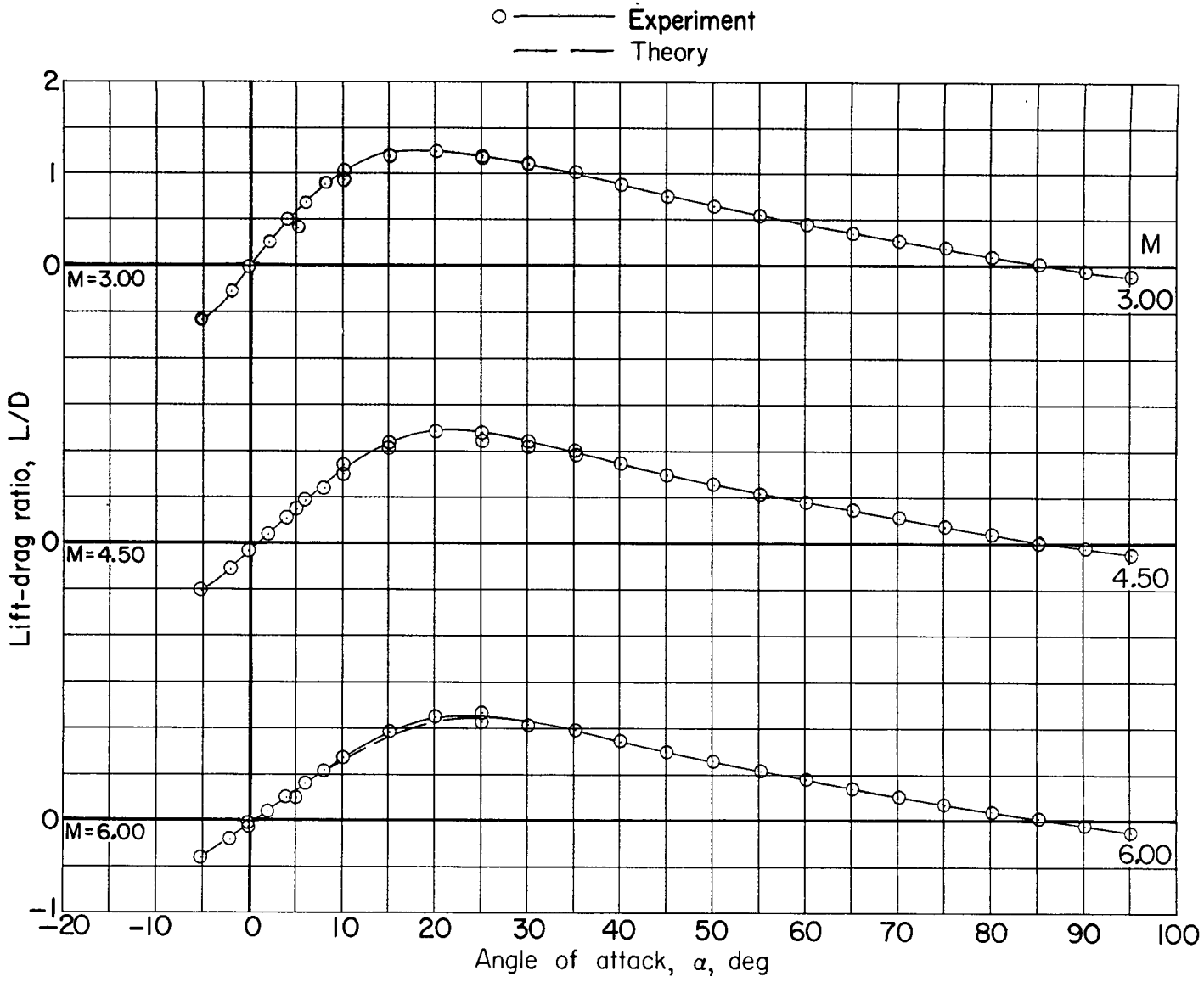

(f) Lift-drag ratio.

Figure 6.- Concluded.

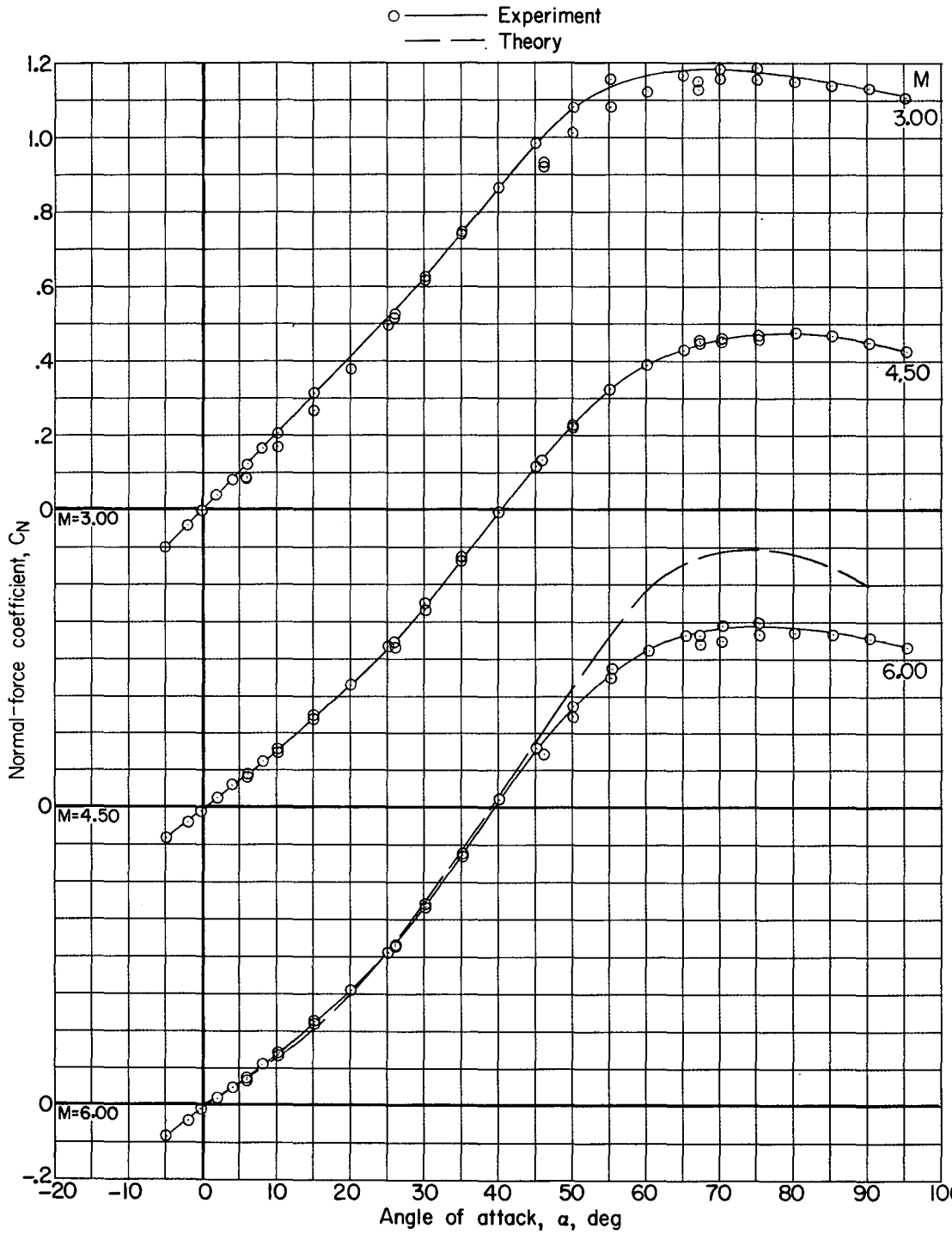

(a) Normal force.

Figure 7.- Longitudinal aerodynamic characteristics of model 3.

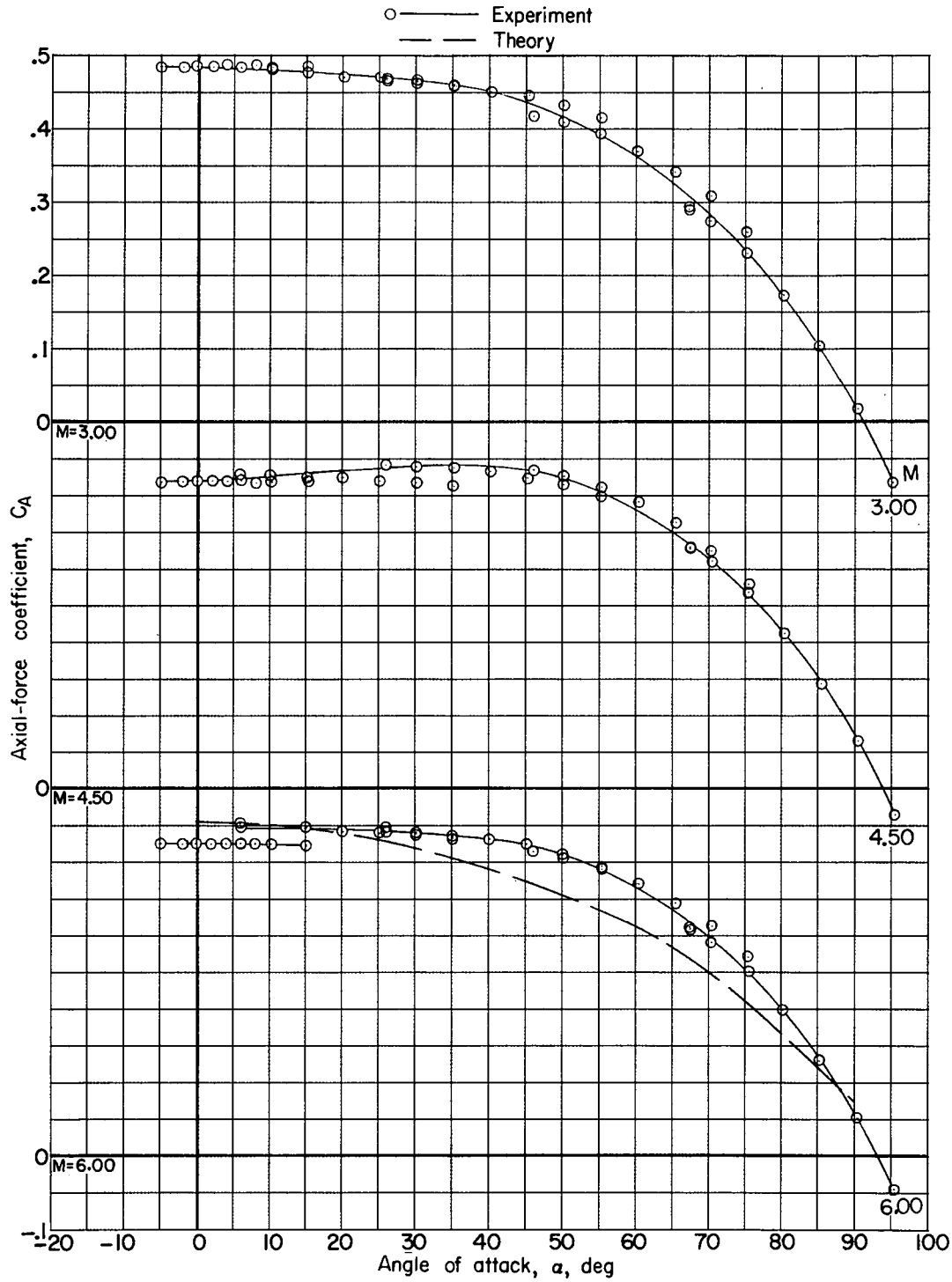

(b) Axial force.

Figure 7.- Continued.

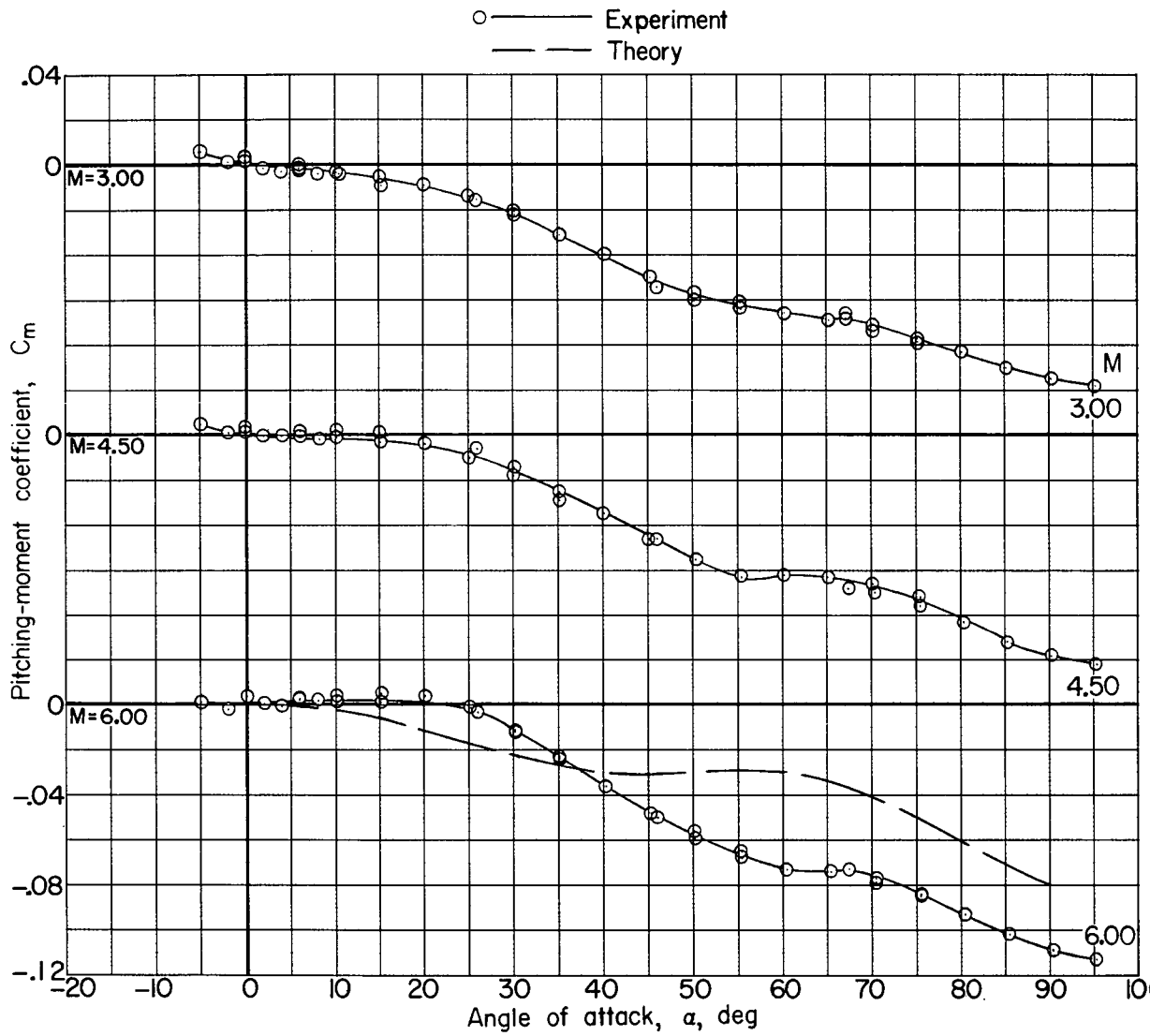

(c) Pitching moment.

Figure 7.- Continued.

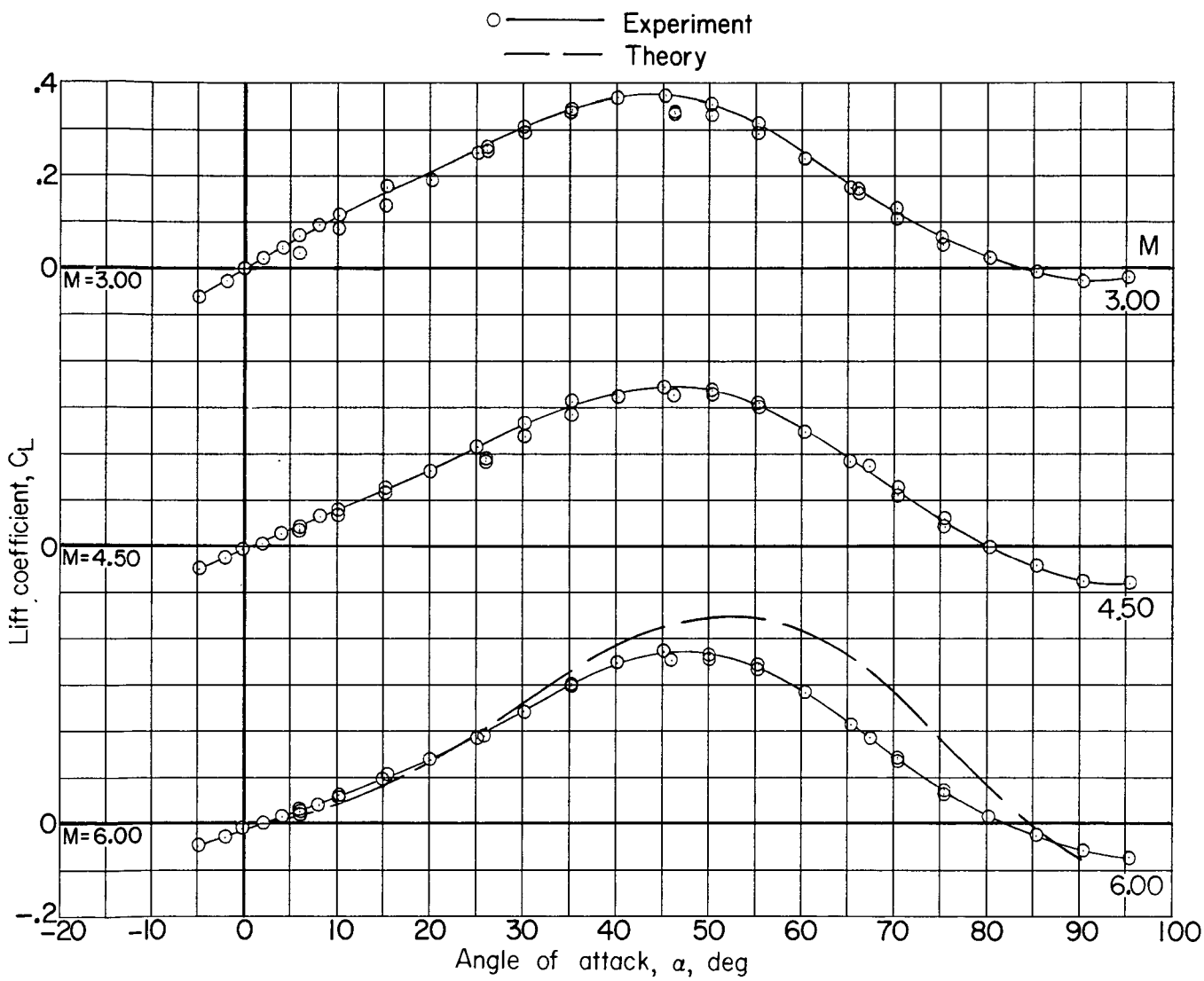

(d) Lift.

Figure 7.- Continued.

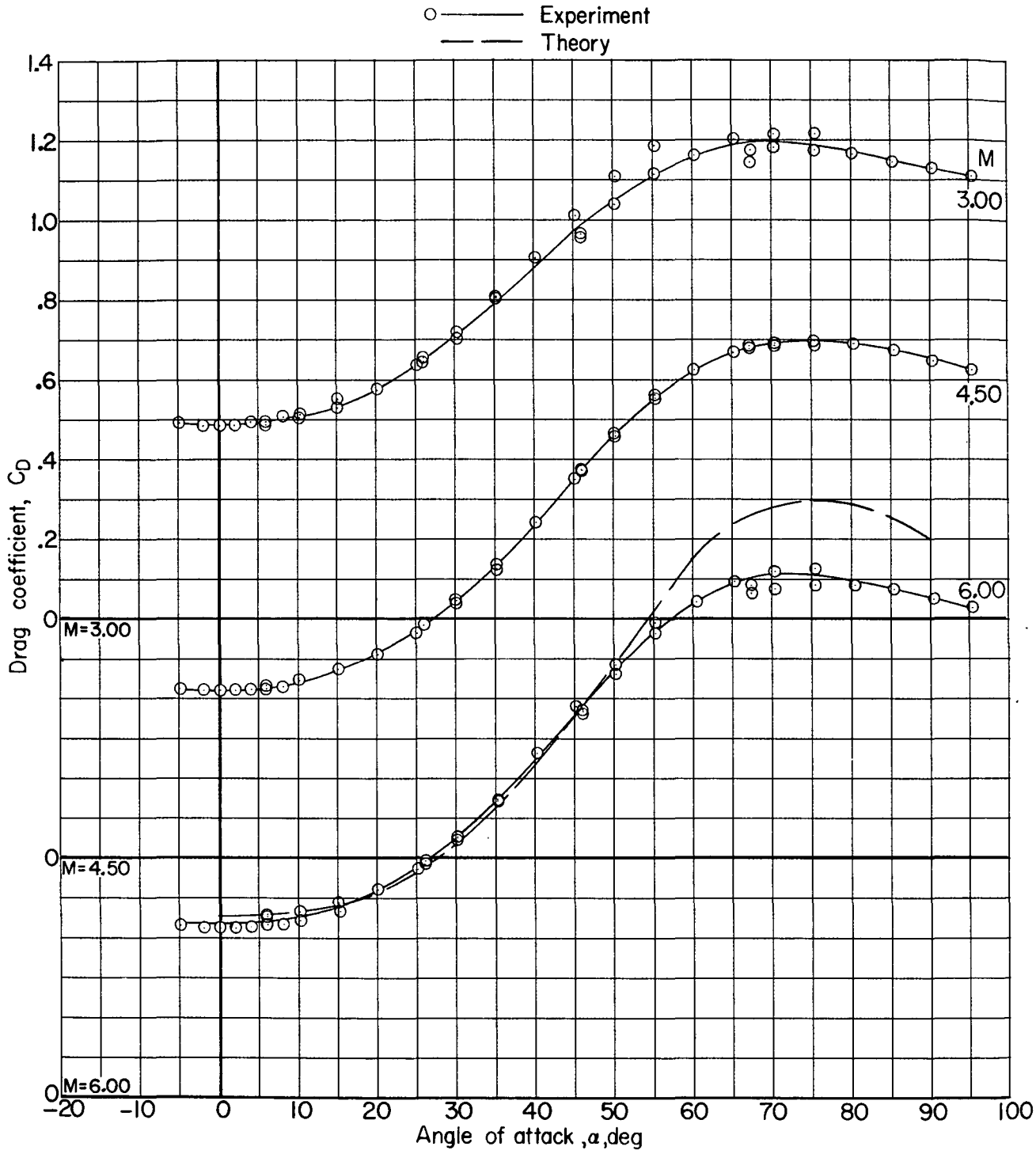

(e) Drag.

Figure 7.- Continued.

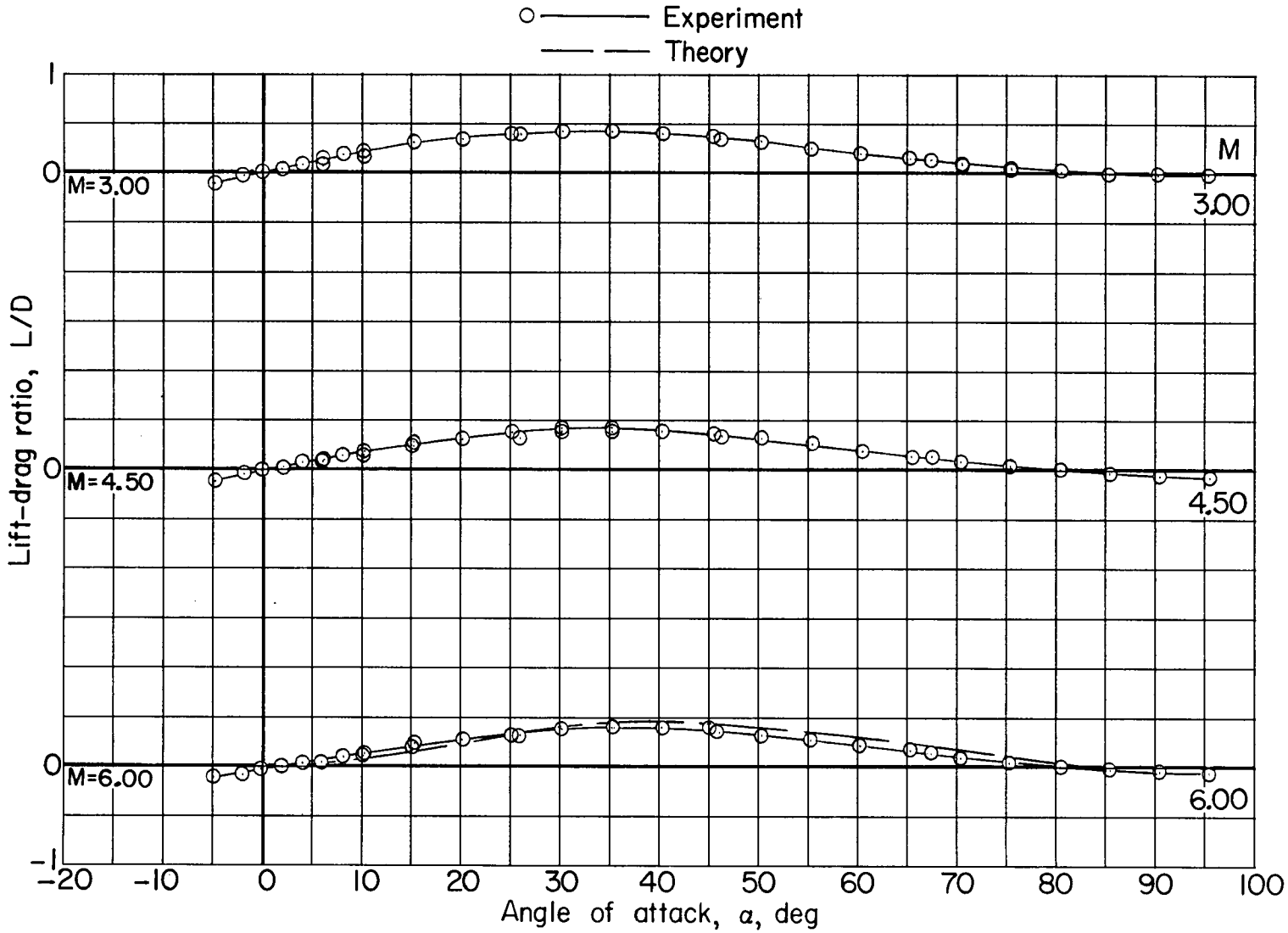

(f) Lift-drag ratio.

Figure 7.- Concluded.

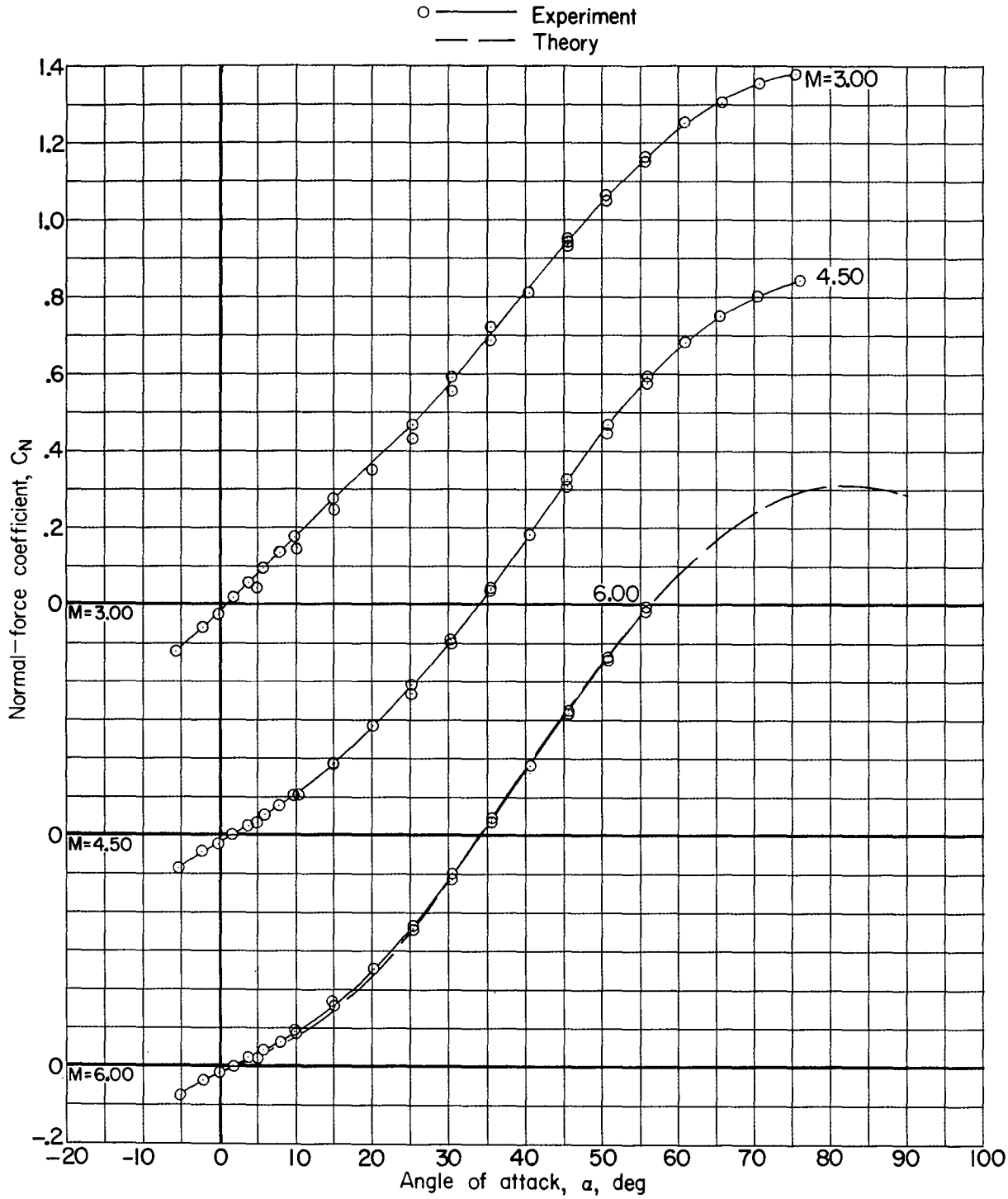

(a) Normal force.

Figure 8.- Longitudinal aerodynamic characteristics of model 4.

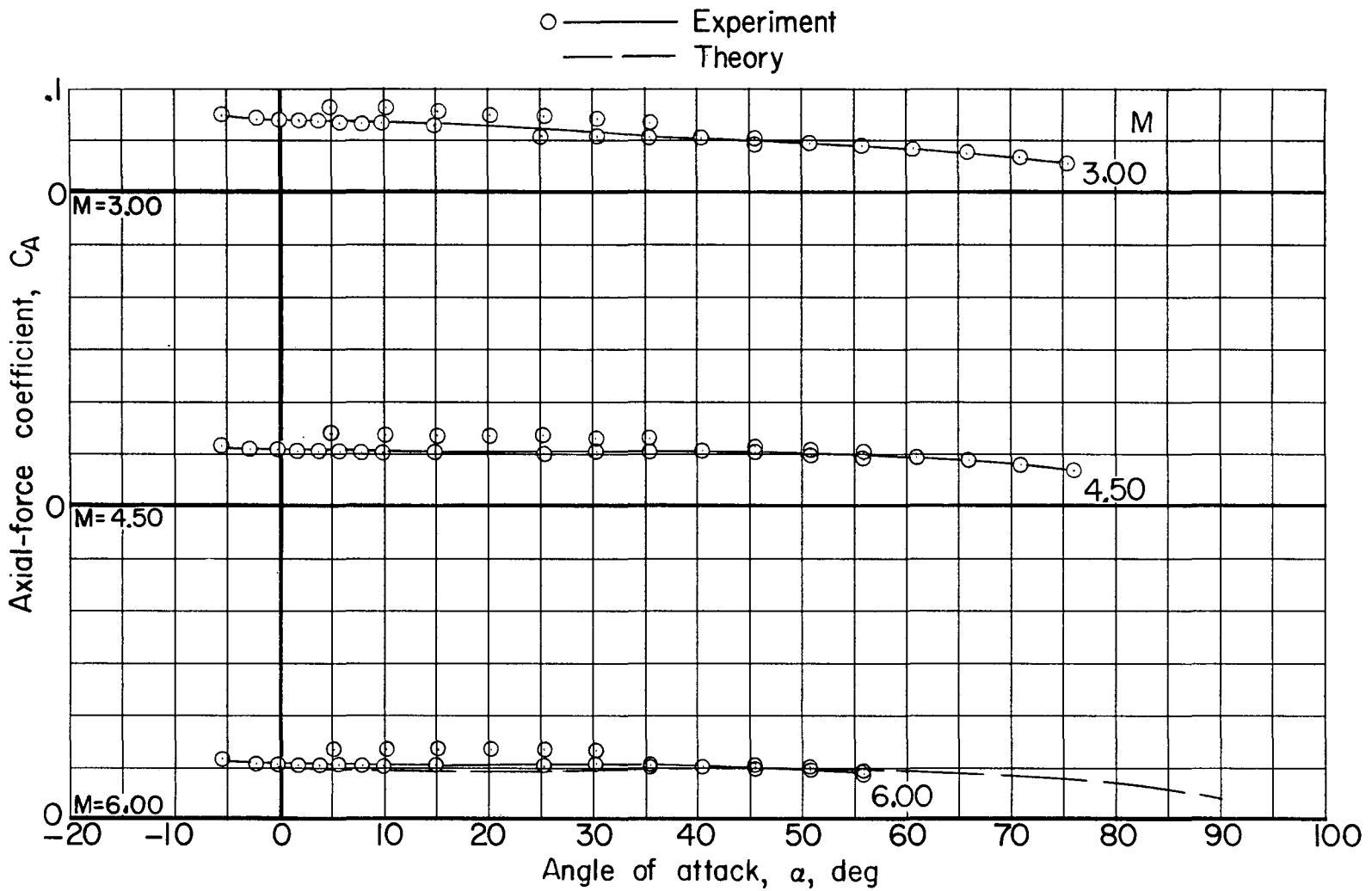

(b) Axial force.

Figure 8.- Continued.

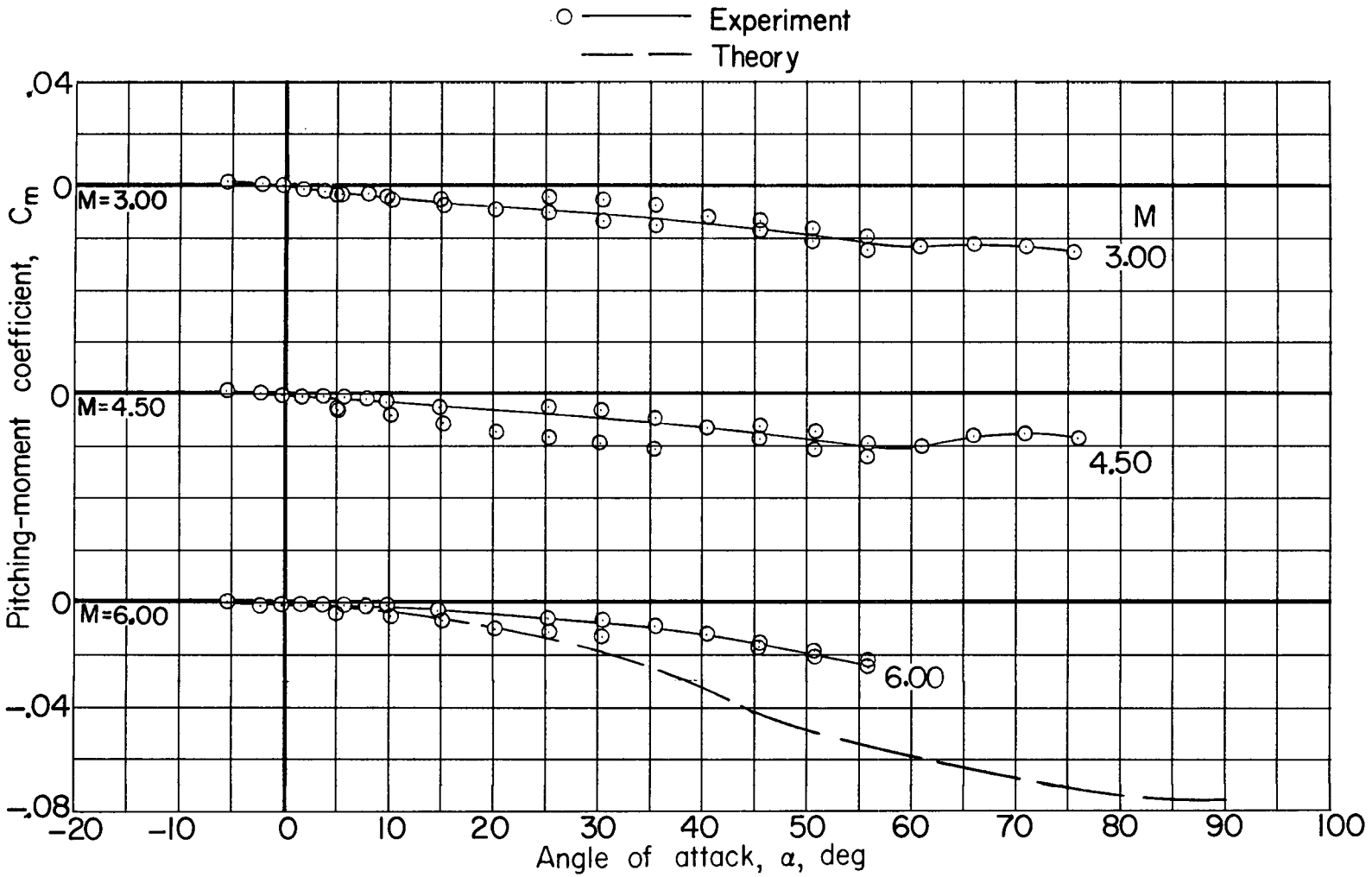

(c) Pitching moment.

Figure 8.- Continued.

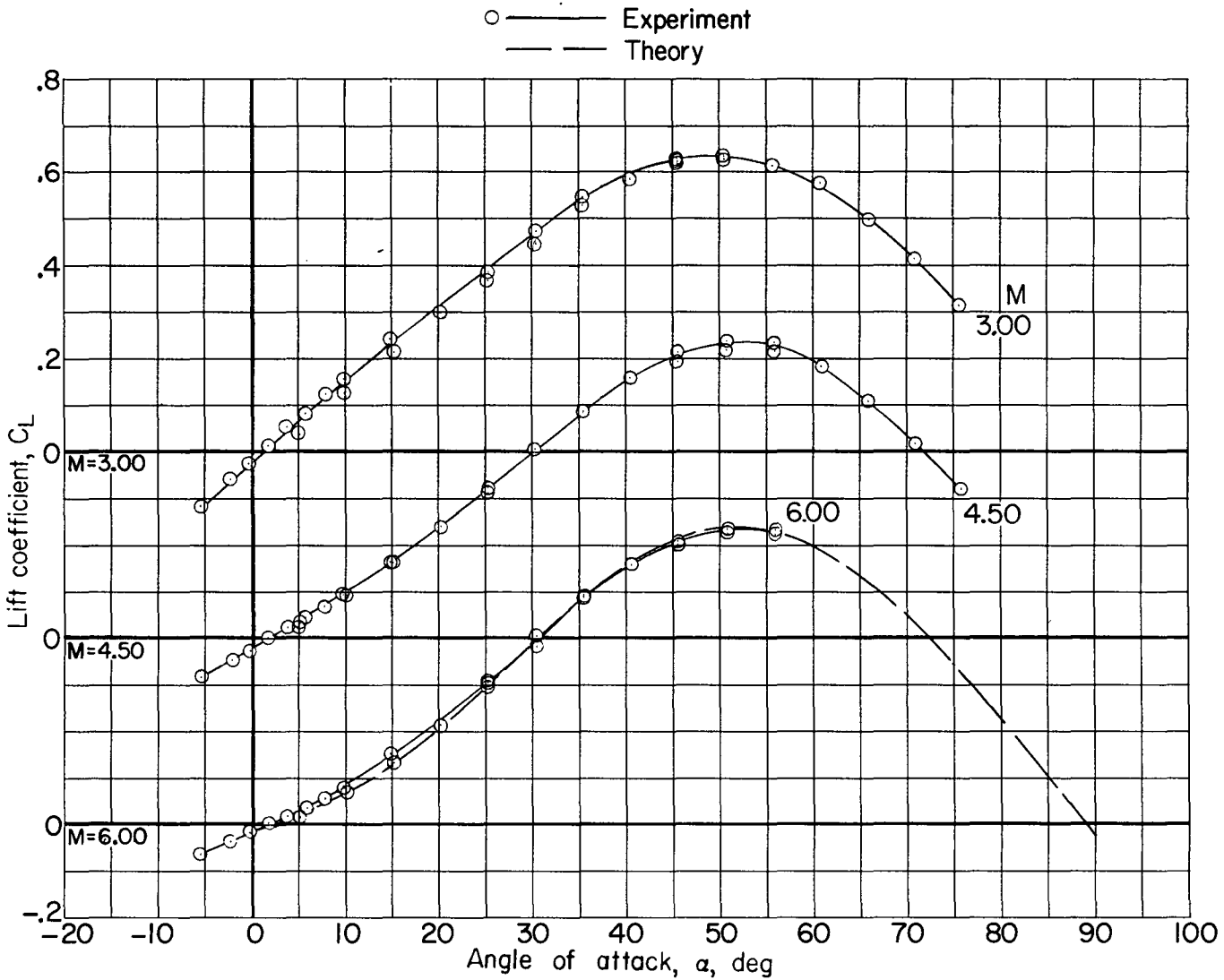

(d) Lift.

Figure 8.- Continued.

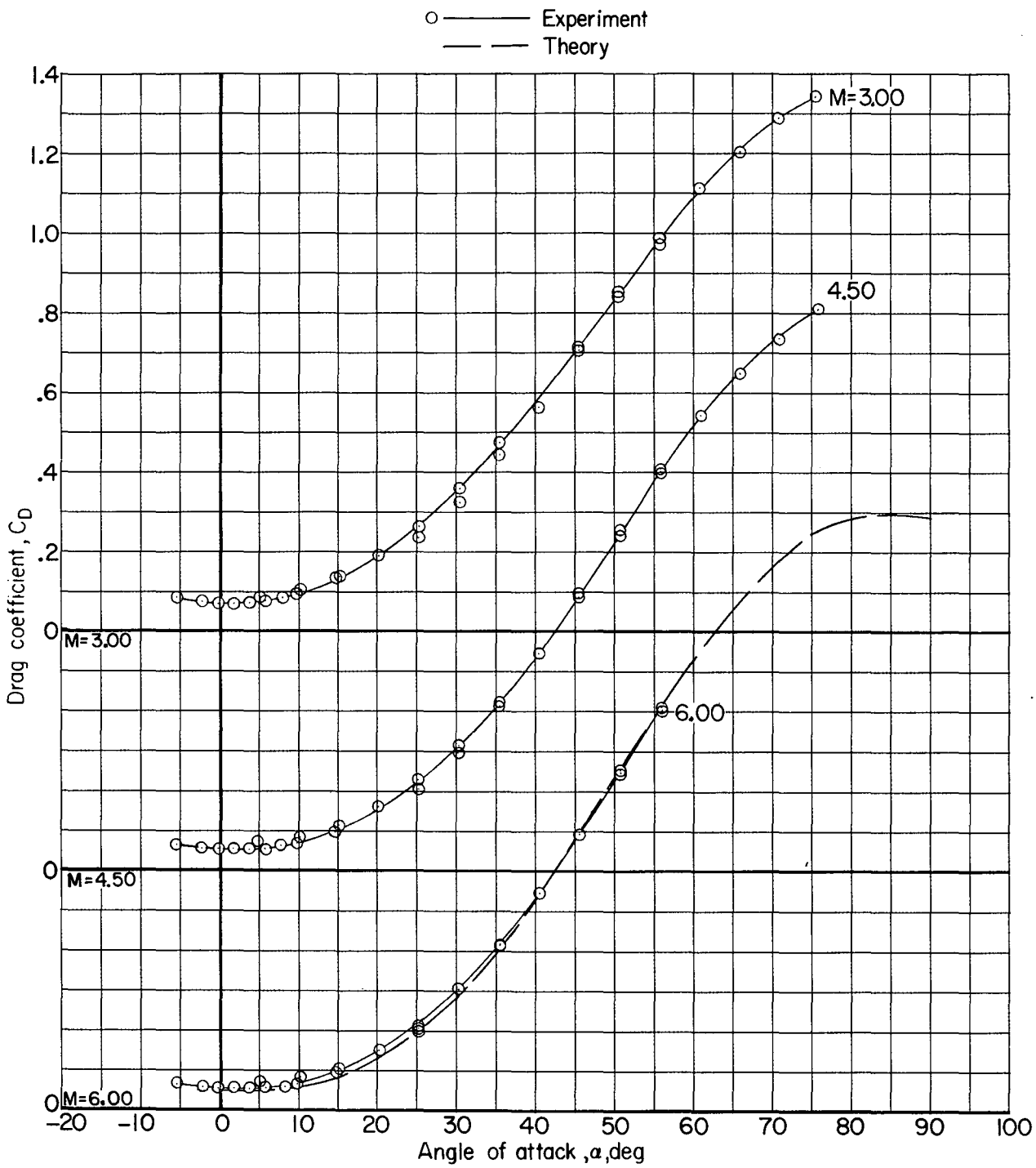

(e) Drag.

Figure 8.- Continued.

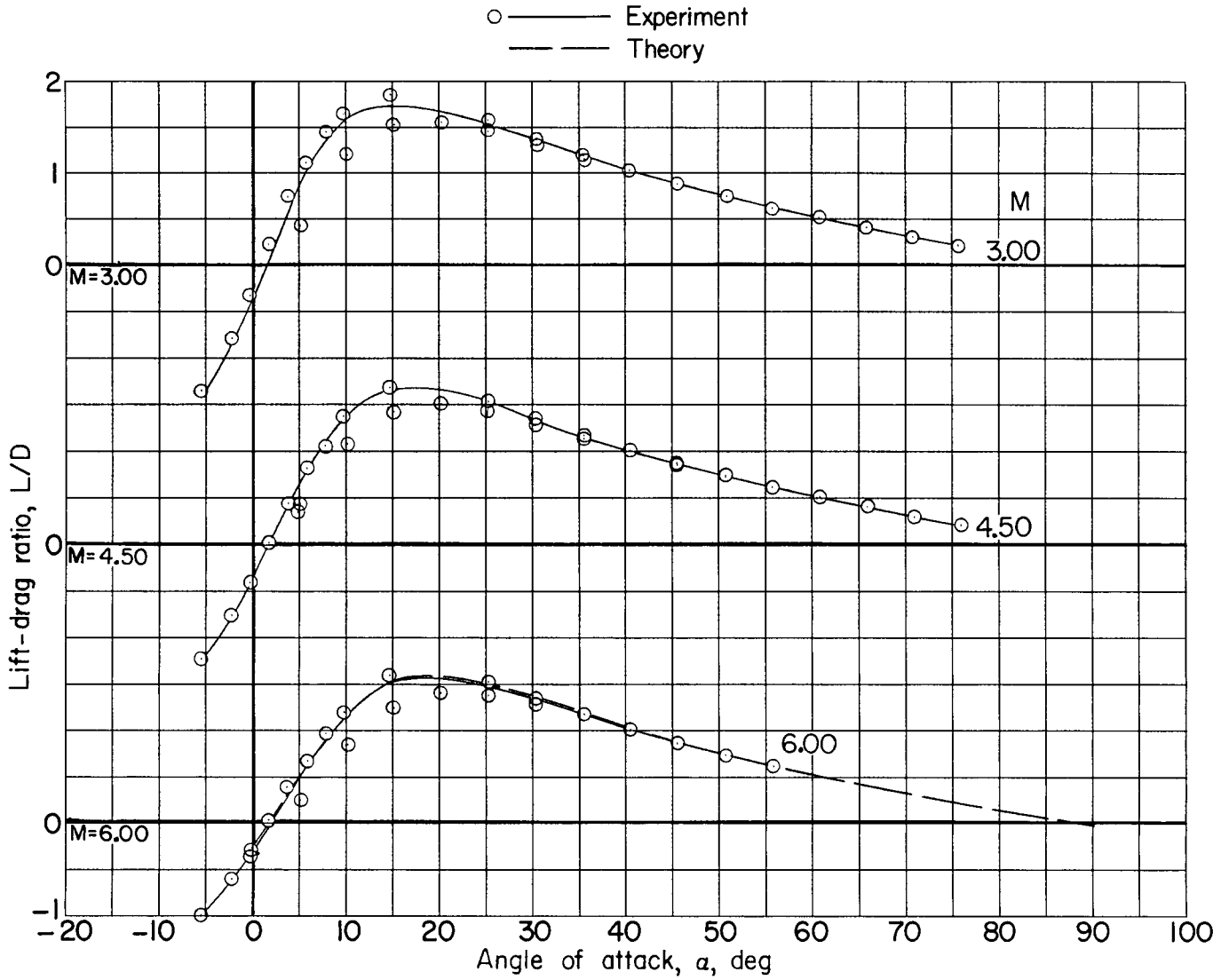

(f) Lift-drag ratio.

Figure 8.- Concluded.

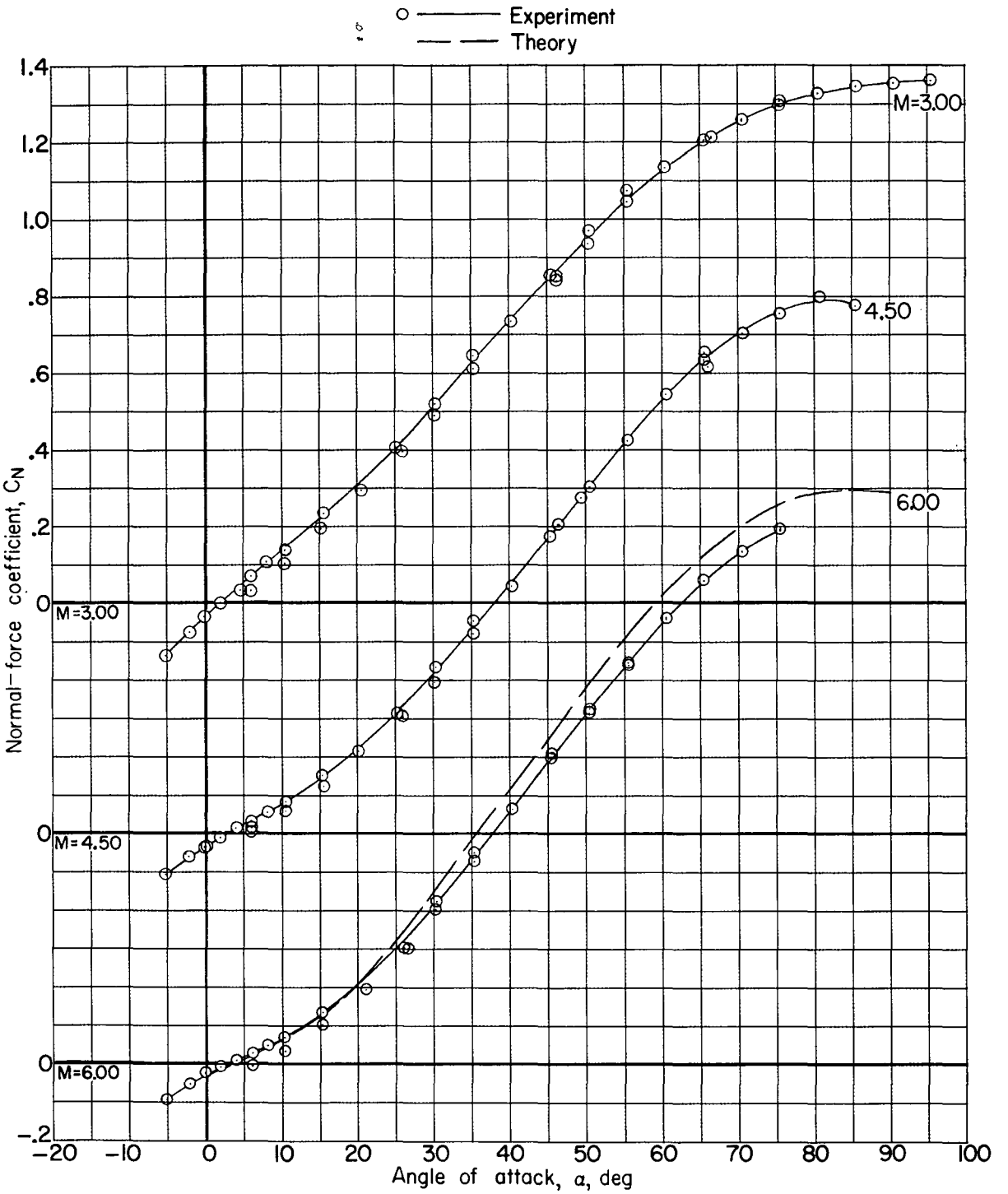

(a) Normal force.

Figure 9.- Longitudinal aerodynamic characteristics of model 5.

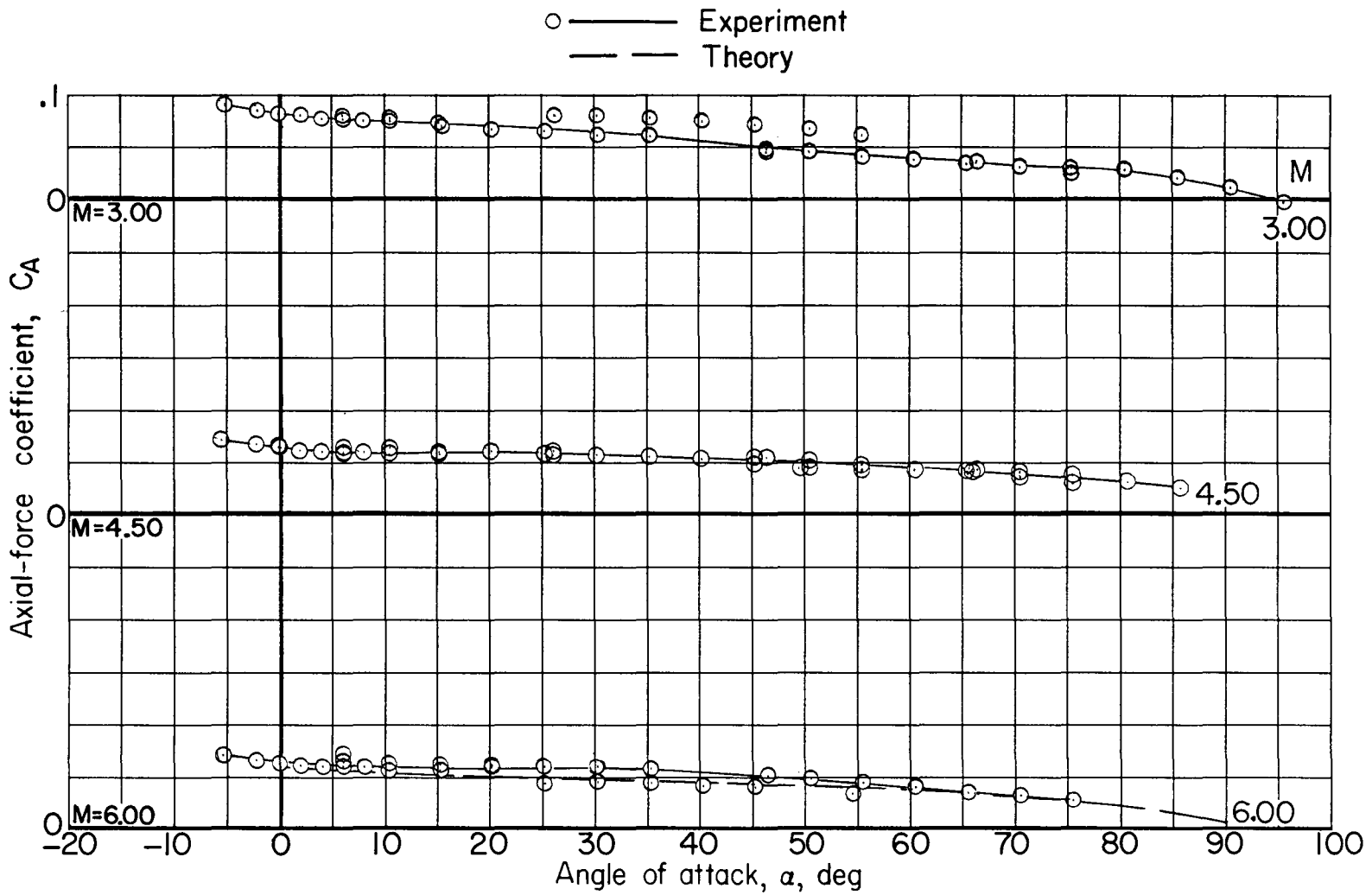

(b) Axial force.

Figure 9.- Continued.

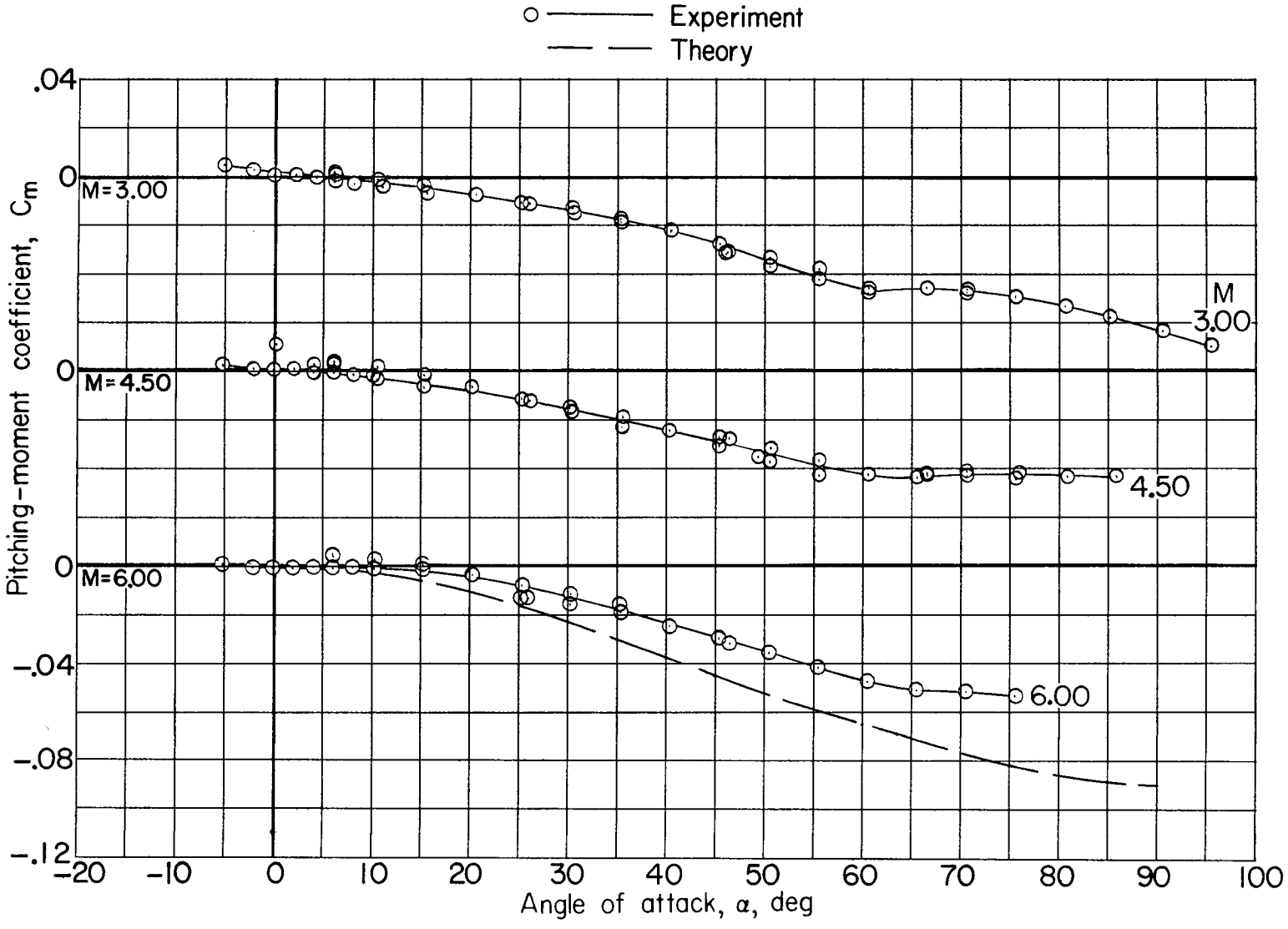

(c) Pitching moment.

Figure 9.- Continued.

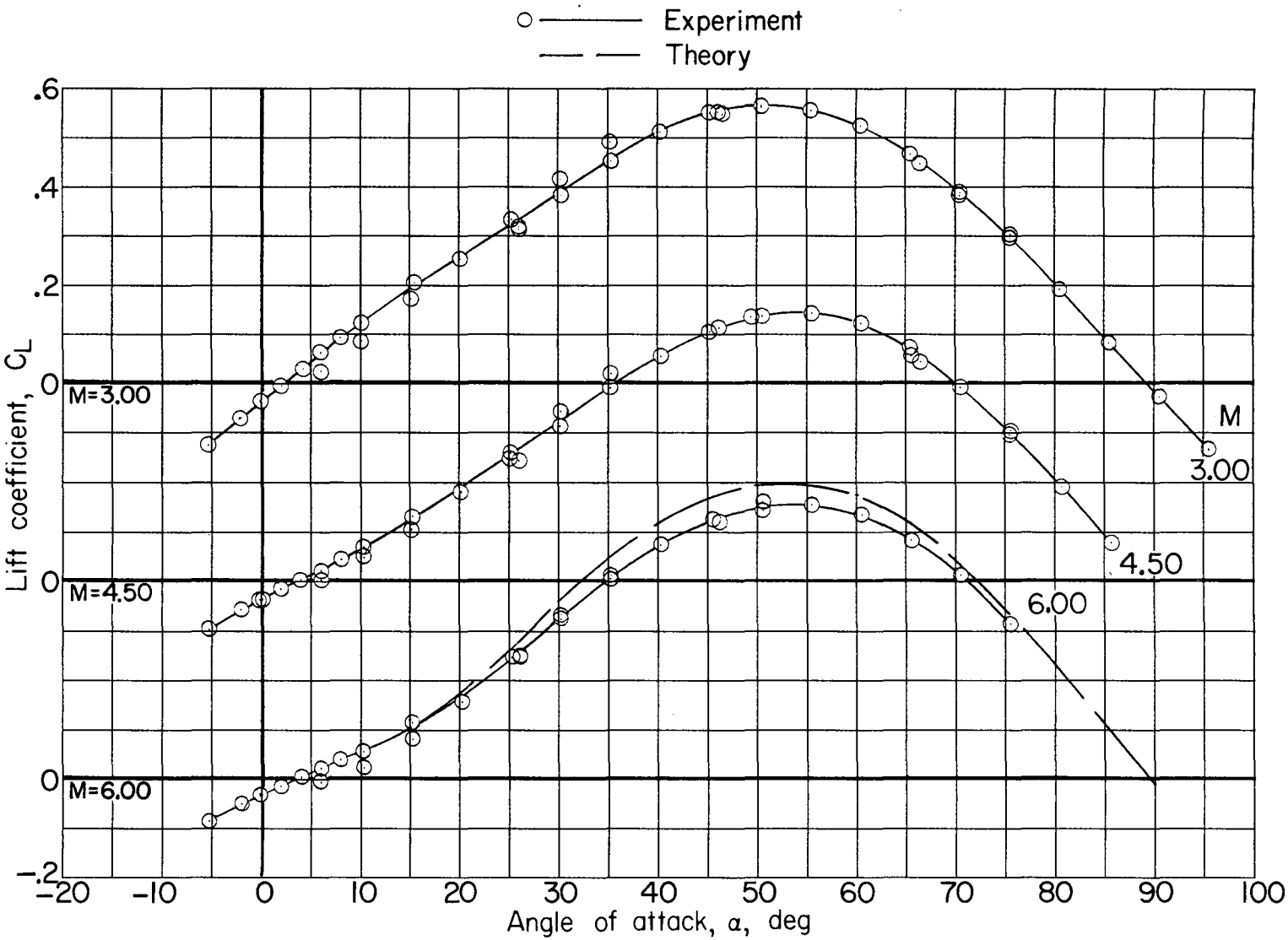

(d) Lift.

Figure 9.- Continued.

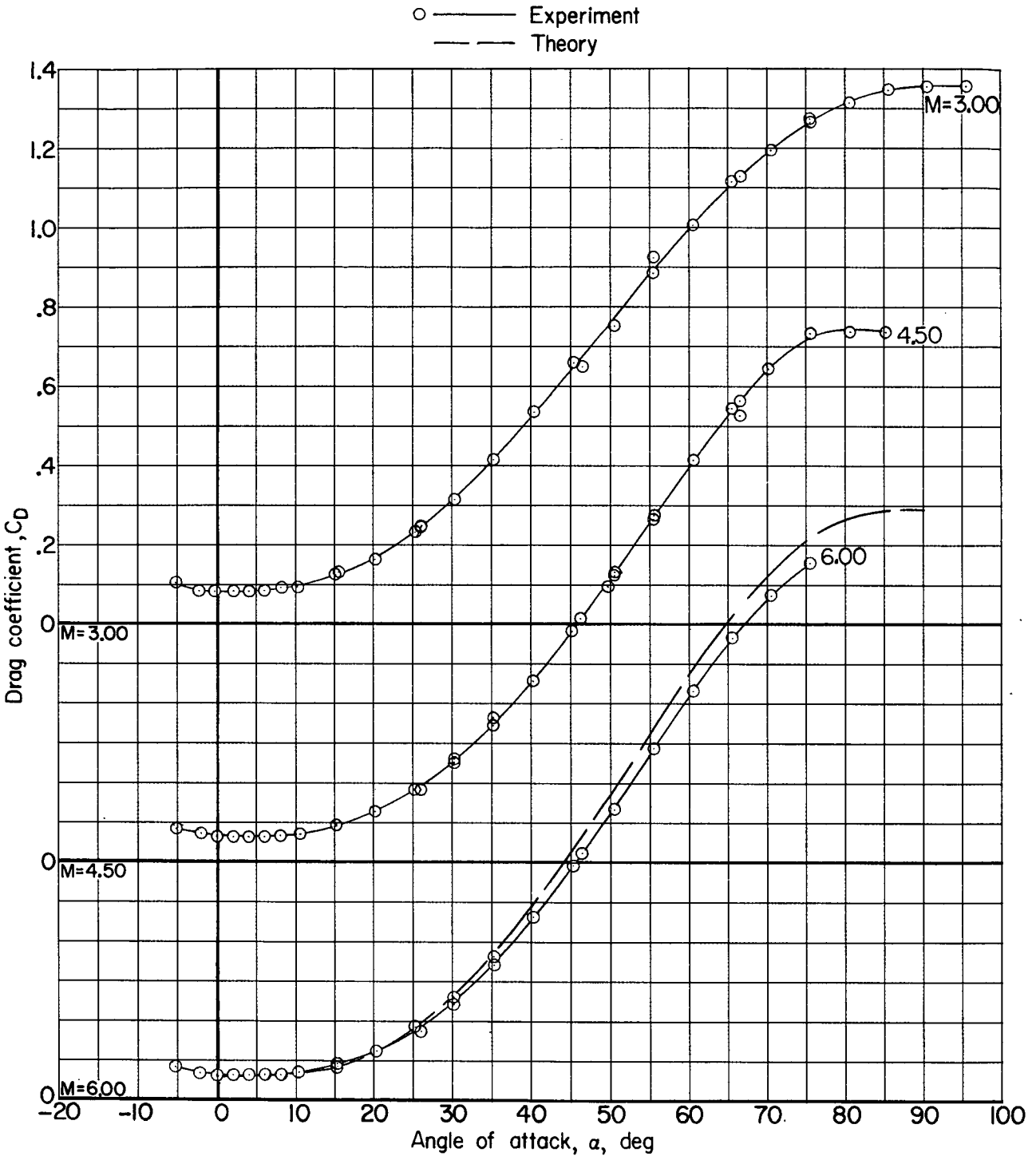

(e) Drag.

Figure 9.- Continued.

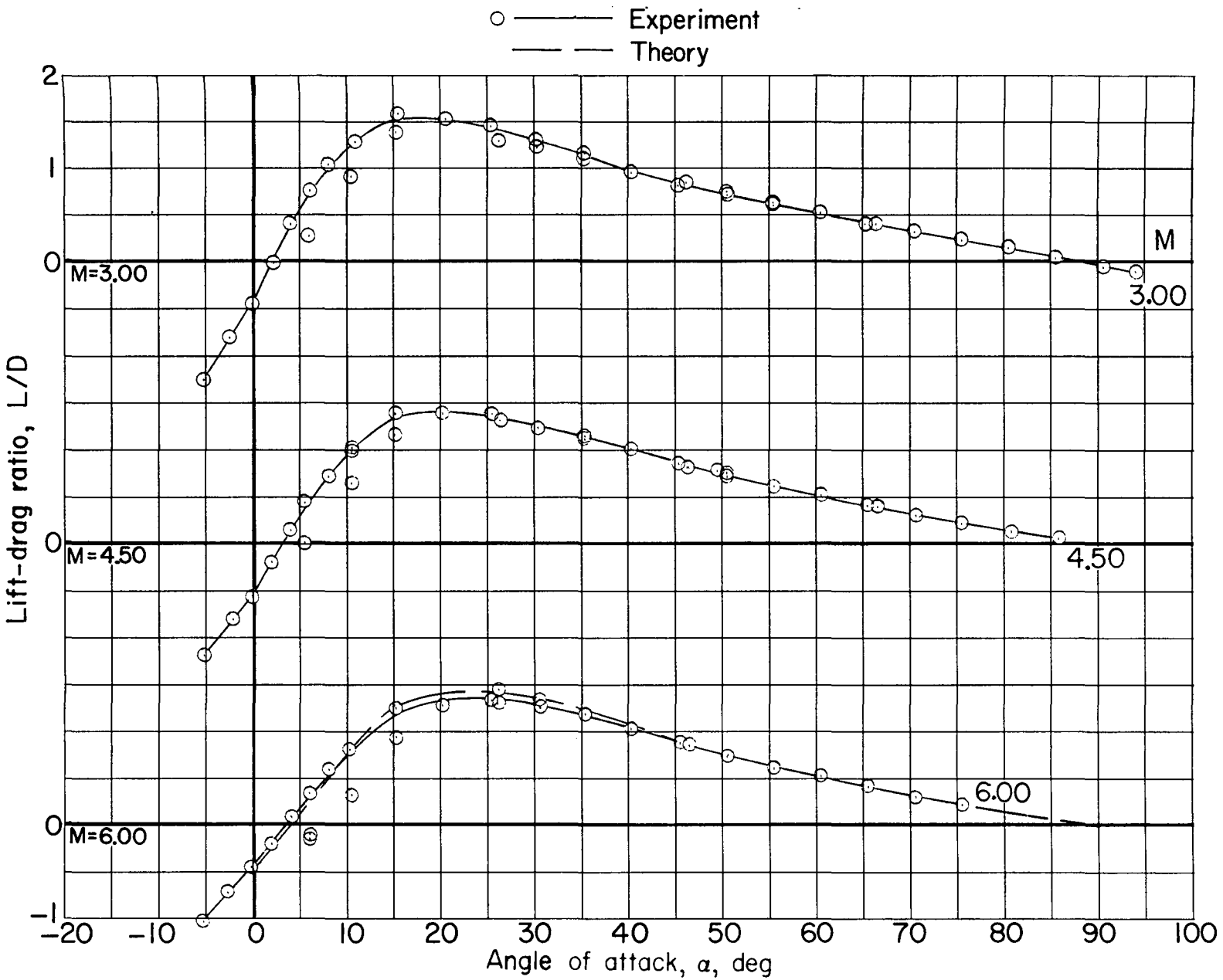

(f) Lift-drag ratio.

Figure 9.- Concluded.

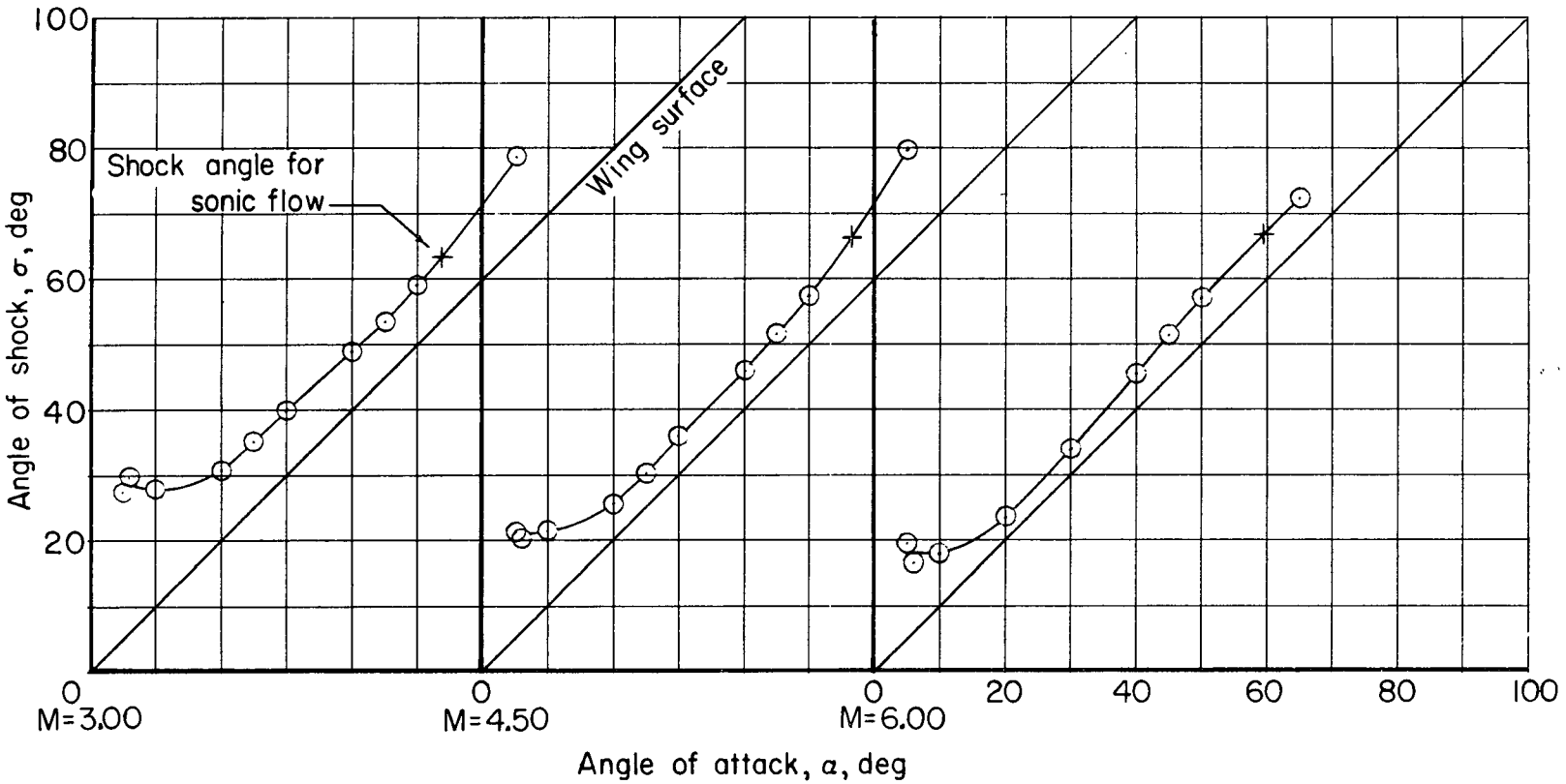

Figure 10.- Variation of the shock angle with angle of attack for model 2.

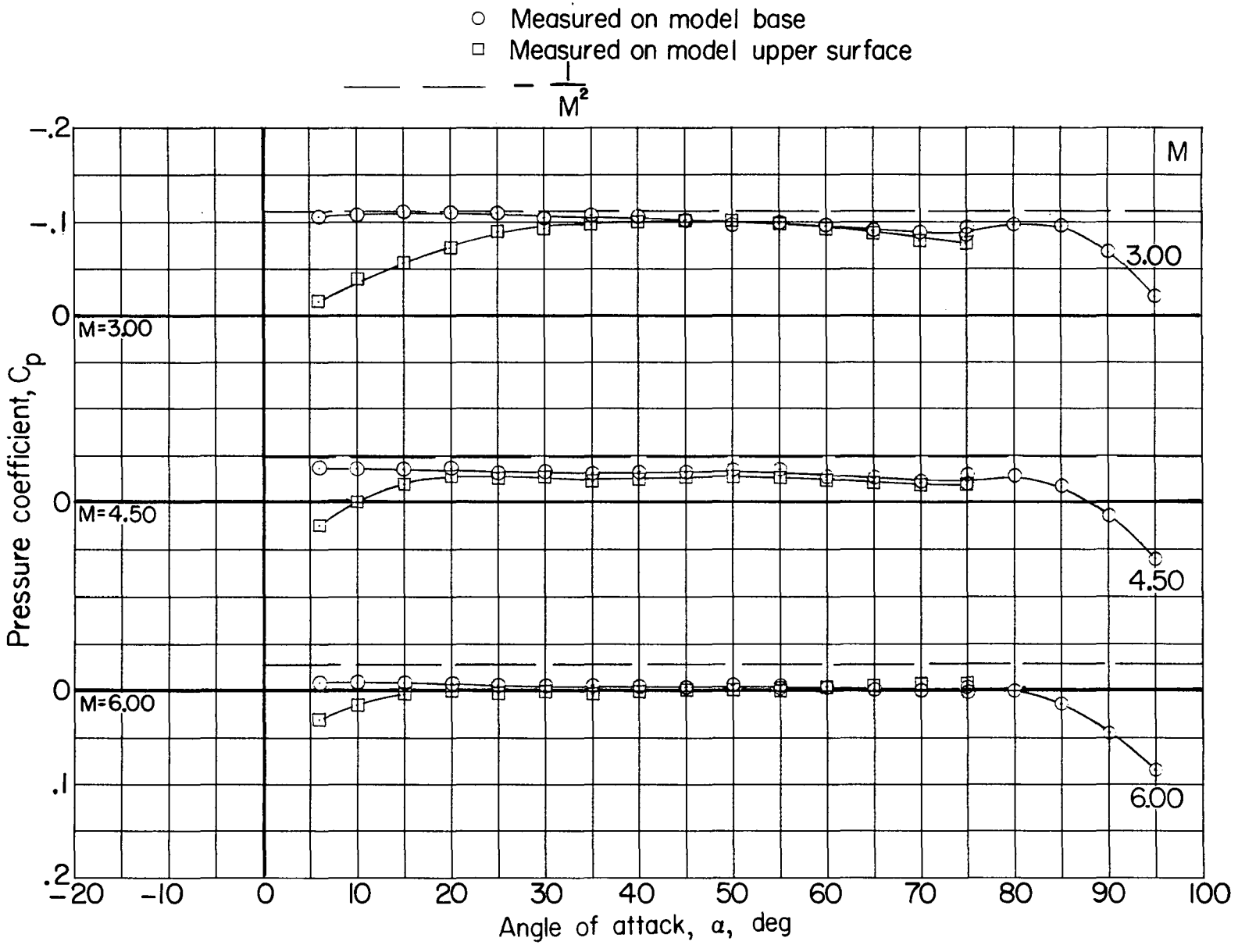

Figure 11.- Measured pressure coefficients at the base and upper surface of model 2.

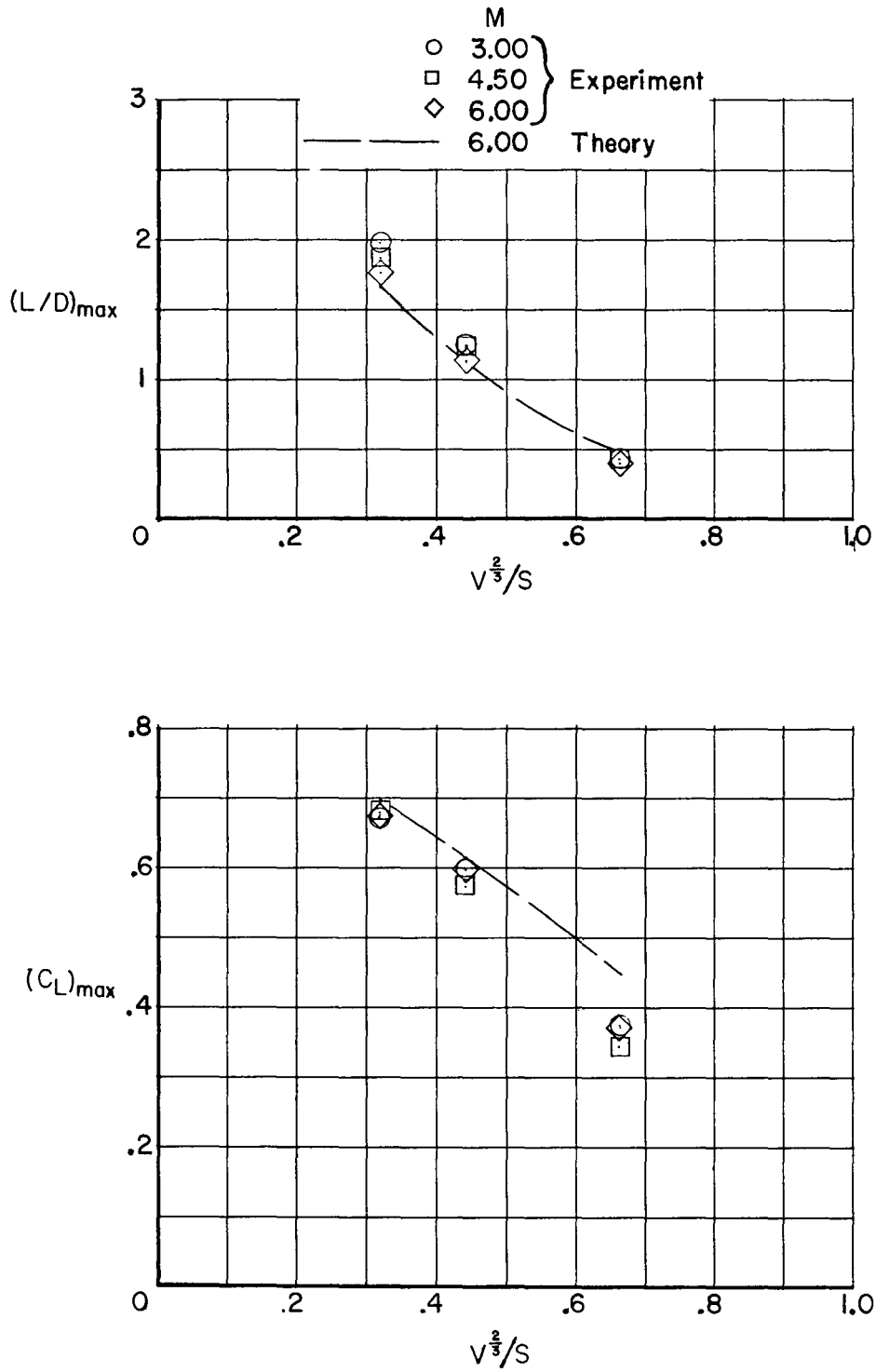

Figure 12.- The effect of the volume parameter on the aerodynamic performance of a thick-slab delta wing.

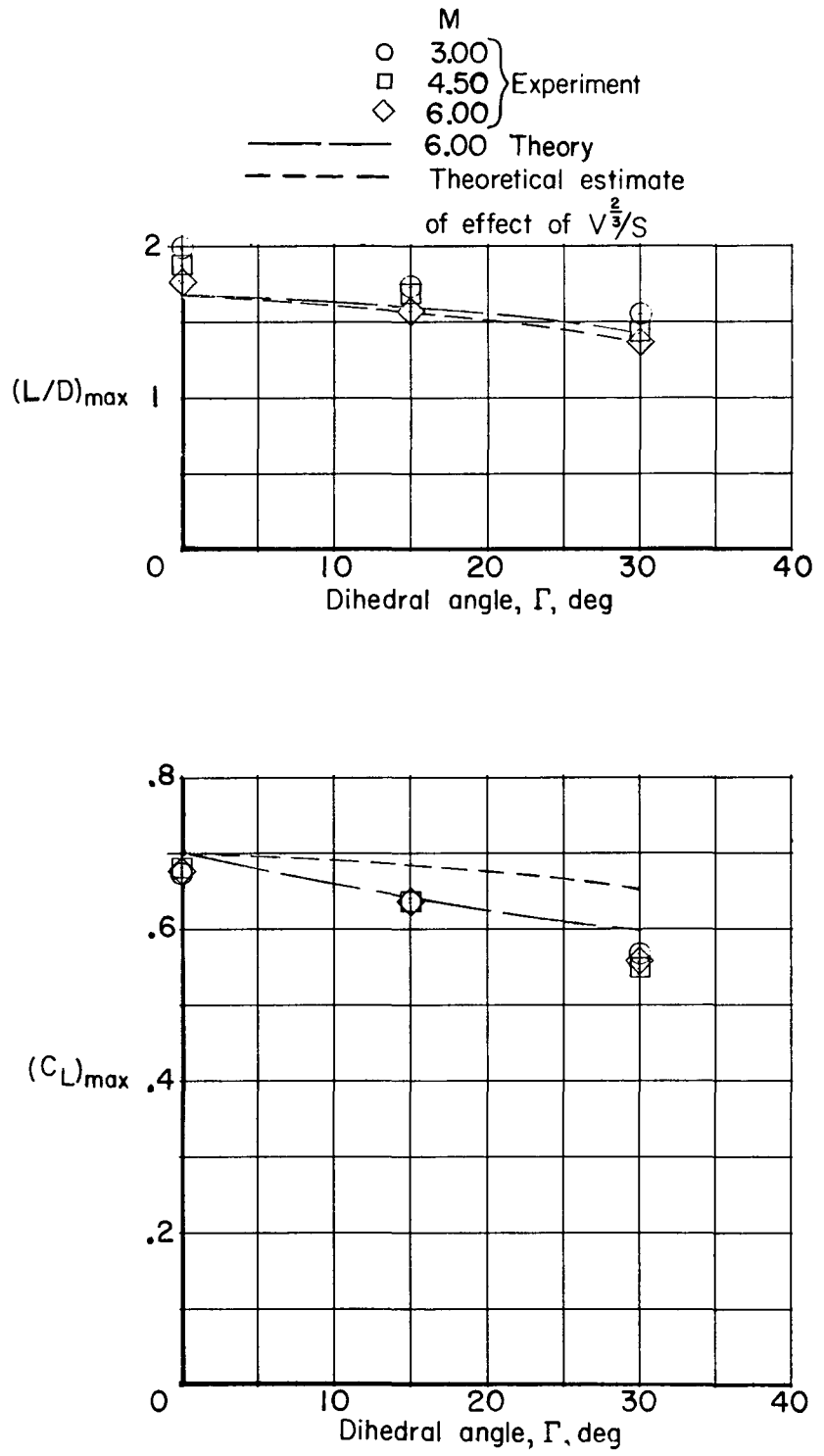

Figure 13.- The effect of dihedral on the aerodynamic performance of a thick-slab delta wing.

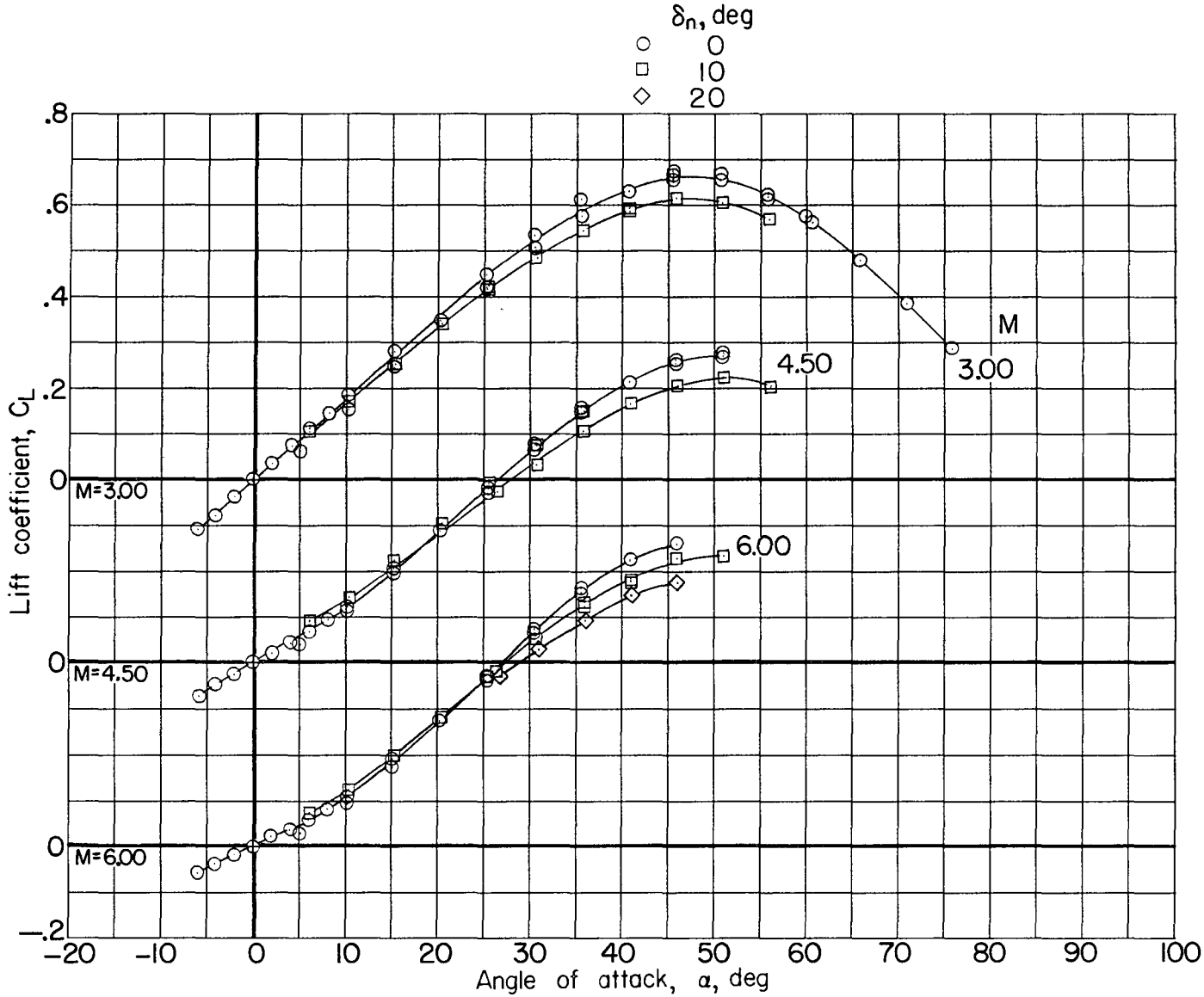

(a) Lift.

Figure 14.- The effect of nose deflection on the aerodynamic characteristics of model 1.

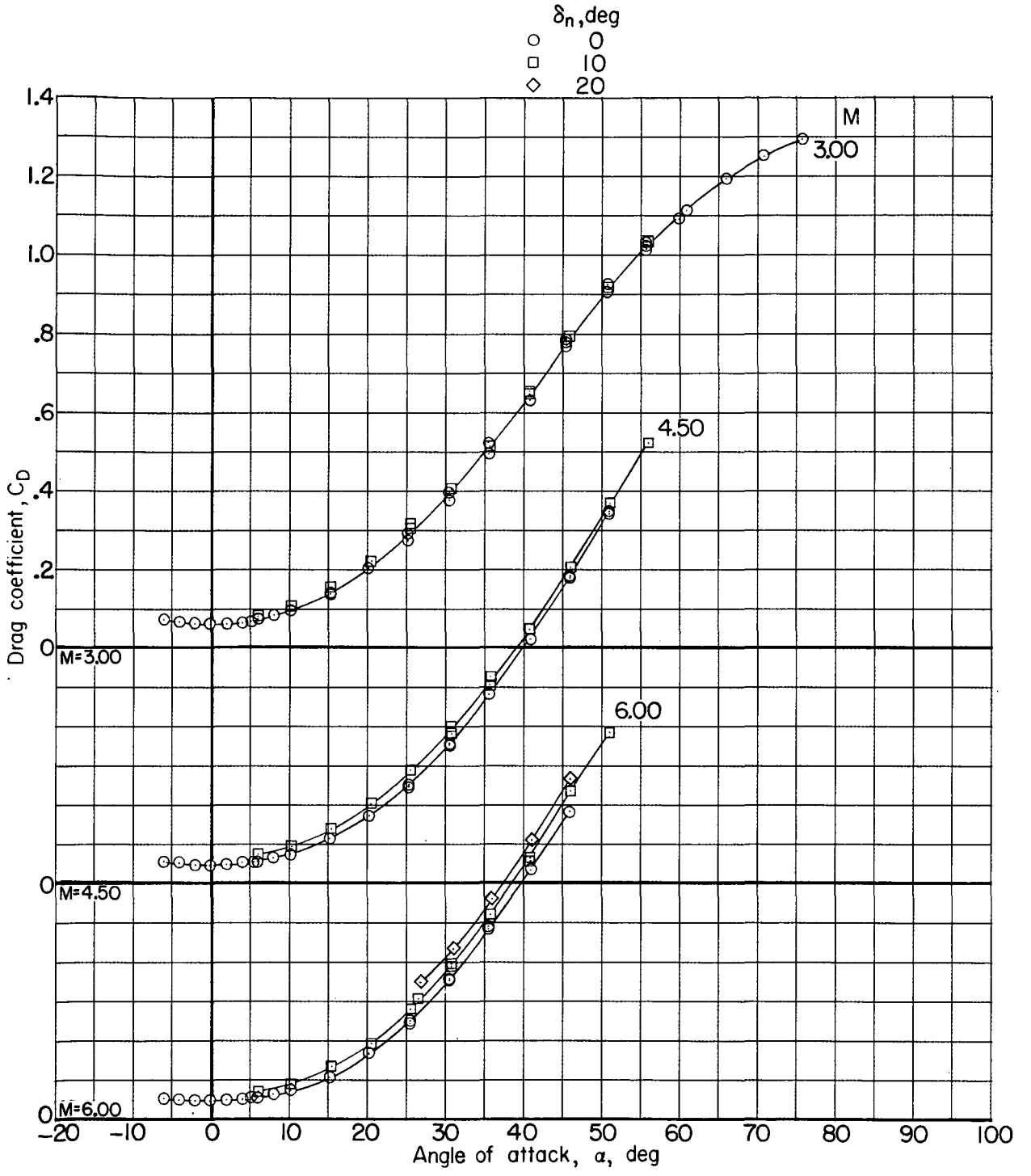

(b) Drag.

Figure 14.- Continued.

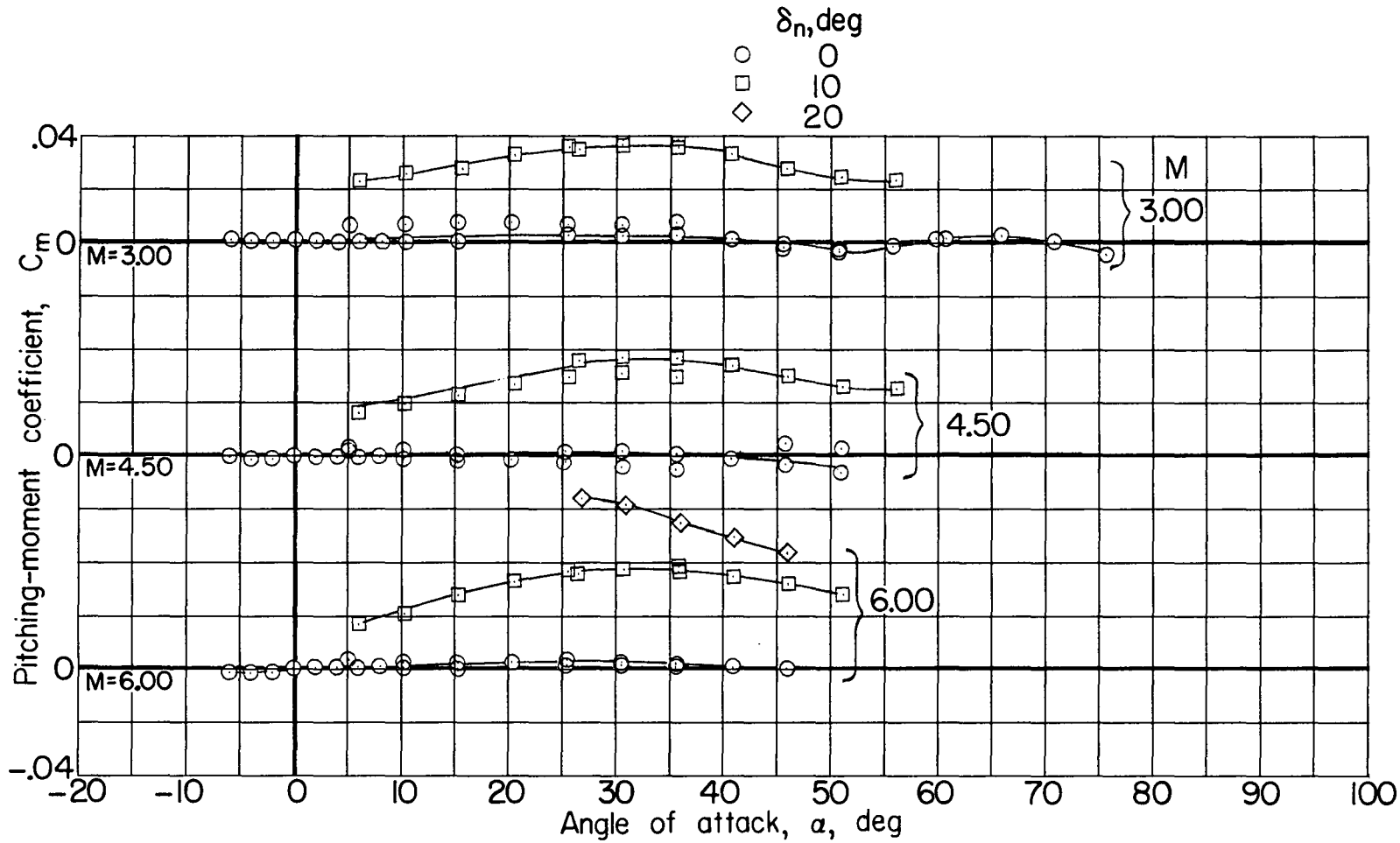

(c) Pitching moment.

Figure 14.- Continued.

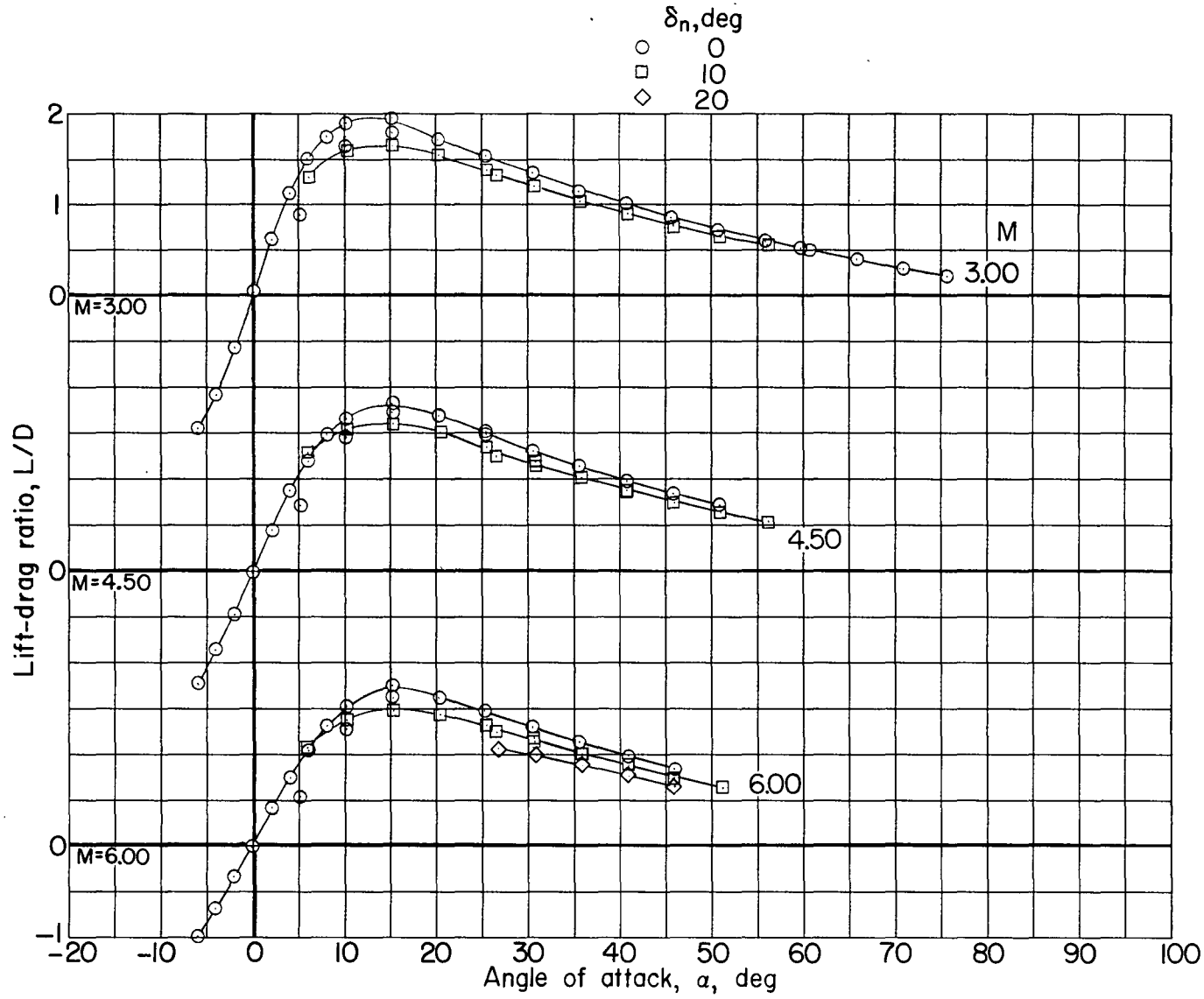

(d) Lift-drag ratio.

Figure 14.- Concluded.

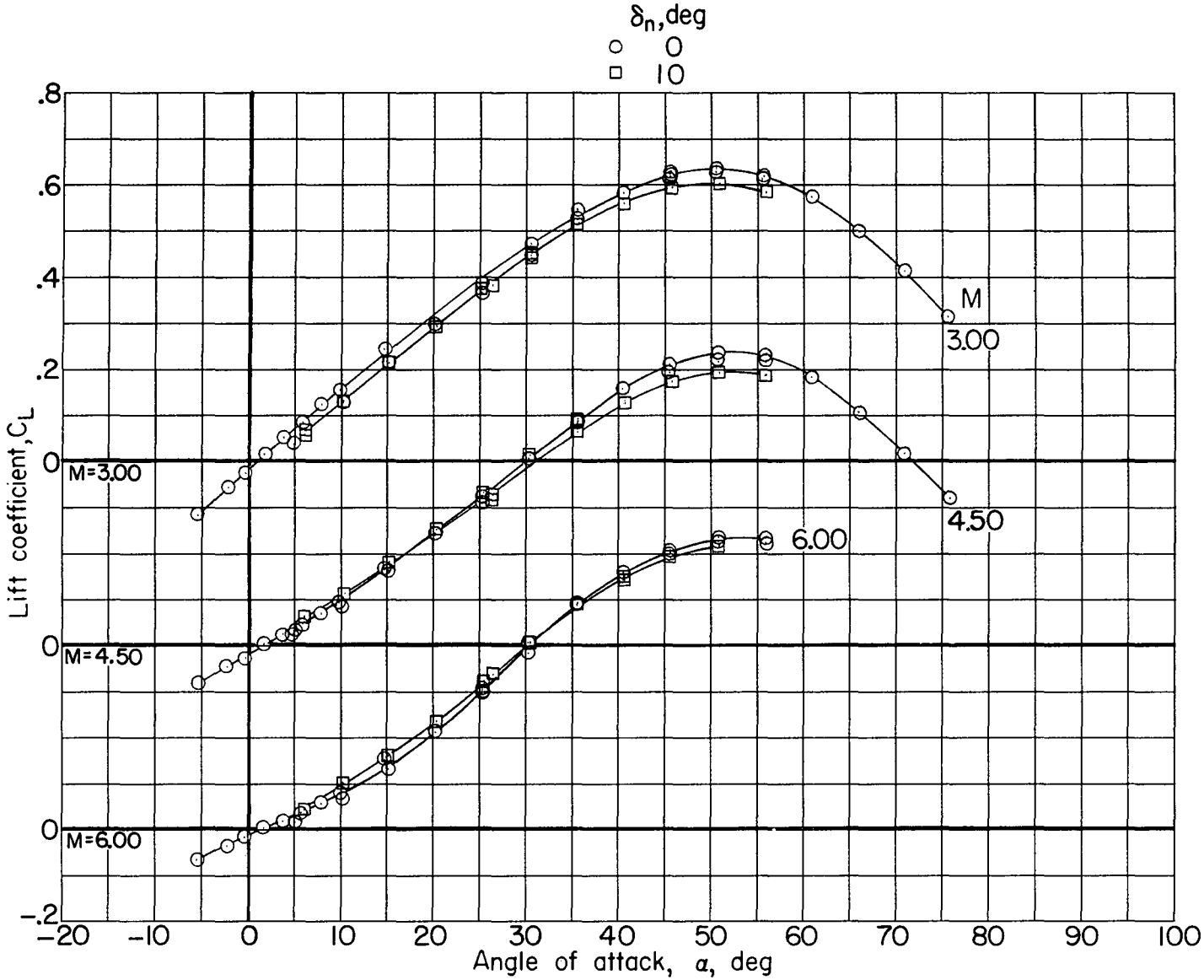

(a) Lift.

Figure 15.- The effect of nose deflection on the aerodynamic characteristics of model 4.

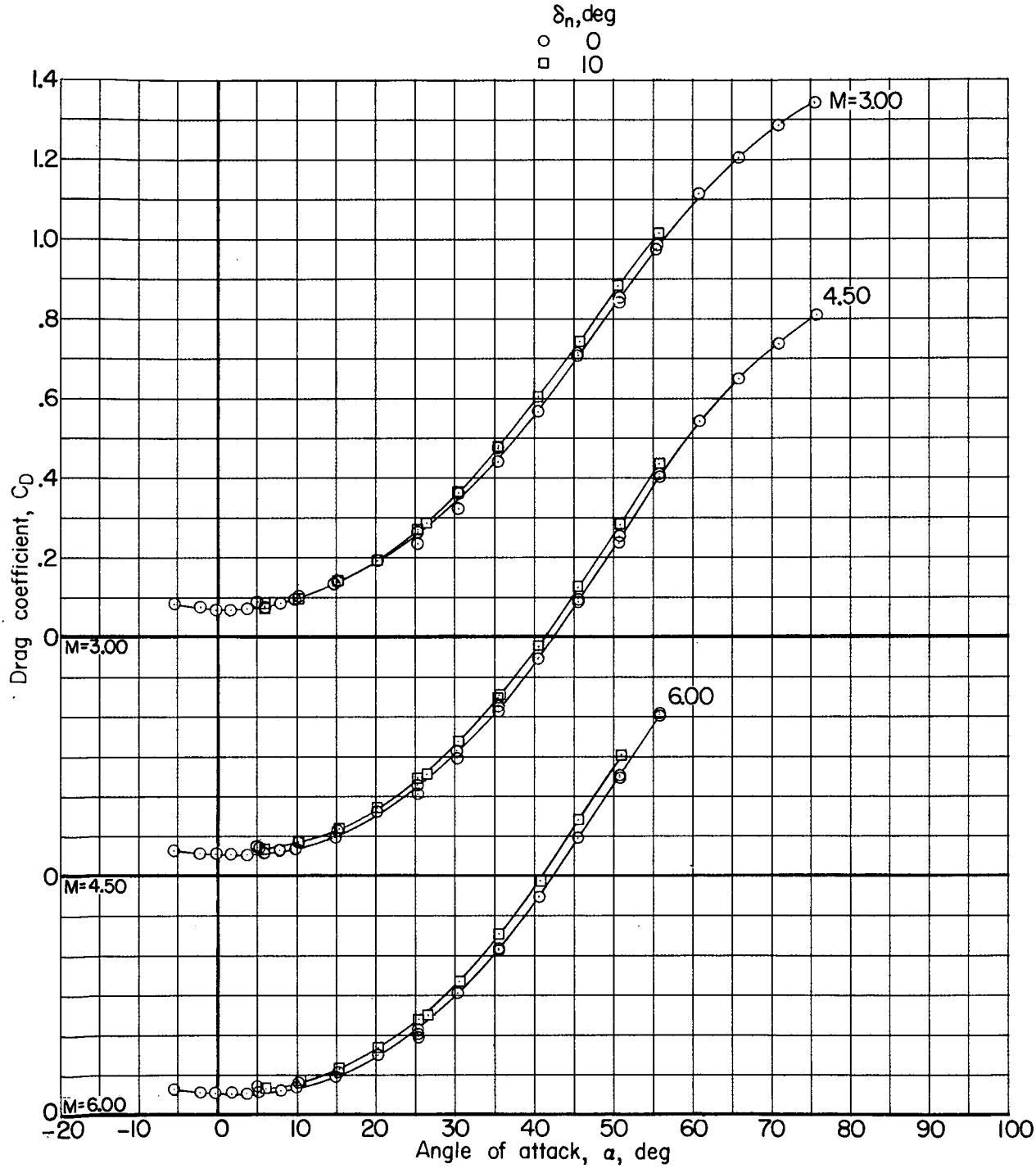

(b) Drag.

Figure 15.- Continued.

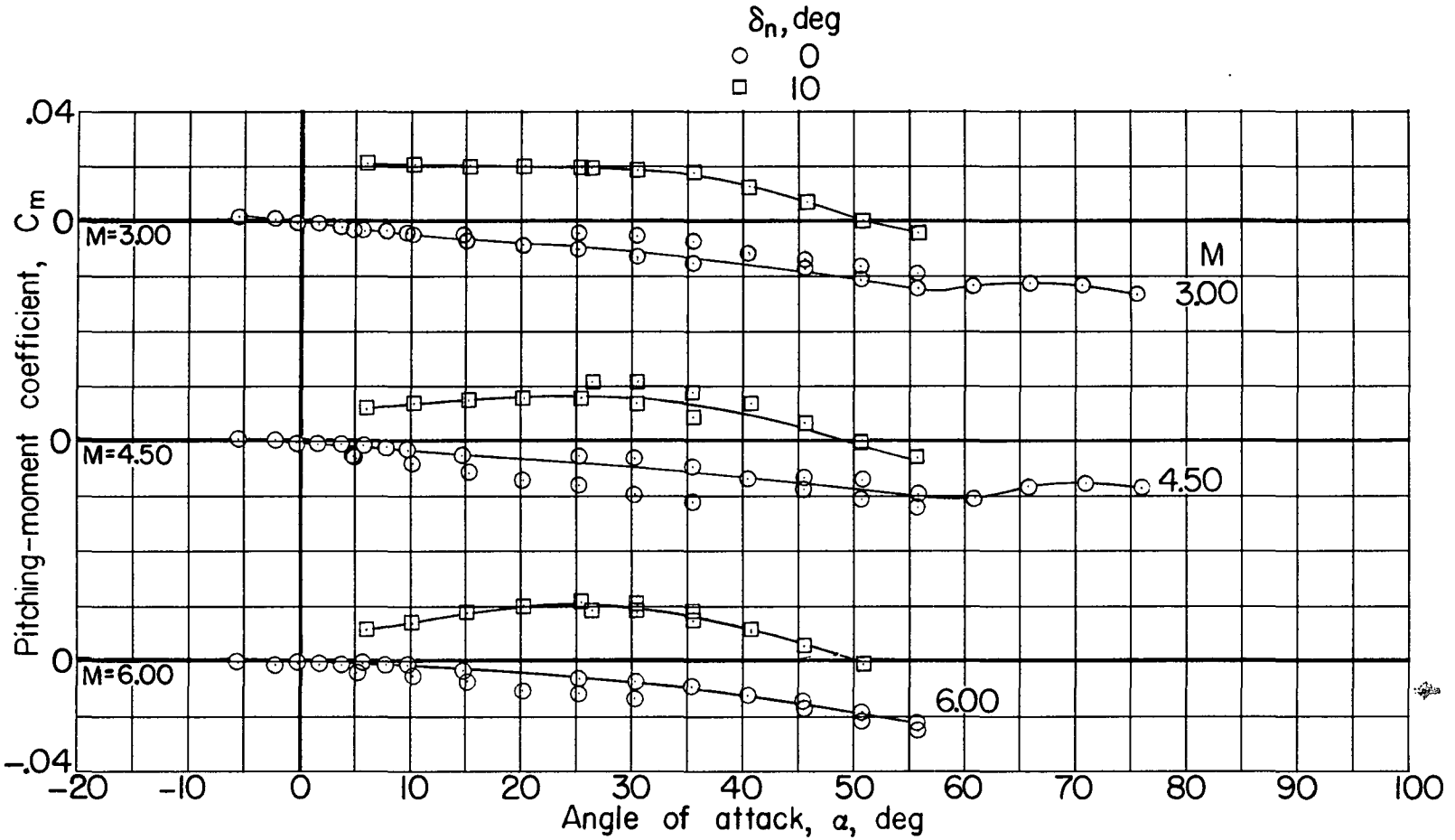

(c) Pitching moment.

Figure 15.- Continued.

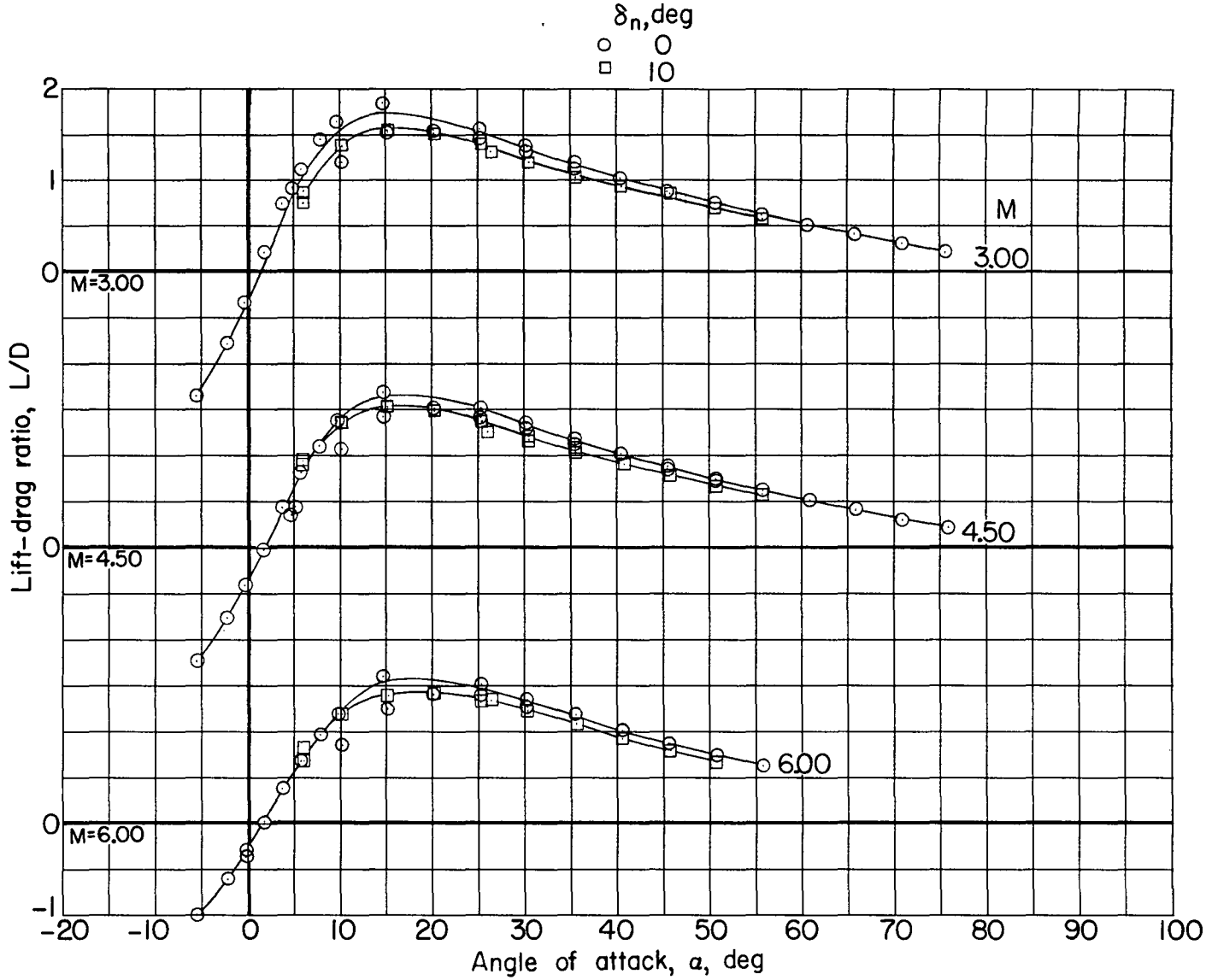

(d) Lift-drag ratio.

Figure 15.- Concluded.

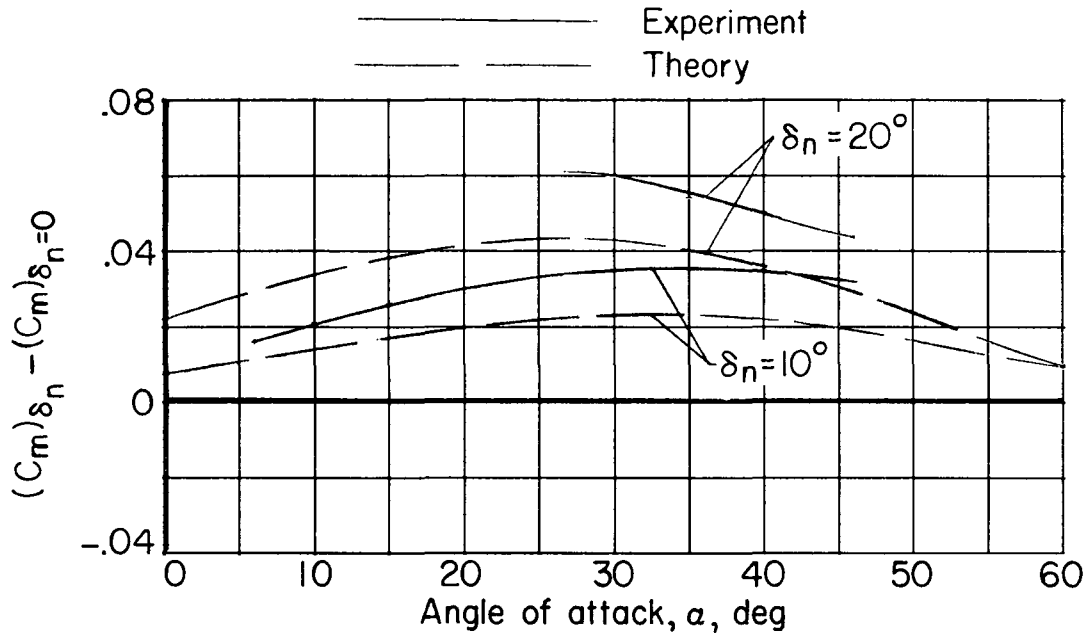

(a) Model 1.

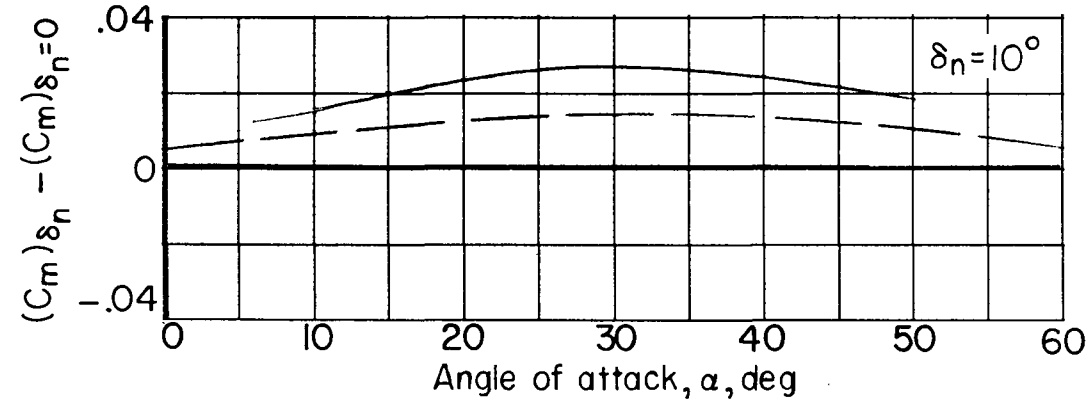

(b) Model 4.

Figure 16.- Variation of incremental pitching-moment coefficient due to nose deflection with angle of attack for models 1 and 4. M = 6.00.

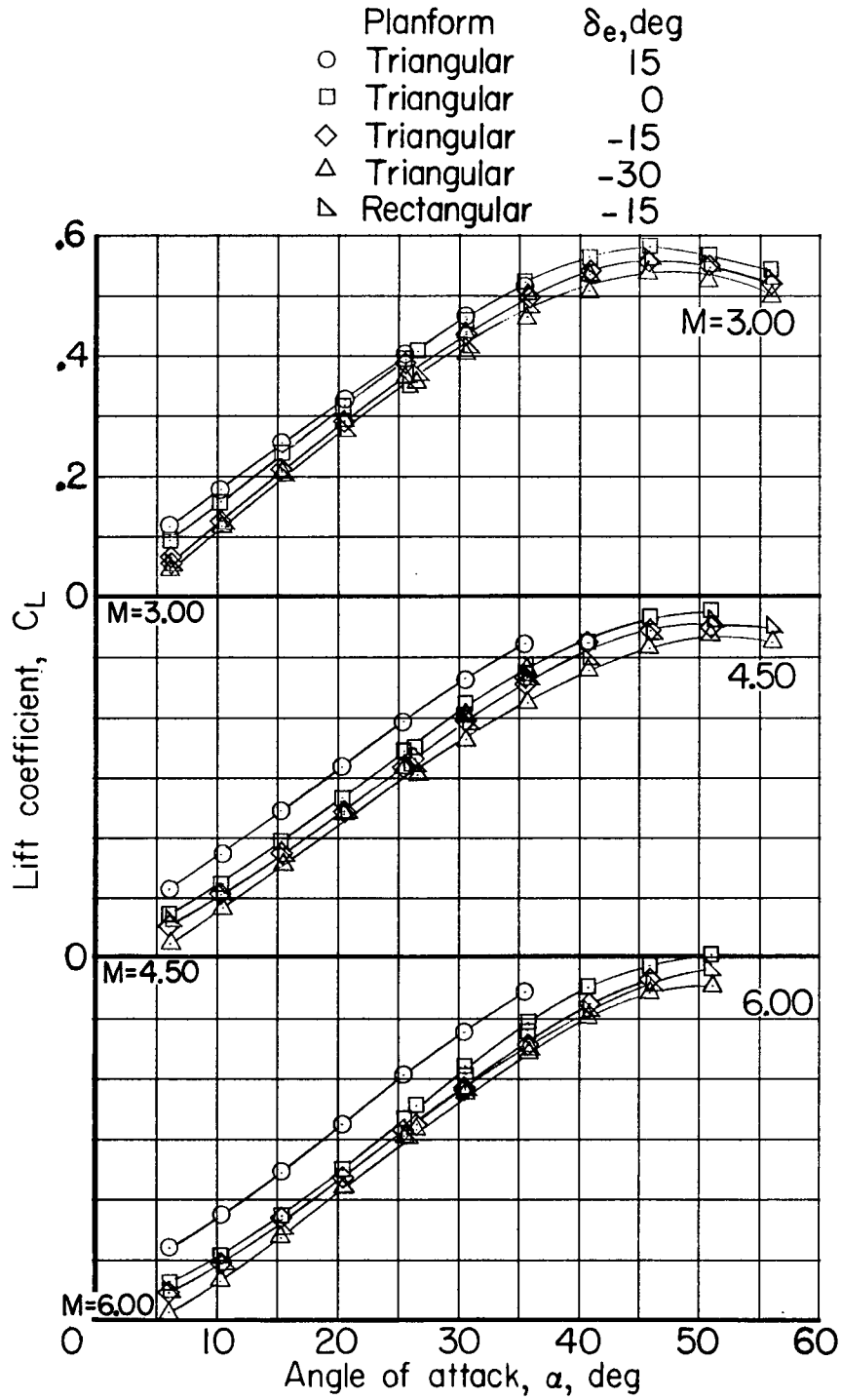

(a) Lift.

Figure 17.- The effect of elevon planform and deflection angle on the aerodynamic characteristics of model 1. $\delta_n = 10^o$.

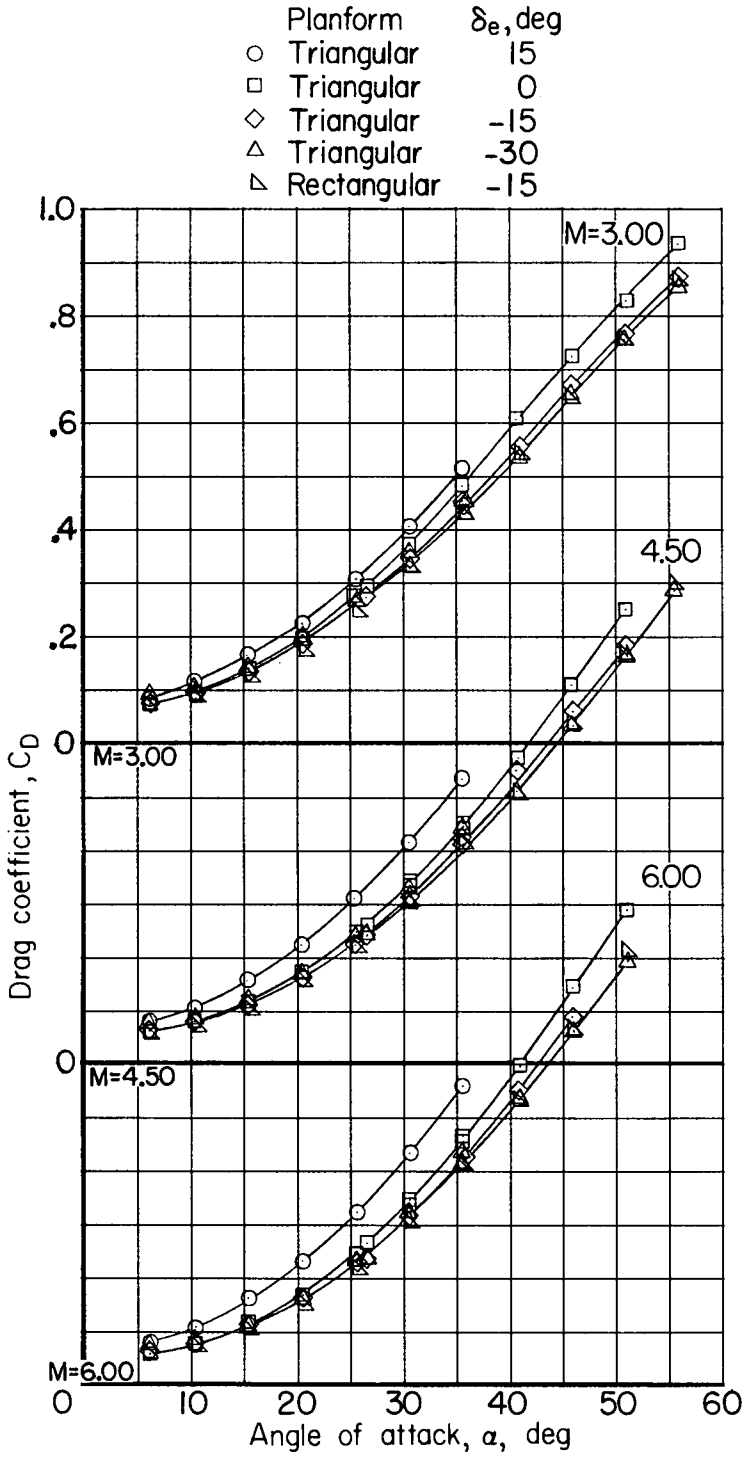

(b) Drag.

Figure 17.- Continued.

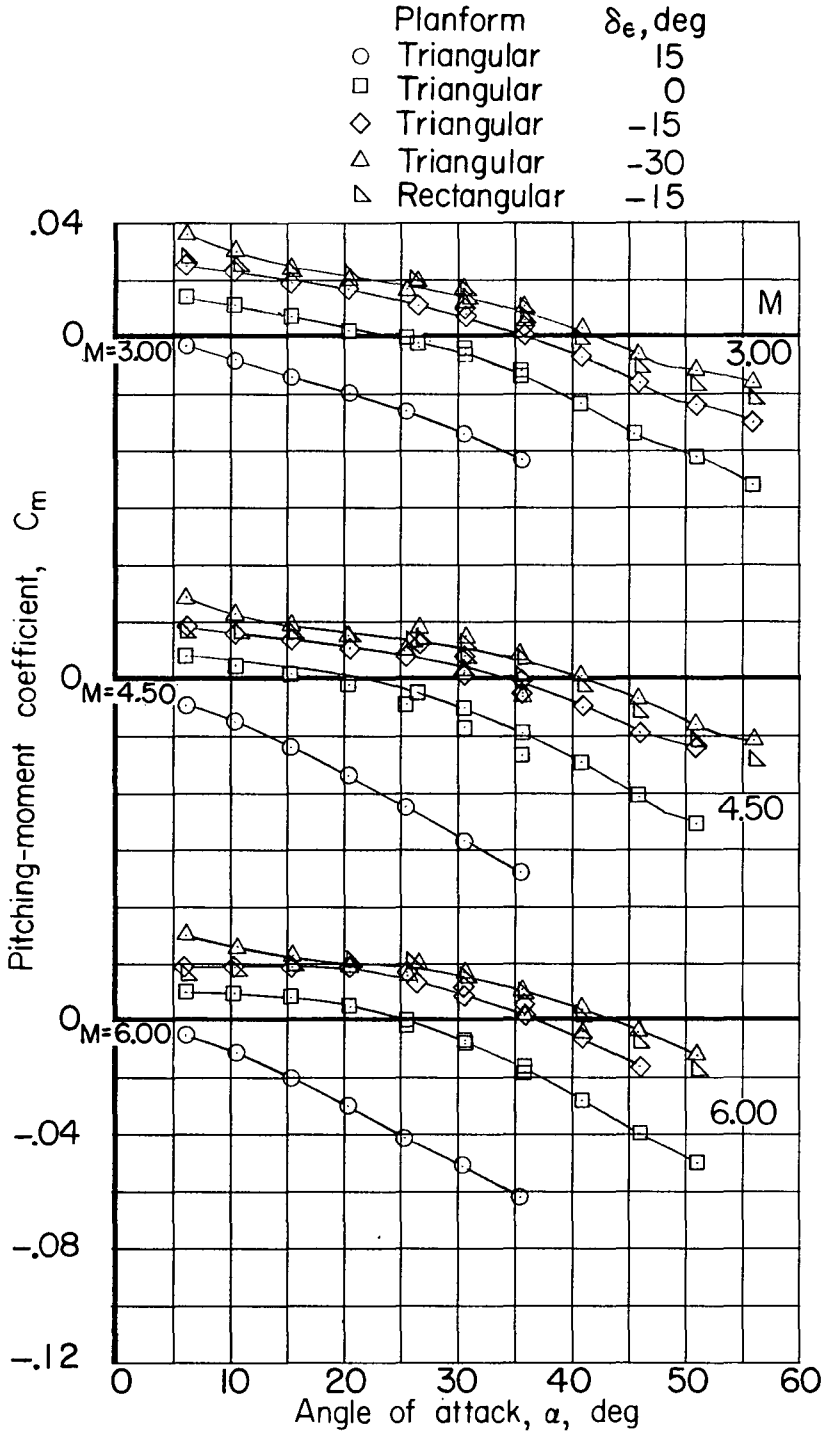

(c) Pitching moment.

Figure 17.- Continued.

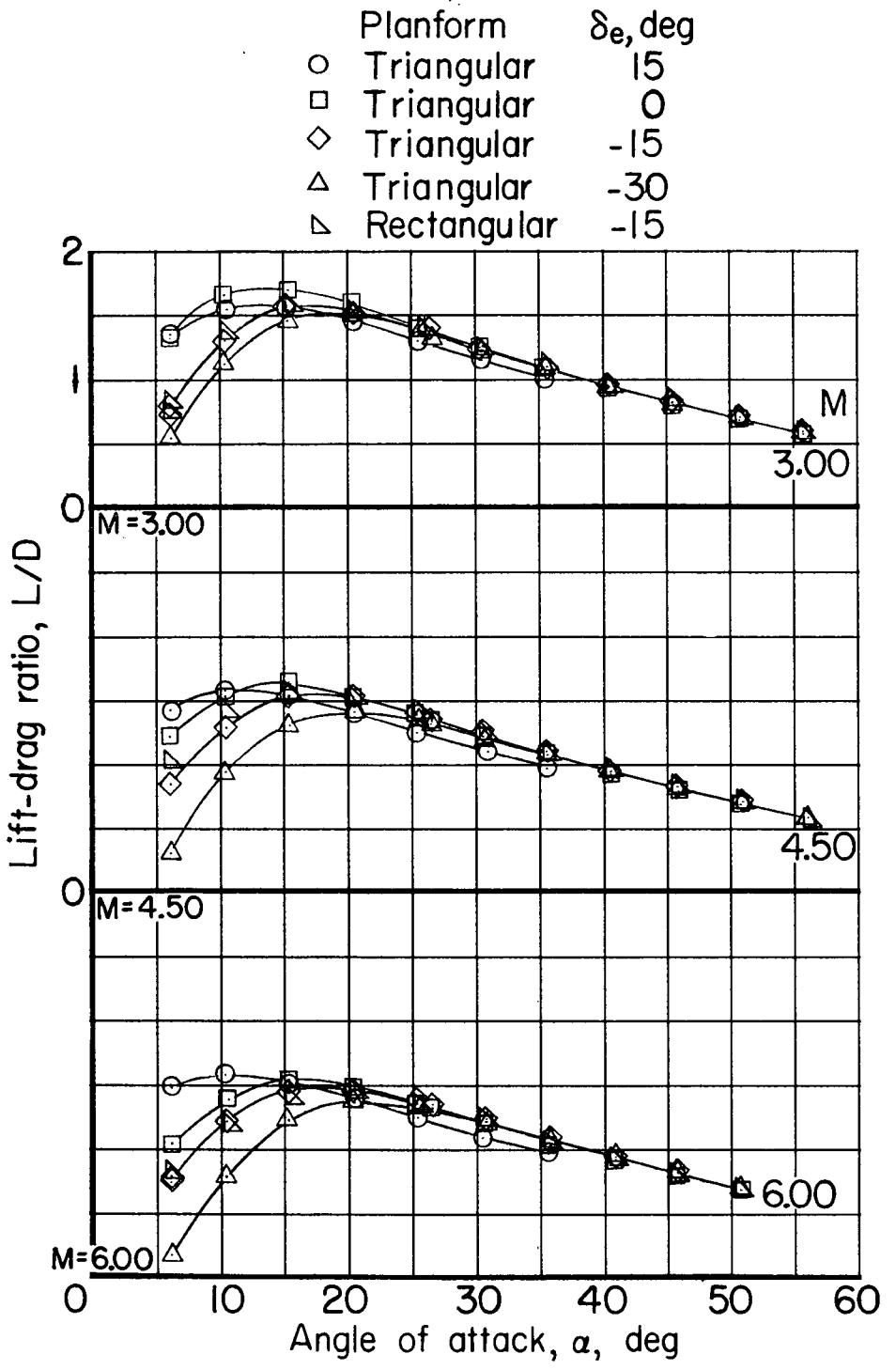

(d) Lift-drag ratio.

Figure 17.- Concluded.

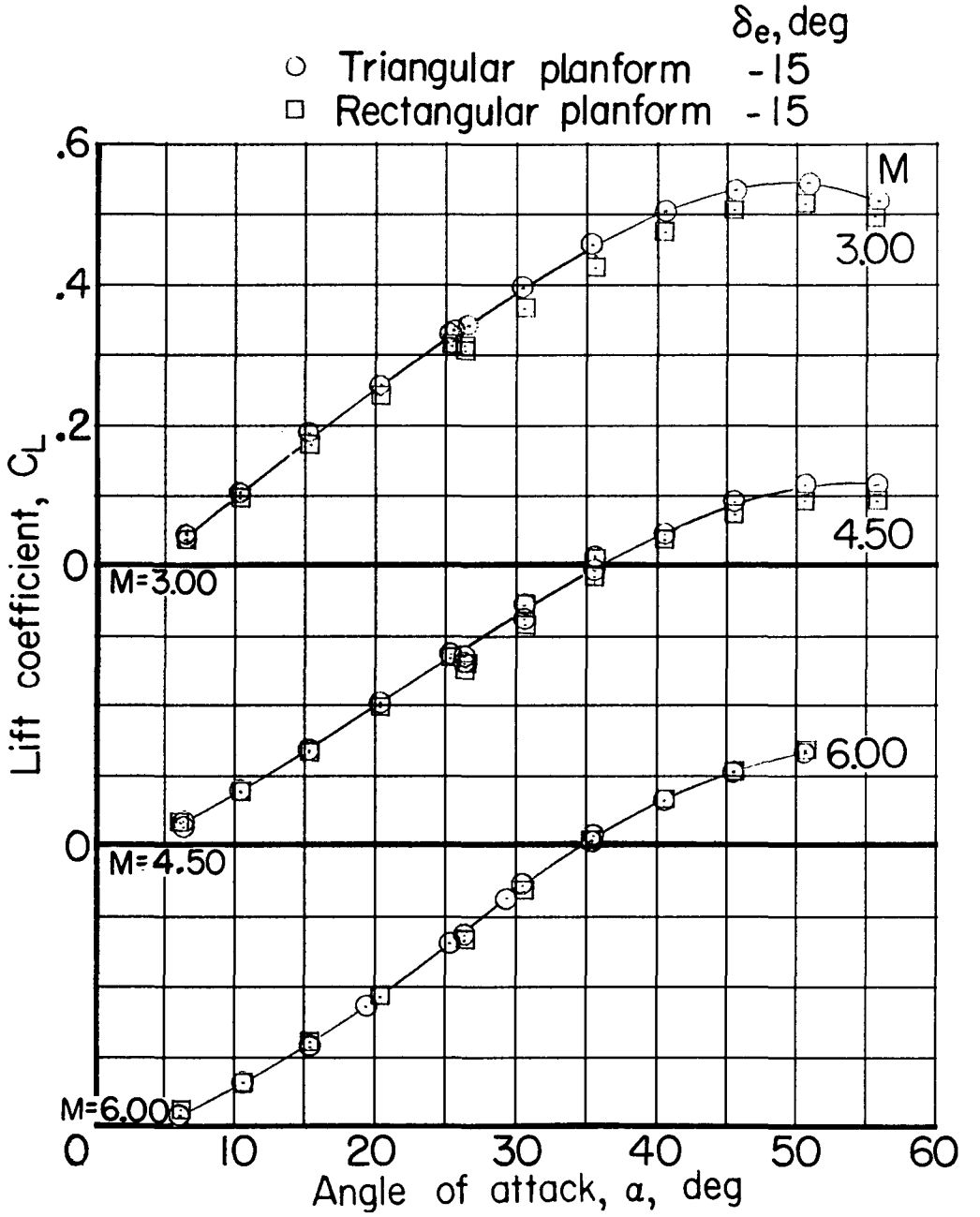

(a) Lift.

Figure 18.- The effect of elevon planform on the aerodynamic characteristics of model 4. $\delta_n = 10^\circ$.

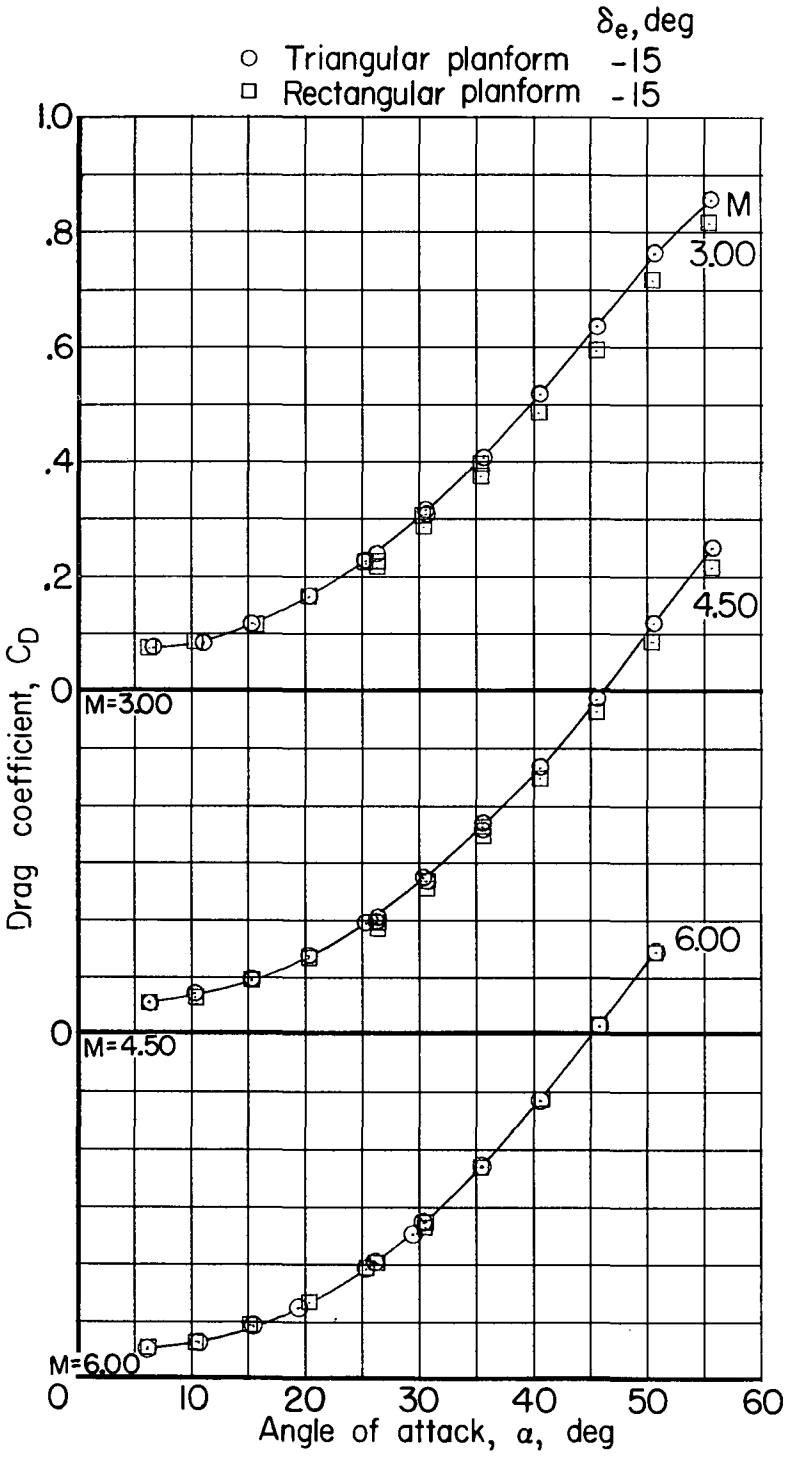

(b) Drag.

Figure 18.- Continued.

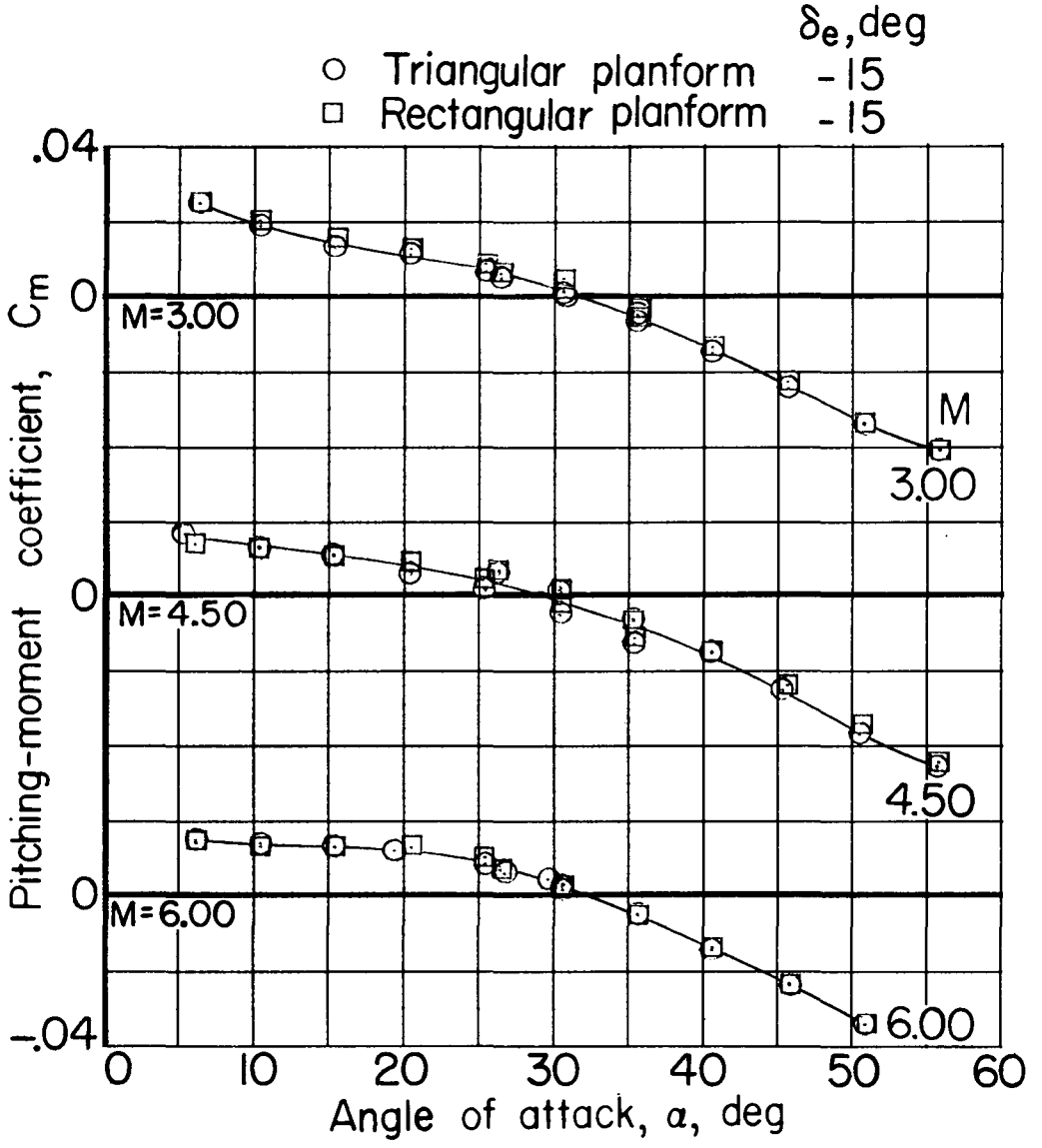

(c) Pitching moment.

Figure 18.- Continued.

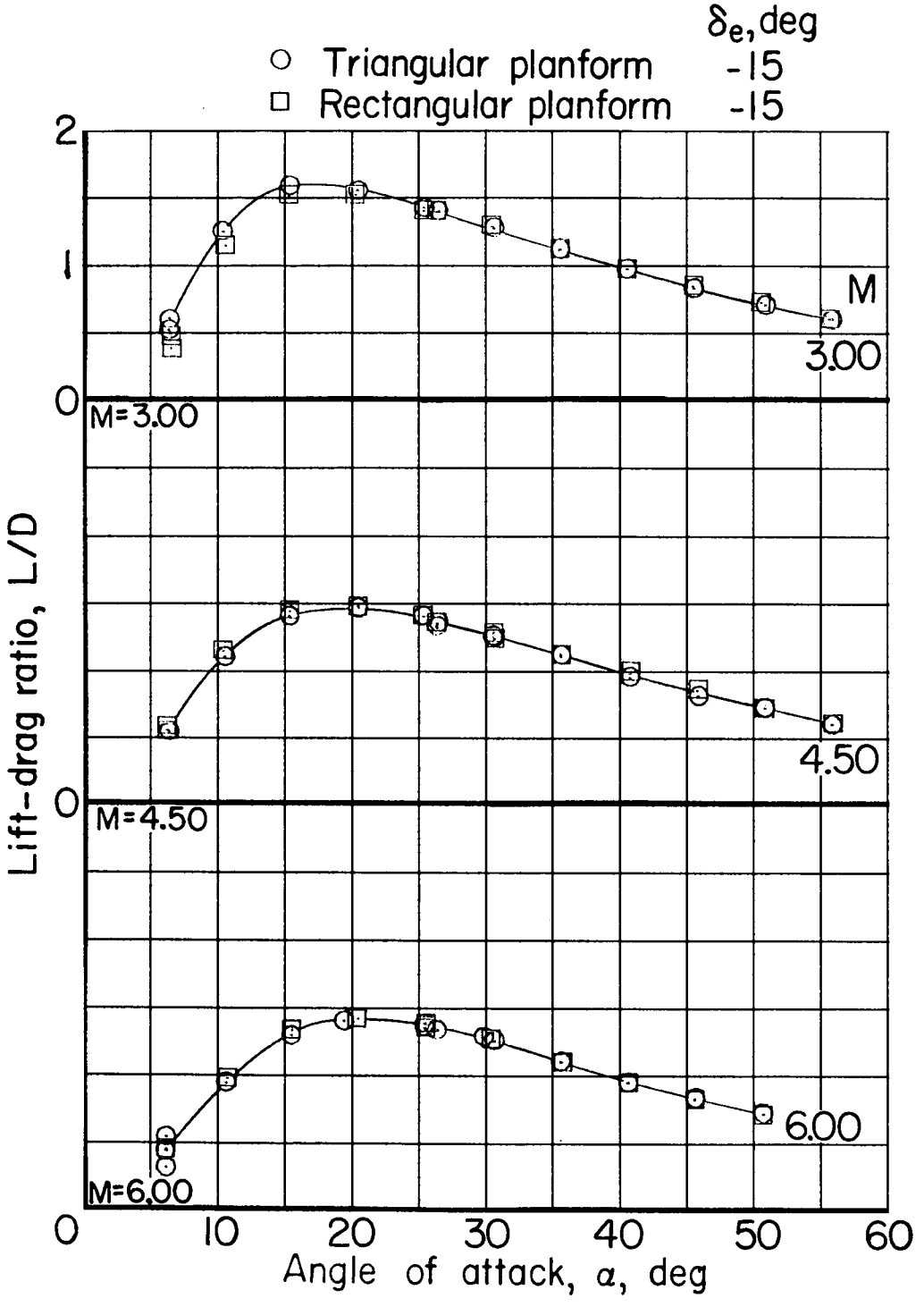

(d) Lift-drag ratio.

Figure 18.- Concluded.

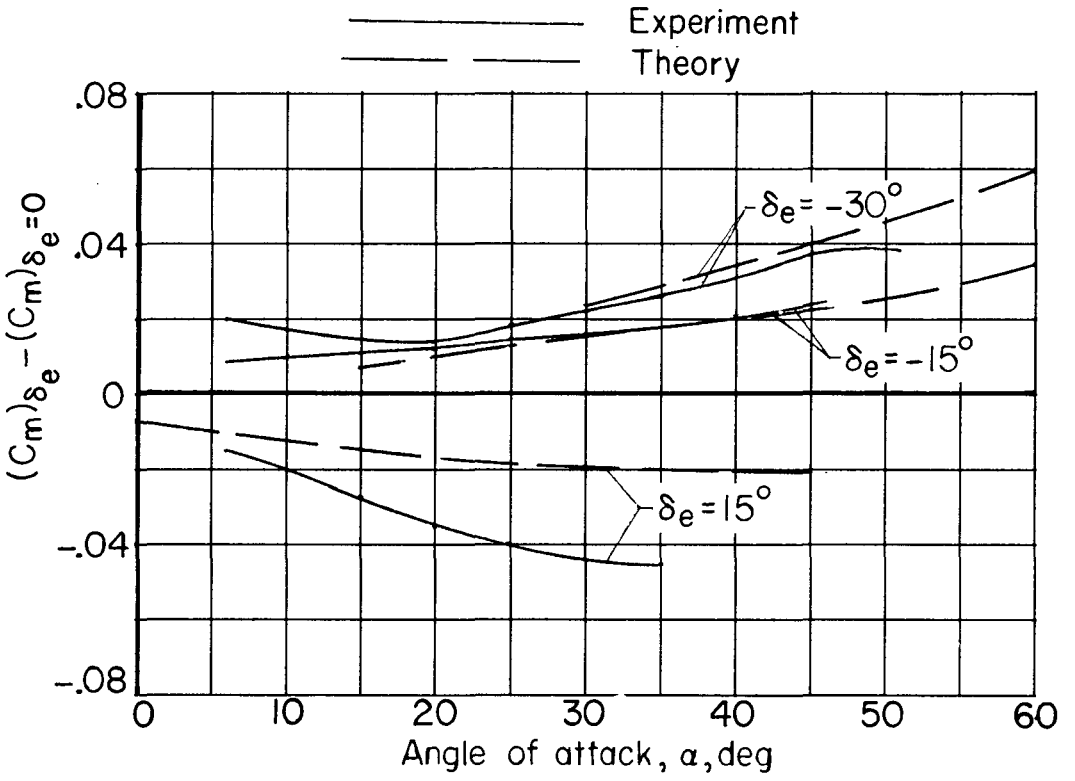

Figure 19.- Variation of incremental pitching-moment coefficient due to elevon deflection with angle of attack for model 1. M = 6.00.